MONTHLY NOTICES

OF THE

ROYAL ASTRONOMICAL SOCIETY

Vol. 109 No. 4

MEETING OF 1949 MAY 13

Professor W. M. Smart, President, in the Chair

The election by the Council of the following Fellows was duly confirmed:—

Nirad Gopal Basu, B.Sc., 39/1 Suburban School Road, Calcutta, India (proposed by A. K. Das);

William Bernard Cribb, 20 Dore Avenue, Manor Park, London, E. 12 (proposed by J. F. Griffiths); and

Cyril Rosen, Northlands, 17 Highbury Quadrant, London, N. 5 (proposed by F. M. Holborn).

The election by the Council of the following Junior Members was duly confirmed:—

Geoffrey Martin Brown, Department of Physics, University College of Swansea, Singleton Park, Swansea (proposed by G. L. Clark); and

Edward Kendrick, B.Sc., 402 Wilbraham Road, Chorlton-cum-Hardy, Manchester (proposed by J. C. Farrer).

One hundred and ten presents were announced as having been received since the last meeting, including:—

C. F. Baeschlin, *Lehrbuch der Geodäsie* (presented by the publisher);

Survey of India, *Air Survey for Development* (presented by Brigadier G. F. Heaney, C.B.E.);

J. E. Kerrich, *An Experimental Introduction to the Theory of Probability* (presented by the author);

Georges Lemaître, *Rayons Cosmiques et Cosmologie* (presented by the author); and

Henri Memery, *L'Action Individuelle des Taches Solaires sur les Phénomènes Terrestres* (presented by the author).

ADDITIONAL MEETING OF 1949 JULY 1

in the Physics Department of the University of Manchester

Professor W. M. Smart, President, in the Chair

The President announced that this meeting was the second in the history of the Society to be held outside London. He expressed the thanks of the Society to the University of Manchester for their hospitality on this occasion; and also to the Manchester Astronomical Society, with whose cooperation the meeting was being held.

A number of Fellows signed the Admission Book. Several papers communicated to the Society were read by their authors, and a detailed account was given of the investigations being carried out at Jodrell Bank on the daytime meteor streams.

On the evening of 1949 June 30 a popular lecture entitled "Sun, Radio and the Stars" was given by Dr M. A. Ellison, in the Chemistry Theatre of the University of Manchester; Mr J. C. Farrer, President of the Manchester Astronomical Society, being in the Chair.

On the morning of 1949 July 1, Fellows were invited to visit the Jodrell Bank Experimental Station of the University, where they were given demonstrations of the work being done on meteors, galactic noise and related subjects.

On the evening of 1949 July 1 the Council of the University of Manchester invited Fellows to dinner in the Staff House, together with members of the Astronomical Society of Manchester.

On the morning of 1949 July 2 a Geophysical Discussion on Ionization in the Earth's Upper Atmosphere was held in the Physics Department of the University, under the Chairmanship of Professor L. Rosenfeld.

HIGH-RESOLUTION INTERFEROMETRY OF THE SOLAR SPECTRUM

*P. J. Treanor, S.J.**

(Communicated by the Director, University Observatory, Oxford)

(Received 1949 June 22)

Summary

Many fundamental problems in solar physics are likely to remain unsolved until a spectroscopic resolving power of the order of 10^6 becomes available. Grating or prism spectroscopes have not yet been constructed to satisfy this need. The writer investigates the possibility of obtaining the required resolving power by interferometric means.

The chief difficulty, in obtaining a high-resolution interferometric analysis of a continuous spectrum broken by absorption lines, lies in the fact that high primary monochromatization is required in order to present the interferometer with a range of spectrum small enough to be analysed without overlap of orders. This consideration sets a limit to the factor of gain obtainable by interference methods, and defines somewhat narrowly the correct conditions of employment of the spectroscope and interferometer.

An experimental arrangement is described which is designed to satisfy these conditions. A short etalon of high reflectivity is placed behind the spectrum of the Sun formed by the Oxford Solar Spectroscope. Recollimated light from this spectrum is analysed by the etalon, and produces an interference pattern in a plane conjugate to that of the spectrum, in the focal plane of a camera. This pattern consists of a system of circular heterochromatic channels, and within these channels a system of monochromatic absorption fringes appears. These absorption fringes are interferometric spectra of the solar absorption lines, and their definition is determined by the resolving power of the etalon only. The sharpness of the fringes makes possible wave-length measurements of high precision. Measurements in the D region show that the probable error for a single plate will be about 0·001 A.

The interference photographs display continuously, without overlap of orders, an interferometric spectrum exceeding many times the range of the etalon used. This feature, combined with the resolution, makes the method suitable for the photometric determination of line contours. Results of applications in this field will be presented in a subsequent paper.

Introduction

It has been realized for many years that the profiles of solar absorption lines, observed with ordinary spectroscopes, are seriously distorted by instrumental slit pattern. This effect, which is far from negligible even in the profiles of the broader solar lines observed with large spectroscopes, mainly determines the inner part of the observed profile of lines of Rowland intensity 3 and less (**18, 26**). If the form of the instrumental pattern is known, it is possible to correct the observed profile, at least of the broader lines, but the only real solution of the difficulty, as Redman (**20b**) has pointed out, is to obtain an actual resolving power of the order of 10^6. Solar spectroscopes have at present a resolving power not greatly exceeding 10^5. Although it is reasonable to suppose that this figure may

* Skynner Student in Astronomy, Balliol College, Oxford.

gradually be increased, interferometric methods offer a more immediate prospect of effecting the necessary improvement.

Following the important experiment of Fabry and Perot (**11a**) in 1902, which revealed systematic differences between Rowland's solar wave-length measurements and those determined by the newly invented etalon interferometer, and Kayser's demonstration (**16**) that these discrepancies were attributable to errors inherent in grating measurements, the Fabry-Perot interferometer secured a permanent place in astronomical spectroscopy. Although the possibility of using the interferometer to study the intensity distribution within the solar lines was adumbrated by Fabry and Perot, the first applications were, naturally, to absolute wave-length measurements. In this field, however, it was the freedom from systematic error and the high dispersion of the etalon that was considered of prime importance, and its resolving power was not exploited; indeed it was frequently used under conditions in which its resolving power would have been no greater than that of the spectroscope. Shane first showed (**22**) that the interferometer could be combined with a spectroscope with a narrow slit, in such a way as to improve the resolving power of the spectroscope, and his method has been applied successfully to contour measurements by Cherrington and by Panofsky (**6, 19**).

Now the Fabry-Perot interferometer is itself essentially a high-resolution spectroscope and as such is widely used in the study of emission spectra. From this point of view, the problem of its application to the high-resolution interferometry of the solar spectrum involves first a discussion of the conditions in which the etalon can be used to analyse spectroscopically a continuous spectrum. This discussion forms the first part of the paper. The remaining problem is a practical one; namely the designing of a system which will satisfy these conditions. The description of such an optical system forms the second part of the paper. Finally, in Part III, the application of this system to wave-length measurements is discussed.

Part I. The transition from emission to absorption spectra interferometry

Fundamental properties of the monochromatic fringe pattern.—The general theory of the etalon has frequently been treated at length, for example by Meissner (**17**); it is convenient however to recall here its fundamental characteristics and to quote the results to which reference will have to be made.

The interferometer consists essentially of a pair of partially transparent metal on glass mirrors of reflectivity r, held in exact parallelism by a silica spacer of thickness t. Light from a perfectly monochromatic source of wave-length λ, after passage through the etalon at an angle ϕ to the silvered surfaces, will produce a series of beams in a condition to interfere, according to the equation

$$n\lambda = 2\mu t \cos\phi, \tag{1}$$

where μ is the refractive index of air, henceforth assumed equal to unity. If the source of light is extended, there will be formed in the focal plane of a camera of focal length f a system of bright circular interference fringes. The sharpness of the fringes increases as the reflectivity r of the etalon increases, the intensity distribution within the fringes being given by

$$R(z) = a^2 \Big/ \left\{ 1 + \frac{4r}{(1-r)^2} \sin^2 \frac{2\pi t(1-[z^2/2f^2])}{\lambda} \right\}, \tag{2}$$

where z is the distance from the axis of the system, this axis being defined by a line through the pole of the camera lens perpendicular to the silvered surfaces.

If the light instead of being strictly monochromatic consists, say, of a strong emission line with a train of satellites, each satellite will produce its own ring system, so that a repeated pattern of bright and satellite rings is built up (Plate 9*a*). Each pattern is composed of corresponding orders of the line and its satellites, and so forms a high-dispersion spectrum of the group. The dispersion in these interferometric spectra is

$$d = f^2/\lambda z \text{ mm./A.} \tag{3}$$

Though this expression is independent of t it is not convenient in practice to make measures in the innermost rings, and the dispersion at a given order from the centre, say the third, increases with t. The use of higher t values results therefore in higher available dispersion.

Evidently, if a satellite group is sufficiently extensive, adjacent orders will overlap (Plate 9*a*). The range of the etalon, that is, the amount of spectrum which it can analyse without overlap, is approximately

$$\Delta = \lambda^2/2t. \tag{4}$$

In consequence of the finite width of the fringes, entailed by (2), the interferometer has a finite resolving power which, as Meissner (**17**) shows, may be written

$$P = [2{\cdot}98r^{\frac{1}{2}}/(1-r)]n, \tag{5}$$

n being the order of interference. By analogy with the grating spectroscope this may be written

$$P = m\,.\,n, \tag{6}$$

where m is the effective number of interfering beams and has the value

$$m = 2{\cdot}98r^{\frac{1}{2}}/(1-r). \tag{7}$$

It follows from (4) that the range is very small except for short spacers, which by (1) and (5) yield low resolving powers. Consequently, even in the examination of emission spectra it is necessary to eliminate by a low-powered monochromator all the lines except the group under examination. If, as frequently occurs, the group is itself of greater extent than the range, overlapping will occur between orders, but it will still be possible, if the group is not too complicated, to sort out the overlapping patterns.

Application to absorption spectra.—Now consider what happens when the emission-line source is replaced by a source with a continuous spectrum. Every elemental wave-length present will contribute its own set of interference circles. Hence, provided that the range of continuous spectrum presented for analysis is less than the range $\lambda^2/2t$ of the interferometer, a set of broadened circular fringes will be produced, the radial distribution of intensity in each fringe representing the interferometric analysis of the range of spectrum in question. Absorption lines will appear as dark concentric circles within this broadened system.

A closely analogous case, which may be used to illustrate this analysis of a short range of continuous spectrum containing an absorption line, is provided by the self reversal of emission lines. Here, the true finite breadth of the emission line proper provides the "continuous" spectrum, while the self-reversed core constitutes a true absorption line. The diametral section of the interferometric analysis of this phenomenon, for the D_2 line from a discharge tube, is shown in Plate 9*b*.

Up to this point the analogy with emission spectra is perfect. It breaks down, however, when the range presented is greater than that of the etalon. It is clear

that adjacent orders of interference will then overlap, as in the emission case, but this will now involve the superposition of the continuous spectrum from one order on the absorption lines of the next, and the structure of the spectrum will be obscured. Hence, whereas in emission spectra an overlap, even of several orders, can be tolerated in the interests of high resolution, this is not the case in the analysis of absorption spectra, which requires the use of a monochromator capable of excluding all radiation except that contained in a narrow wave-length band equal to the range of the etalon.

Now the minimum wave-length range, which an ordinary spectroscope, when used as a monochromator, can supply, is closely related to the spectroscopic resolving power. The satisfying of the fundamental condition, that the etalon range shall be at least equal to this minimum range, relates the maximum resolving power of the etalon, under correct conditions of employment, to the resolving power of the spectroscope. This is a very serious fact, in view of the purpose of the etalon, which is to secure a much higher resolving power than that of the spectroscope, and its quantitative implications must now be established.

The spectroscope as a monochromator.—Consider very nearly monochromatic radiation of wave-length λ (corresponding to position x in the focal plane) incident on the slit (Fig. 1 *a*). This will be smeared out by the instrumental pattern, so that at position x_1 in the focal plane its intensity will be $S(x_1 - x)$, or in terms of nominal wave-lengths $S(\lambda_1 - \lambda)$ (Fig. 1 *b*). Hence, if $T(\lambda)$ is the intensity of this closely monochromatic radiation, the intensity of λ-radiation at nominal position λ_1 will be

$$T(\lambda)S(\lambda_1 - \lambda).$$

If the radiation has a continuous distribution $T(\lambda)\,d\lambda$, then similarly the intensity of λ-radiation at nominal wave-length λ_1 will be

$$T(\lambda)S(\lambda_1 - \lambda)\,d\lambda,$$

and this will be, for example, the intensity of λ-radiation passed by a slit at nominal wave-length λ_1 in the focal plane (Fig. 1 *c*).

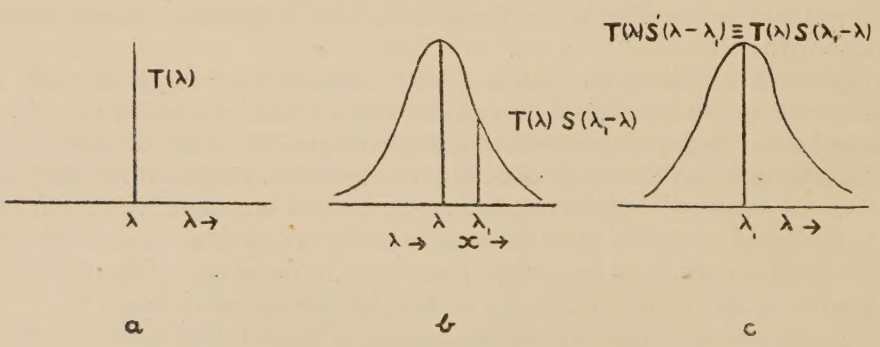

FIG. 1.—*The spectroscope as a monochromator.*

(*a*) *Incident closely-monochromatic radiation.*
(*b*) *Instrumental pattern in plane of spectrum.*
(*c*) *Transmission of spectroscope at nominal* λ_1 *for continuous spectrum.*

The interferometer-pattern for monochromatic wave-length λ and position x has an intensity distribution $R(\lambda)$ of the form given by equation (2). Now consider a short wave-length range λ' to $\lambda' + d\lambda'$ incident on the etalon. The

intensity of this radiation incident on the etalon is $T(\lambda')S(\lambda_1-\lambda')\,d\lambda'$ and the observed intensity at a point z in the focal plane of its camera, corresponding to a nominal ring position for wave-length λ, will be

$$O(\lambda)=\int_0^\infty T(\lambda')S(\lambda_1-\lambda')R(\lambda-\lambda')\,d\lambda'. \tag{8}$$

Now $R(\lambda-\lambda')$ is a periodic function such that $R(\lambda-\lambda'\pm n\Delta)=R(\lambda-\lambda')$, where Δ is the range of the etalon. This means that light, not only of wave-length λ' but also of wave-length $(\lambda'\pm n\Delta)$, will produce fringes at the ring position corresponding to λ'. We may make these contributions from adjacent orders explicit by splitting up (8) into the form

$$\begin{aligned}O(\lambda)=&\int_{\lambda-\frac{\Delta}{2}}^{\lambda+\frac{\Delta}{2}} T(\lambda')S(\lambda_1-\lambda')R(\lambda-\lambda')\,d\lambda'\\
&+\int_{\lambda\ \frac{\Delta}{2}}^{\lambda+\frac{\Delta}{2}} T(\lambda'-\Delta)S(\lambda_1-\lambda'+\Delta)R(\lambda-\lambda'+\Delta)\,d\lambda'\\
&+\int_{\lambda-\frac{\Delta}{2}}^{\lambda+\frac{\Delta}{2}} T(\lambda'-2\Delta)S(\lambda_1-\lambda'+2\Delta)R(\lambda-\lambda'+2\Delta)\,d\lambda'+\ldots\\
&+\int_{\lambda-\frac{\Delta}{2}}^{\lambda+\frac{\Delta}{2}} T(\lambda'+\Delta)S(\lambda_1-\lambda'-\Delta)R(\lambda-\lambda'-\Delta)\,d\lambda'\\
&+\int_{\lambda-\frac{\Delta}{2}}^{\lambda+\frac{\Delta}{2}} T(\lambda'+2\Delta)S(\lambda_1-\lambda'-2\Delta)R(\lambda-\lambda'-2\Delta)\,d\lambda'+\ldots.\end{aligned} \tag{9}$$

Noting that $R(\lambda-\lambda'+n\Delta)=R(\lambda-\lambda')$ and that over the range of integration of each of the integrals $T(\lambda')$, $S(\lambda_1-\lambda')$ are changing slowly with wave-length, we may take their mean values outside the integral sign. We thus get for the observed intensity at nominal wave-length λ in a particular fringe

$$\begin{aligned}O(\lambda)\simeq&\left[T(\lambda)S(\lambda_1-\lambda)+\left\{\begin{matrix}T(\lambda-\Delta)S(\lambda_1-\lambda+\Delta)+T(\lambda-2\Delta)S(\lambda_1-\lambda+2\Delta)+\ldots\\+T(\lambda+\Delta)S(\lambda_1-\lambda-\Delta)+T(\lambda+2\Delta)S(\lambda_1-\lambda-2\Delta)+\ldots\end{matrix}\right\}\right]\\
&\times\int_{\lambda-\frac{\Delta}{2}}^{\lambda+\frac{\Delta}{2}} R(\lambda-\lambda')\,d\lambda'.\end{aligned} \tag{10}$$

The term in curly brackets represents light of wave-lengths other than λ scattered from adjacent orders on top of wave-length λ. It is clear that we must choose a slit pattern and etalon spacer such that $S(\lambda_1-\lambda+\Delta)$, etc. are less than one or two per cent of $S(\lambda_1-\lambda)$, so that these contributions do not prevent a reasonably pure spectrum from being formed. If this condition is satisfied, the observed intensity will be given to a close approximation by the first term of (9), which, if the reflectivity is high, has a very condensed kernel $S(\lambda_1-\lambda')R(\lambda-\lambda')$ and will therefore approximate closely to $T(\lambda)$ in the neighbourhood of $\lambda=\lambda_1$.

Table I gives, for different instruments, the approximate value of the scatter produced at the centre of the range examined ($\lambda=\lambda_1$) when an etalon is used with a range 1, 2, 3 or 4 times the width of the slit pattern. (The width of the pattern has been taken at 40 per cent maximum intensity.) The published instrumental curves for narrow slit of the Potsdam (**14**), Mount Wilson (**4**) and Cambridge (**20a**) instruments and a provisional curve for Oxford have been used in making this calculation.

TABLE I

Percentage scatter for different ratios of range to pattern width

Instrument	Ratio : 1	2	3	4
Mt. Wilson	46	14	7	4
Potsdam	39	13	6	2
Cambridge	27	4	1	(0)
Oxford	50	15	8	6

It will be seen from this table that the scatter can be reduced to reasonable proportions at the centre of the range only by using an etalon with a range not less than three times the breadth of the pattern with narrow slit. At points removed from the centre of the range, the elimination of scatter is still more difficult.

In Table II the instrumental widths and corresponding maximum spacers, *on the assumption of this factor* 3, are given for the instruments in Table I.

TABLE II

Instrumental pattern widths and maximum spacers

	λ=4000 A.		λ=6000 A.	
	Width	Spacer	Width	Spacer
Mt. Wilson	0·040 A.	6·7 mm.	0·060 A.	10 mm.
Potsdam	·032	8·3	·049	12
Cambridge	·067	4·0	(·39)	1·5
Oxford	0·030	8·9	0·066	9·0

This restriction on the maximum length of etalon that can be used makes it necessary to have recourse to very high reflectivity in order to achieve high resolving power. Referring to equation (7) we see that the number of effective reflections m can be increased to about 40 by using reflectivities of about 0·93, which is nearly the practical limit. To obtain a resolving power of 10^6 with this reflectivity, an etalon of 5 mm. is required at λ4000 A. and one of 7·5 mm. at λ6000 A.

According to Table II it is possible to use such etalon lengths without undue overlapping of orders, at least when the spectroscope is used with a narrow first slit, a procedure which is very uneconomical of light. The effect of opening up the slit will be to broaden the instrumental pattern, and therefore to diminish the maximum allowable etalon length. The exact effect in any particular case may be calculated from (10) if the form of the broadened pattern is known (7). Fortunately, the effect of opening the slit is mainly to broaden the core of the pattern, without increasing the scatter-producing wings in the same proportion.

The practical problem which now presents itself is therefore to design a method of using the spectroscope and interferometer which will satisfy the conflicting demands of high light-efficiency on the one hand and high reflectivity and primary resolving power on the other, and which will at the same time use the spectroscope as a monochromator.

Part II. The method of circular channels

The first question which arises in attempting to realize practically the conditions laid down in the preceding section is how to use a high-resolution spectroscope as an efficient monochromator. Previous work in this field suggests two different lines of development. The most common way of using a spectroscope in conjunction

with an interferometer is to focus the ring-pattern onto the slit, and to observe, in the plane of the spectrum, the laterally separated diametral sections of the rings formed by the different radiations in the spectrum. This procedure, too well known from its application to emission spectra to need discussion, forms the basis of the method of parabolic channels suggested by Fabry and Perot (**11a**) and used in many studies of solar wave-lengths (**5, 2, 1, 10, 23**), and of the modified form introduced by Shane (**22**). In these methods the monochromatizing action is deferred until after the interferometric analysis.

In the method first proposed by Fabry and Perot (**11a**), and since used with modifications by Thiessen (**23**), sunlight illuminates the spectroscope slit and forms the ordinary spectrum. A narrow second slit in the plane of the spectrum and parallel to the first slit passes on light with a very limited spectral distribution. This light is then analysed by an etalon followed by a camera, as if the second slit were an independent source. In this case the monochromatizing action precedes the analysis by the interferometer.

That the order of monochromatization and analysis is not necessarily a matter of indifference may be seen from the following analogy. If one were examining the green emission-line of *Hg* with an interferometer, and were obliged to use a green glass filter of spectroscopically good but optically poor quality, it would be natural to place it between the lamp and the etalon, not between the etalon and the eye. For in the first position it would be acting purely as a monochromator, whereas in the second it would form part of an image-forming system, and its optical imperfections would spoil the definition of the pattern.

In arrangements where the spectroscope follows the interferometer it is called upon not only to separate laterally ring-systems of different wave-lengths, but also to image the ring-sections without altering the form, given by (2), of the distribution along the slit. This it can do only if it has a larger angular aperture perpendicular to the direction of spectroscopic dispersion than is usually the case with spectroscopes which have very high resolving powers and if it is free from astigmatism. This aspect is developed in an appendix.

To short-circuit these difficulties, it was thought preferable to develop an arrangement in which the spectroscope precedes the etalon, as in the second slit method, while avoiding the heavy loss of light entailed by this method in its classical form, and maintaining conditions in which the integral equation would be applicable.

It is clear from the discussion which led to equation (8) that the second slit method, with a *very narrow* second slit, is, in principle, an ideal method. In practice, however, it is necessary to open the second slit considerably, thus departing from the ideal conditions, and even so the light-loss is so heavy that photographic work is very difficult. How this loss of light occurs may be seen from Fig. 2 *a*. If the camera alone were placed behind the second slit, its focal plane would contain an out-of-focus image of the illuminated collimator. On introducing the etalon, the fringes will extend over the region of this image (Fig. 2 *a*). Fabry and Perot (**11b**) pointed out that it is convenient to have an optical system to image the second slit on the camera objective and, in conjunction with the latter, image the collimator in the focal plane of the camera. This they achieved by a system of cylindrical lenses. Under these conditions, in the absence of the interferometer, a uniform rectangle of illumination appears on the plate, and when the interferometer is introduced, the ring system appears over this area. The loss of light occurs

because the narrow strip of spectrum passed by the second slit is spread out into a very much larger area on the plate.

It is clearly possible to effect a great improvement in intensity by imaging the second slit on the focal plane of the camera. This may be done by inserting a second collimator between the second slit and the interferometer, and constitutes the first stage in the development of the method actually adopted. The pattern will now extend over only the image of the slit on the plate and, if the slit is infinitely narrow, over only a line. But since the plate is now in the image plane of the spectrum, the second slit may be dispensed with altogether, since the light, previously occulted by the walls of the second slit will form its own fringe pattern on a different part of the plate.

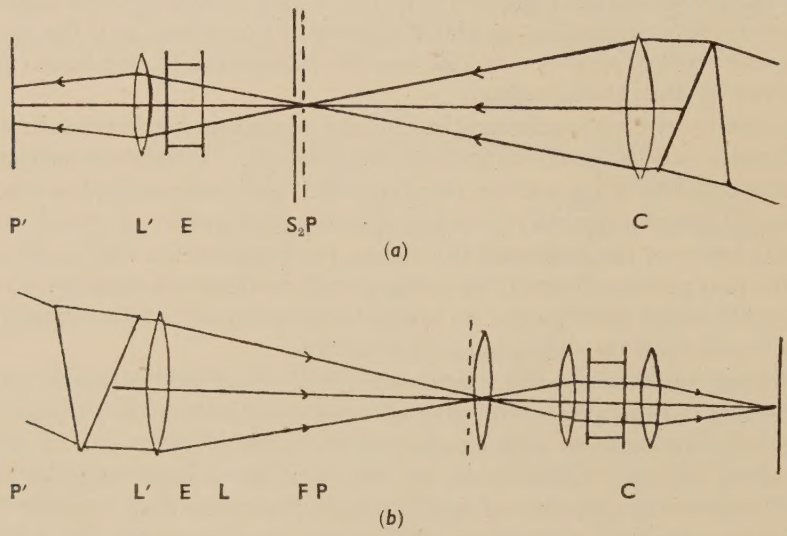

FIG. 2.—*Development of the method of circular channels from the second slit method.*

(*a*) *The second slit method.*
(*b*) *The method of circular channels.*

It will be clear that what is then observed at any line on the plate perpendicular to the spectroscopic dispersion is the analysis of the light that would have passed through a *narrow* second slit placed at the corresponding position of the spectrum. The intensity distribution will be of the form given by (8); but in general the sections observed will be chordal instead of diametral. The arrangement shown in Fig. 2 *b*, which was that finally adopted, differs from that just described in only one detail, namely the presence of the field lens F. The reason for this lens is that in its absence light from parts of the spectrum remote from the etalon-camera axis will be directed somewhat away from the axis, and so will not enter the etalon. This will result in the field of view at the camera being heavily vignetted. The field lens F images the prism diaphragm on the etalon, and gives an unvignetted field over the whole area of its own image in the focal plane of the camera.

Details of apparatus.—The Oxford Solar Spectroscope, a Littrow prismatic instrument with a dispersion of about 1½ A./mm. at λ 5890 A. and a resolving power in this region of about 90,000 formed a highly suitable source of primary monochromatization. The centre of the image of the Sun formed by the solar telescope was focused immediately on the slit. The ordinary plate holder of the spectroscope

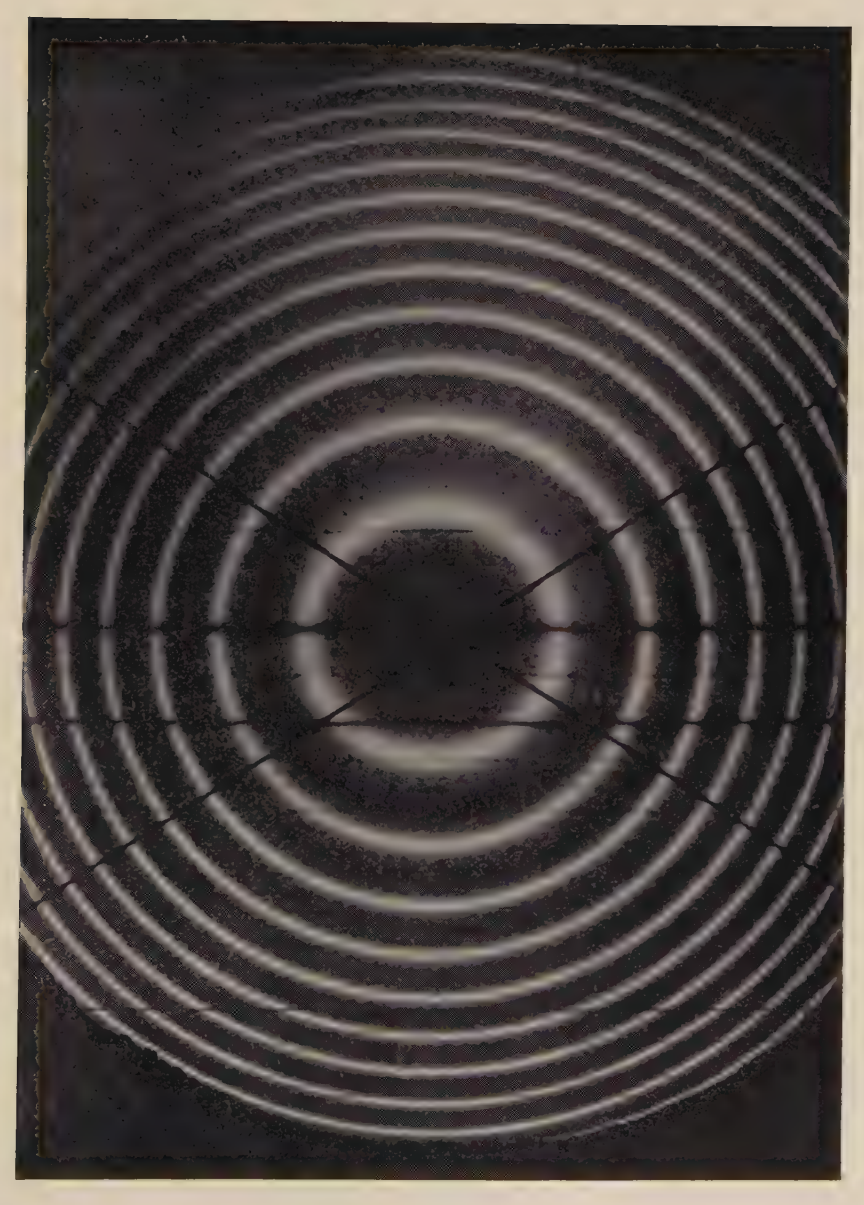

Centre of the heterochromatic pattern with narrow slit. (Positive print.)

P. J. Treanor, High-Resolution Interferometry of the Solar Spectrum.

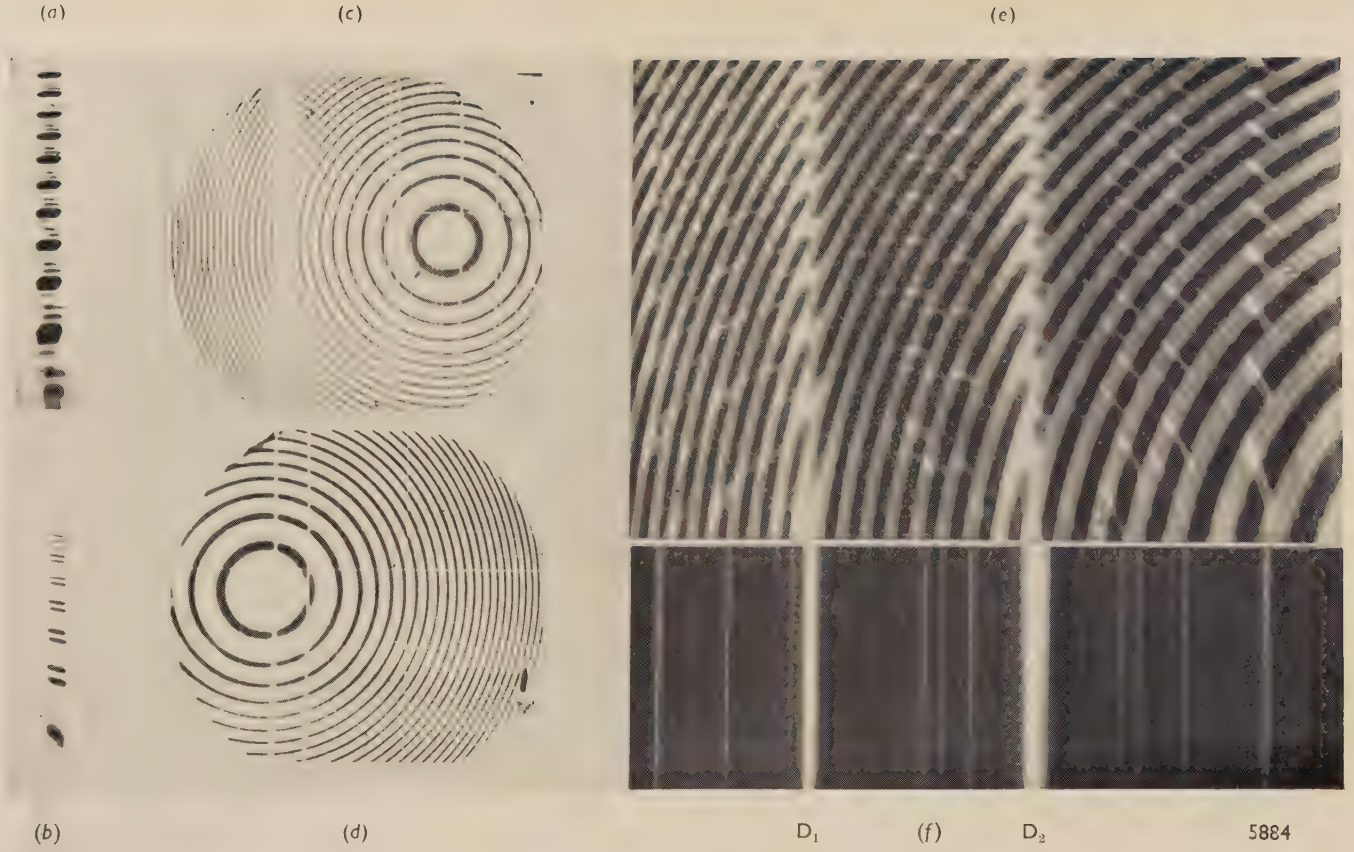

(*a*) *Hg* 4358. (*b*) D_2 *self absorption.* (c) *Heterochromatic fringes with narrow slit (Mg b region).* (d) *D region, showing shift of centre.* (e) *D region with wide slit, near monochromatic centre.* (*f*) *Normal spectrum of D region.* (*All* negative *prints.*)

P. J. Treanor, High-Resolution Interferometry of the Solar Spectrum.

was removed and the field lens F (a scratch-free spectacle lens of 50 cm. focal length) was mounted in the plane of the spectrum. This was followed by a corrected second collimating lens L at its focal distance from F. The focal length of L was initially 50 cm. but a lens of 25 cm. focal length was used in later experiments. L was followed by the etalon and a camera of 50 cm. focal length. The etalon usually had a length of 2·655 mm. With longer spacers it was found that the scatter from adjacent orders increased rapidly, owing mainly, it is believed, to the rather extensive wings of the instrumental pattern of the spectroscope. The plates were silvered over a circular area about 2 cm. in diameter. The reflectivity of the plates finally used was high; an estimate from the ratio of fringe breadth to order interval using a narrow spacer (0·1 mm.) and D lines in emission gave 0·93. The area of etalon used is limited by the aperture ratio of the spectroscope and by the focal length of the second collimator and was only a few millimetres broad. This is an advantage with high silverings, since the effects of surface imperfection and maladjustment of parallelism of the etalon plates are rendered less serious.

Since the instrument is of a Littrow type, it was necessary to erect the collimator-camera system in the immediate neighbourhood of the solar image, so that some thought had to be given to eliminating scattered light. General daylight was eliminated by screening off the whole cubicle containing the optical bench of the spectroscope. The path of direct sunlight to the slit was enclosed in a tube passing through the screen. A single removable cover eliminated residual light during exposures, while enabling the necessary adjustments to be made.

Though the loss of light entailed by the heavy silvering was large, exposure times for the D region did not usually exceed 15 minutes.

The circular channels.—Although the writer was led to adopt the arrangement just described by the foregoing reasoning, the actual appearance of the interference system which it produces had not been anticipated, and is in fact a surprising one. Before the etalon is inserted, one observes in the plane P′ (Fig. 2 *b*) an ordinary spectrum, covering a region of about 25 A. When the etalon is inserted, a system of concentric interference fringes, strongly resembling ordinary Fabry-Perot fringes, appears (Plate 8). They differ however from these, since they are heterochromatic; that is to say, the wave-length of light forming a given fringe changes as one moves along the fringe, the order of interference remaining constant. This can be seen from the fact that the system is crossed by absorption lines. Furthermore, the centre of the pattern does not coincide with the axis of the etalon camera system, but is displaced, in this case by a few degrees, and in order to bring the centre of the heterochromatic system into the centre of the plate, it is necessary to tilt the etalon about a vertical axis by a corresponding amount. Plate 8 shows the actual appearance under these conditions (in this case with only moderately high reflectivity).

The amount of the displacement of the fringe-centre depends upon the linear dispersion of the spectroscope and the centre therefore shifts as the spectral region is altered, owing to the varying prismatic dispersion (Plate 9*c* and *d*). Moreover, as the spectral region examined is gradually altered, by changing the minimum deviation link-work of the prisms, the heterochromatic pattern appears to expand, or contract, after the manner of Newton's rings. A similar effect occurs when the etalon is tilted about a vertical axis.

It was soon realized that, in spite of their very different geometry, these heterochromatic fringes were of a similar character to the parabolic channels of Shane's

experiments, and result from placing side by side the chordal-section analysis of the spectrum at each nominal wave-length, just as the juxtaposition of the analysis of the continuous spectrum into diametral sections results in parabolic channels.

This being the case, it is to be expected that on opening the slit, and so increasing both the range of wave-lengths presented for analysis along any section and the breadth of spectrum over which any particular wave-length is represented, the heterochromatic pattern will broaden, as in the parabolic channel method, and reveal the analysis of the chordal sections of the absorption lines. This analysis is of course present, though in a fragmentary and less visible form, in the narrow fringe system. The absorption-line sections on Plate 8, for example, are in fact chordal sections of this kind, though the centre of the monochromatic system is very remote.

The slit was accordingly opened to 0·2 mm., using an etalon of high reflectivity (Plate 9*e*). It was then perceived that the absorption lines did appear as sharp chordal sections *concentric with the axis of the etalon*. What, however, had not been anticipated was that the relation of the heterochromatic to the monochromatic absorption system would result in the continuous display of an interferometric spectrum over the regions where the two systems intersected more or less orthogonally, a display which makes plainly visible the detail of the solar spectrum over a range many times exceeding that of the etalon. The dip in the centre of each broadened heterochromatic fringe in Plate 9*e* calls for a word of explanation. It is suggested that its cause is the hole in the collimator-illumination, produced by the Cassegrain mirror's shadow, which gives rise to a peculiar broadened slit pattern.

The D region, selected more or less arbitrarily, proved to have been a happy choice for showing up the features of the method of circular channels. In particular it contained the line 5884, an iron line with a water-vapour companion of nearly equal strength, which though unresolved in the Utrecht Atlas and at the limit of resolution of the Oxford spectroscope, is not only clearly resolved in the interference photograph but is shown to consist of two lines of different character, the iron line having a "softer" core. The D_2 line itself, in spite of the small nominal "range" of the etalon, is displayed in its whole extent, together with the wv blend on the side of shorter wave-length. The original plate also shows the redward companion detected by Evershed in limb spectra (**9**).

The theoretical resolving power of the arrangement, as calculated from the rather rough estimate of reflectivity and the order of interference (9000), would be about 360,000. The general appearance of the interference photographs leaves no doubt that the actual resolving power is of a different order of magnitude to that of the spectroscope, which is about 90,000*, and supports the above estimate of the resolving power.

It is not yet certain how much this value may be increased. It is certain that the arrangement used did not go to the very limit of reflectivity or etalon length. However, a few experiments with a 5·3 mm. etalon, although performed in difficult observing conditions in late autumn, suggest that this length is already too long for the Oxford instrument, and no longer satisfies the condition established in Part I, at least in the D region. This was a not altogether unexpected result, in view of the rather heavy wings of the instrumental slit pattern of the spectroscope,

* This value, confirmed from emission-line tests, does not conflict with the fact that the spectroscope barely resolves 5884, on account of the finite width of the components of this line.

and probably means that the limit of resolution obtainable with it would not greatly exceed half a million. It is worth noting however that the use of "apodising" filters (**3**), which reduce the wings of instrumental patterns at the cost of a slight increase in the breadth of the core, may, if the promise of their recent development is fulfilled, offer a relatively simple solution to this difficulty, and may thus contribute very directly to the general improvement of resolving power obtainable by interferometric means.

The geometry of the heterochromatic fringe system.—Consider a perfectly pure spectrum formed in a plane PP (Fig. 3). Erect in this plane a system of rectangular

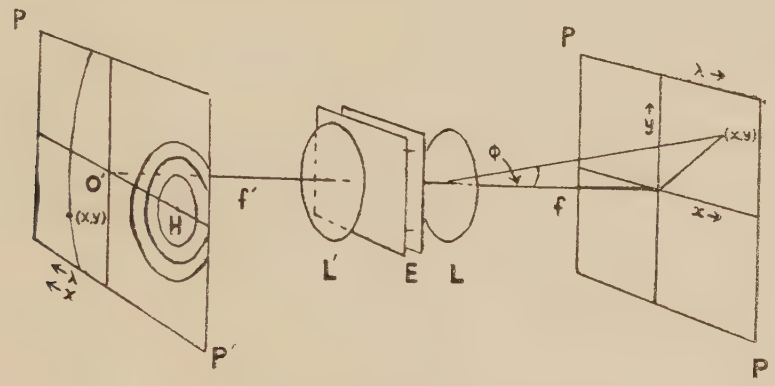

FIG. 3.—*Geometry of the circular channels.*

coordinates, the origin of coordinates O being the projection of the etalon-camera axis on the plane PP. This axis is defined as a perpendicular from the pole of L′ to the mirror surfaces of the interferometer. The etalon is adjusted so that these surfaces are parallel to the plane PP. Let the axis of x be parallel to the spectroscopic dispersion, x increasing with increasing λ, and let the axis of y be perpendicular to the direction of dispersion. Denote the wave-length at $x=0$ by λ_0; assuming then that the dispersion is constant over the wave-length range examined, the wave-length of light from any point x, y will be $\lambda_0+x\,.\,d\lambda/dx$. Light from this point, after collimation by L, a lens of focal length f, will form a beam, making an angle with the axis whose cosine is given by $\cos\phi=f/(f^2+x^2+y^2)^{\frac{1}{2}}$, as may be seen from Fig. 3. The order of constructive interference of the resulting reflected beams in the interferometer will be given, according to (1), by

$$n(x,y)=\frac{2t\cos\phi}{\lambda_0+x\,.\,d\lambda/dx}=\frac{2tf}{(f^2+x^2+y^2)^{\frac{1}{2}}.(\lambda_0+x.\,d\lambda/dx)}. \qquad (11)$$

The locus of curves of constant order n is therefore given by

$$2tf=n(f^2+x^2+y^2)^{\frac{1}{2}}(\lambda_0+x\,d\lambda/dx). \qquad (12)$$

Assuming linearity of dispersion, this expression has involved no approximation up to this point. But since x and y are in our case much smaller than f, then to a good approximation $(f^2+x^2+y^2)^{\frac{1}{2}}\simeq f/(1-[x^2+y^2/2f^2])$, so that (12) becomes

$$x^2+y^2=2f^2-(f^2n\lambda_0/t)-f^2nx(d\lambda/dx)/t. \qquad (13)$$

On completing the square, this becomes

$$x^2+f^2nx(d\lambda/dx)/t+[f^2n(d\lambda/dx)/2t]^2+y^2=2f^2+[f^2n(d\lambda/dx)/2t]^2-f^2n\lambda_0/t. \qquad (14)$$

Hence finally

$$(x+f^2n(d\lambda/dx)/2t)^2+y^2=2f^2+[f^2n(d\lambda/dx)/2t]^2-f^2n\lambda_0/t. \qquad (15)$$

Since $d\lambda/dx$ is a constant, this equation states that the loci of points on the spectrum which produce interference of order n will be circles with centre $(-f^2n(d\lambda/dx)/2t, 0)$. Since n is a large number, successive circles ($dn=1, 2$, etc.) will be very nearly concentric. The displacement of the centre from the origin, which is also the monochromatic fringe centre, will be approximately $-f^2(d\lambda/dx)/\lambda$ and is therefore independent of the spacer-length t. It may be altered by increasing the primary dispersion or by altering the focal length of the second collimator. This last variable provides a convenient means of obtaining the most favourable relation between the fringes.

Equation (15) gives the loci of points in the primary spectrum which give rise to constructive interference of order n. The actual interference pattern occurs in the images of these loci in the plane of the camera of focal length f'. If we construct on the plate axes of coordinates X, Y, parallel to those defined in the plane of the spectrum and with the same origin, the equation in plate coordinates of the circles of constructive interference on the plate will be defined by the equation:

$$(X+ff'n(d\lambda/dx)/2t)^2+Y^2=2f'^2+(ff'n(d\lambda/dx)/2t)^2-(f'^2n\lambda_0/t). \qquad (16)$$

The choice of f' clearly makes a difference only in the scale of the picture; it is chosen to give adequate dispersion in the chordal sections according to (3).

Consider finally what happens when the wave-length range presented is altered by moving the prism system until the wave-length present at the origin is $\lambda_0+\delta\lambda$. The order of interference produced by light at any point on the spectrum changes from $(2t\cos\phi)/\lambda$ to $(2t\cos\phi)/(\lambda+\delta\lambda)$, that is by $2t\,d\lambda/\lambda^2$ orders. The whole system will therefore appear to contract by this amount. The contraction or expansion which results from tilting the etalon has a similar explanation.

The foregoing theory explains the phenomena which would be observed with a perfect spectroscope, narrow slit and unit reflectivity. It will however be clear from the earlier discussion that the distribution of light along any line perpendicular to the direction of spectroscopic dispersion is given by an equation of the same form as (8), where, however, $R(\lambda-\lambda')$ is the distribution in a chordal section. The effect of opening the slit is to widen the function $S(\lambda_1-\lambda')$ of this equation; i.e. to increase the range analysed in each chordal section, an effect which is reflected in the broadening of the heterochromatic fringes. Since the absorption lines have a finite breadth, they cannot be conveniently seen until the range is somewhat increased in this way, but it is not necessary to open the slit until adjacent orders both of the chordal sections and of the heterochromatic fringes simultaneously coalesce, as in the method of parabolic channels; for there is here no corresponding gain in clarity, and the only effect is greatly to increase the scatter from adjacent orders discussed in the first part of this paper. As may be seen from the plate of the D region, even when the orders are well separated, this scatter is very considerable. The clear separation of the heterochromatic fringes is in fact the best practical test of the adequacy of the primary monochromatization provided by the system.

A note on equivalent arrangement.—It may be observed here that an arrangement, sometimes employed in the study of emission spectra, in which the etalon is mounted internally in the parallel beam between prism and camera (**24**) is geometrically equivalent to the one described. There are two practical differences.

The first is that the etalon aperture limits the area of the prism actually in use. Since it is undesirable with high silverings to use more than a few square millimetres of etalon surface, this arrangement would be completely unsuitable in the present context, even if a very large etalon were available. A second difference is that the camera lens of the spectroscope determines the linear dispersion at the plate both of the prismatic and of the interferometric spectrum. It is the possibility of varying these two quantities independently which enables the heterochromatic and monochromatic fringe systems to be brought into their most favourable conjunction for displaying the spectrum. The arrangement used by Dufay and Gauzit (**8**) was an adaptation of this equivalent arrangement to an objective prism system, for the measurement of stellar radial velocities. The heterochromatic fringes then observed, though described by equation (12), are centred so far from the etalon axis that they resemble the well-known parabolic channels.

Part III. Wave-length measurements in the method of circular channels

Since the sharp monochromatic absorption fringe sections in Plate 9*e* fall on the loci of ordinary Fabry-Perot rings of constant wave-length, it is clear that they can, in principle, be used for the determination of wave-length by methods not essentially different from those employed in the study of emission spectra.

In the case of emission spectra, wave-lengths are determined by using the fundamental relation

$$(n+\epsilon)\lambda = 2t, \tag{17}$$

where t is the etalon length, ϵ the fractional order of interference at the centre of the plate. This is given by

$$\epsilon = \frac{D_n^2}{D_n^2 - D_{n+1}^2} - p, \tag{18}$$

where D_n is the diameter of a fringe of order n and p is a small integer. The problem of using the channelled spectra to determine absolute wave-lengths by means of these relations is therefore simply that of devising a method of measuring accurately the radii of the monochromatic fringe sections. The detailed process of reduction then follows the conventional methods (**17**).

A *prima facie* difficulty is created by the fact that the interference spectra of an absorption line in different orders form a chordal, not a diametral, section of the complete Fabry-Perot circles. This is far, however, from being an unmitigated evil, since it means that all the absorption fringes on the plate have a common centre. Any superimposed laboratory standard, not necessarily from the same wave-length region, will consist of circles with the same centre, the locating of which enables all the radii to be measured.

To facilitate the making of the necessary measures, the fixed stage of a Hilger measuring machine was replaced by a rotating stage, on which the plate was mounted, and which bore also a circular scale graduated in degrees and read by two pointers separated by 180°.

The ideal procedure for measuring r the true radius of any fringe by means of this machine would be to bring the axis of rotation of the stage onto the locus of the track of the cross-wire of the travelling microscope, and to bring the centre of the monochromatic (absorption) fringe system into coincidence with the axis of rotation. By rotating the stage any fringe could then be brought onto the track of the cross-wire, which it would cut perpendicularly, and a setting could then be

obtained on it with the same ease as on a line in a spectrum. By rotating the stage through 180°, the same section will again cut the track of the cross-wire and a new setting of the microscope will be obtained. The difference between two such settings would be $2r$ and no angular pointer reading would be required.

In attempting to carry out this ideal plan the following procedure is adopted. First the centre of the monochromatic fringe system is estimated and marked quite crudely, by placing the plate on a system of concentric circles and shifting until all the sections appear to run parallel to the circumference of adjacent circles. In any case it is impossible to bring this marked centre into perfect coincidence with the axis of rotation of the stage. Hence the axis of rotation O′ will not coincide with the true centre O, but will be displaced by an amount ρ (Fig. 4 *a*). The axis

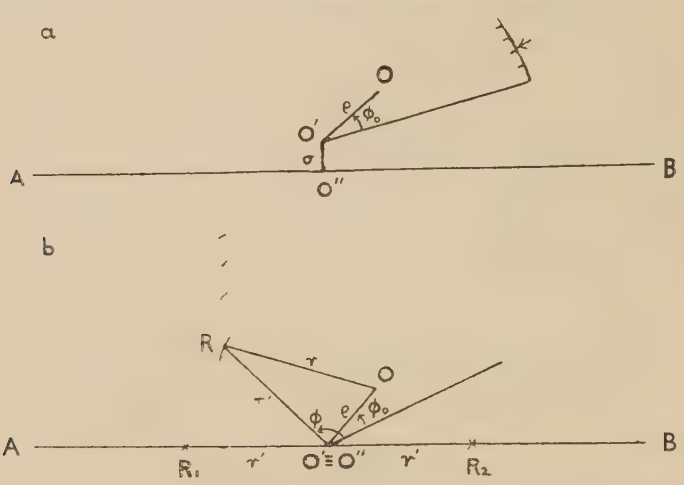

FIG. 4.—*Determination of the centre of a monochromatic chordal fringe section.*

of rotation of the stage will not coincide with the locus AB of the cross-wire's track, but the perpendicular O′O″ to AB will have a length σ. The magnitude of σ, however, depends upon a permanent adjustment of the stage, and may be made less than 0·03 mm. It may be shown that a value of σ of this magnitude has a negligible effect on the measured r values, and in the following treatment O″ will be considered as coinciding with O′. It is then only necessary to take into account the adjustment error ρ.

If we now choose as axis of polar coordinates a line on the plate which passes through the centre of rotation O′ and coincides with AB when the pointer P reads zero, the polar coordinates of O will be ρ, ϕ_0 (Fig. 4 *a*).

If now any fringe R (Fig. 4 *b*) is brought on the track of the cross-wire by rotation to R_1, and a microscope setting obtained; and similarly a second setting is made on the *same* fringe at R_2, the difference of the microscope setting will be $2r'$. To pass from r' to the true radius r, we must use the relation deduced at once from Fig. 4 *b*,

$$r^2 = r'^2 + \rho^2 - 2r'\rho\cos(\phi - \phi_0). \qquad (19)$$

To do this, the coordinates ρ, ϕ_0 of the true centre have to be determined. It must be noted that the angular readings, which do not occur at all in the ideal case, only appear in a correction term which decreases in importance for smaller ρ values. It is therefore only necessary for the measuring machine to determine the linear

coordinate with great accuracy, and the angular coordinate with less accuracy. An important mechanical requisite of the rotating stage is that O′, its centre of rotation, shall be free from drift. (The stage constructed for these measurements made use of a large thrust bearing and showed great stability in this respect.)

The determination of the coordinates of the true centre is easily effected provided that at least two different sections of a laboratory source of monochromatic light are superposed on the plate at the time of exposure. This would be the normal procedure, when a laboratory source is being used as a standard.

However, in the plates of the D region which had to be used to test the accuracy of the method, no such standard had been superposed and, moreover, the fringes had only been photographed on one side of the centre, as may be seen from Plate 9*e*. Consequently the method of determining the plate centre was more involved and time-consuming than would normally be the case, and need not be detailed here. The method consisted essentially in assuming the wave-length of two solar lines, for which interferometric measures were available, and generalizing to the case of chordal fringes the off-centre reduction method of Ritschl (**21**).

The fact that existing wave-length measures had to be used in standardizing the plates and determining the monochromatic centre, as the plates had not been calibrated for this work, means that the results of these measures are of interest only in revealing the internal consistency of the method; that is, the reproducibility of the same fractional order value ϵ from fringe to fringe, and the reproducibility of the same wave-length values from plate to plate.

Table III gives the results of measurements on nine lines in the D region on three spectra. Two of these lines which had been measured interferometrically by Burns (5887·217 and 5898·166) were used as standards and for determining the monochromatic centre. The second column of Table III gives the revised Rowland wave-lengths of the other lines measured, for identification purposes only. The next three columns give the wave-lengths as determined from the three plates. This is followed by the mean value for the three plates. Each wave-length on each plate was determined from epsilon values for four successive fringes. From any such four epsilon values the standard deviation of the mean, on which the adopted wave-lengths depend, may be calculated. It is $\sqrt{\Sigma(\epsilon-\bar{\epsilon})^2/12}$ or, interpreted as an error in wave-length, $(\lambda^2/2t)\sqrt{\Sigma(\epsilon-\bar{\epsilon})^2/12}$. The values of these standard deviations in angstroms are given in columns 7 to 9. The remaining columns give the actual differences from the mean values of the wave-lengths of the same line on the different plates. It will be observed that the mean of the standard deviations, calculated from the epsilons, is considerably less than 0·001 A. per plate, and this indicates the real potentialities of the method. The inter-agreement between plate and plate, though not unsatisfactory, indicates that a certain amount of the potential accuracy has been lost, owing, it is believed, mainly to the adventitious difficulties of reducing the particular plates which had to be used.

Since measurements on complete, rather than off-centre, chordal sections and the use of laboratory standards for locating the monochromatic centre should eliminate these particular difficulties, and indeed improve the deviations of the mean epsilons, it is hoped that the method will ultimately lead to wave-length determinations with standard deviations of less than 0·0005 A. by combining observations from a few plates. The main factor favourable to accuracy in the method is the ease with which accurate settings can be made on the sharp absorption fringes in the manner described. A corresponding accuracy in wave-length

TABLE III

*Wave-length measurements**

Line	Nominal λ (Rowland)	λ Plate (33·2)	λ Plate (32·1)	λ Plate (32·2)	λ mean	σ (33·2)	σ (32·1)	σ (32·2)	Actual residuals $\bar{\lambda}-\lambda$ (33·2)	(32·1)	(32·2)
Fe	5883·816	0·8057	0·8035	0·8011	0·8034	0·0018	0·0014	0·0006	−0·0023	−0·0001	+0·0023
wv	5883·908	0·9018	0·9012	0·8983	0·9004	0·0005	0·0005	0·0002	−0·0014	−0·0008	+0·0021
wv	5885·981 (Standard *)	0·9761	0·9737	0·9737	0·9745	0·0006	0·0013	0·0003	−0·0016	+0·0008	+0·0008
wv	5887·217	(0·2170	0·2170	0·2170	0·2170)	0·0007	0·0011	0·0005	...	...	...
wv	5891·665	0·6553	0·6573	0·6550	0·6559	0·0011	0·0009	0·0009	+0·0006	−0·0014	+0·0009
Ni	5892·885 (Standard *)	0·8682	0·8697	0·8678	0·8686	0·0007	0·0013	0·0009	+0·0004	−0·0011	+0·0008
wv	5898·166	(0·1660	0·1660	0·1660	0·1660)	0·0008	0·0014	0·0012	...	...	...
wv	5899·932	0·9328	0·9298	0·9301	0·9309	0·0011	0·0005	0·0011	−0·0019	+0·0011	+0·0008
wv	5900·048	0·0506	0·0468	0·0502	0·0492	0·0010	0·0004	0·0007	−0·0014	+0·0024	−0·0010

* All values are in angstrom units. The wave-lengths quoted for the two standards are those of Burns.

measures will however only be realized by paying very careful attention to the selection of reliable laboratory standards, and to the elimination of systematic errors due to temperature and pressure changes. In this last respect it may be remarked that the position of the etalon in the circular channel method is a favourable one, for it does not lie in a direct solar beam but in a compartment between collimator and camera which can easily have its temperature controlled.

The high resolution available in the circular channelled spectra provides in addition a safeguard against possible systematic errors due to asymmetry in spectral lines. While the main source of such asymmetry will be due to blending effects, it should not be forgotten that some of the physical processes responsible for solar line shifts themselves provide a mechanism for the production of asymmetry in spectral lines, of the type discussed by van de Hulst (**15**).

The method also opens the way to the measurement, with interferometric precision, of lines too broad to be treated properly by the method of parabolic channels, on account of the overlapping of orders. A few measurements on the D_2 line suggest however that the rapid variation of dispersion near the monochromatic centre produces sufficient asymmetry in the line to make a setting on the line centre, at least of the inner fringes, subject to some systematic error. To eliminate this error source completely, a photometric study of the fringes is required.

Other applications.—A method of obtaining photometric traces of the interference spectra, corresponding to a run of several angstroms along a heterochromatic fringe, is being developed, and it is proposed to use these tracings for profile studies. For this purpose a number of calibrated plates in the region of the *Ca* line 4227 have been secured. There is good reason to believe that the method will yield reliable profiles of fairly narrow lines, and will portray them directly without involving the scanning process incidental in Shane's method of studying line contours. An account of this work will be presented in a subsequent paper.

A related question on which the method may be expected to shed light is the existence of lines weaker than those recorded in Rowland's catalogue.

The observed dip in a photometer trace due to a line much narrower than the instrumental pattern is roughly inversely proportional to the resolving power. A substantial increase in resolving power should therefore reveal such lines, if in fact they exist.

APPENDIX

Conditions of high resolution in the method of parabolic channels.—In arrangements in which the interference fringes are formed on the slit of the spectroscope, the spectroscope has both to separate out the ring systems of different wave-length and to reproduce the ring systems with their true intensity distribution in a direction perpendicular to the spectroscopic dispersion. The first function is essentially one of monochromatization, and has been discussed frequently, for example by Meissner (**17**). The spectroscope can fulfil the second function properly only if the whole of the system of interfering wave-fronts which form the pattern on the slit is actually transmitted through the spectroscope and forms the final image. When the spectroscope has a vertical aperture of a few degrees, this condition is very nearly fulfilled. The conditions of interferometric examination of absorption spectra, however, make it necessary, as has been shown, to use spectroscopes of very high resolution which usually have a very limited vertical aperture.

This may under certain conditions lead to a limitation in the number of reflected beams which are effective in forming the final fringe system, and consequently to a loss of sharpness in the image fringe system.

How this comes about may be understood by reference to Fig. 5.

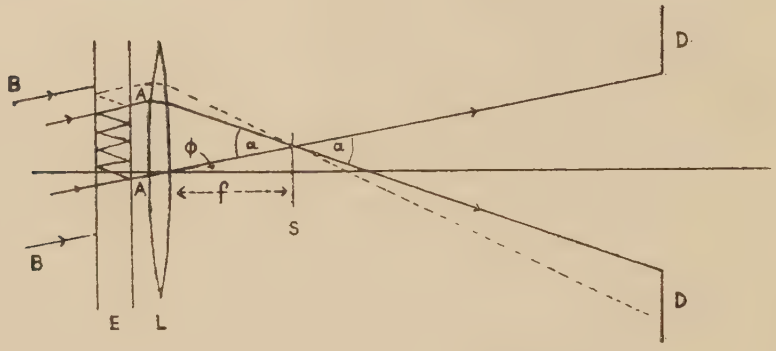

FIG. 5.—*Limitation of beams in the method of parabolic channels.*

Here we assume that the prism has a rectangular diaphragm D subtending at the slit S an angle a in the vertical direction, that is, in the plane containing the slit and the axis of the system. Consider a wide beam of monochromatic rays, proceeding from the illuminated area BB of the etalon at an angle ϕ to the axis, which, after transmission through the etalon, is focused on the slit at a height y by a ring lens of focal length f. Owing to the prism diaphragm, no part of the directly transmitted beam which reaches the ring lens outside the region AA, of length fa, can proceed through the system and be operative in forming the final fringe pattern in the focal plane of the spectroscope. The final pattern is produced mainly by interference between this beam and the *corresponding* reflected beams.

The intensity of the directly transmitted beam will be proportional to fa; while that of the first reflected beam will be proportional to $fa-2t\phi$, owing to its displacement within the etalon of length t. If the first beam has unit amplitude, the amplitude of the nth reflected beam will therefore be reduced by a factor $(1-2nt\phi/fa)^{\frac{1}{2}}$ on this account, and the total number of interfering beams contributing to the resultant t disturbance in the focal plane of the spectroscope will be limited to

$$p=fa/2t\phi. \tag{20}$$

The amplitude of the resultant disturbance at the image point of y in the plane of the spectrum for the wave-length in question will therefore be

$$A_p=de^{i\delta}[1+c_1re^{2i\delta}+\ldots c_{p-1}r^{p-1}e^{2(p-1)i\delta}], \tag{21}$$

where

$$c_n=(1-n/p)^{\frac{1}{2}} \tag{22}$$

and δ is the phase difference between successive reflections.

This expression and its derivation is similar to that used by Geiger (**12**) in discussing the effect of the finite aperture of an etalon, or a stop placed between the etalon and the camera.

Since the higher terms of the series are small in any case, an approximation for $(1-n/p)^{\frac{1}{2}}$ which is good for $n/p \ll 1$ suffices here, and a convenient approximation is

$$c_n = (1-5/8p)^n. \tag{23}$$

Making this substitution, (22) may be written

$$A_p = de^{i\delta}[1 + r'e^{2i\delta} + \ldots + r'^{p-1}e^{2(p-1)i\delta}], \tag{24}$$

where

$$r' = r(1-5/8p). \tag{25}$$

(24) is, however, formally identical with the case of a Lummer plate with p reflections and reflectivity r', and has been thoroughly investigated by Gehrke (**13**) and Hansen (**25**). The distribution of intensity is given by

$$I(\delta) = \frac{d^2(1-r'^p)^2 + 4r'^p \sin^2 p\delta}{(1-r')^2 + 4r' \sin^2 \delta}. \tag{26}$$

The resolving power for this type of intensity distribution has been investigated by Hansen, who gives in graphical form (see Williams (**25**)) the number of effective reflections m for different values of r' and p. By means of equations (20), (25) and this graph, the effective resolving power for any actual case may rapidly be estimated. A numerical example will clarify the procedure. Assuming $f = 25$ cm., $a = 1°$, $\phi = 2°$ and $r = 0{\cdot}925$, then by (20) $p = 25$ and by (25) $r' = 0{\cdot}90$. From Hansen's graph for these values $m = 21$. The value of m for the undistorted pattern, calculated from (7), is about 38. About half the resolving power would therefore be lost with this arrangement. The use of a ring-lens of much longer focal length would reduce this loss.

The above discussion assumes that the spectroscope is free from astigmatism. If this is present, it will, as Fabry and Perot (**11b**) have pointed out, further distort the reflectivity distribution.

Acknowledgments

The writer wishes in conclusion first to thank Professor Plaskett for his generous supervision of the present work and unfailing helpfulness in discussing its difficulties. He also wishes to thank Dr Adam for placing her experience of the method of parabolic channels at his disposal, and Dr Kuhn of the Clarendon Laboratory for the loan of interferometric apparatus. The study has been carried out during the tenure by the writer of the Skynner Studentship in Astronomy at Balliol College, Oxford, since 1946, and the writer here wishes to express his sense of gratitude to his College.

University Observatory,
Oxford:
1949 *June* 20.

References

(1) Adam, M. G., *M.N.*, **108**, 446, 1948.
(2a) Babcock, H. D., *Ap. J.*, **55**, 36, 1922.
(2b) Babcock, H. D., *Ap. J.*, **83**, 111, 1936.
(3) Boutry, G. A., *J. Sc. Inst.*, **24**, 286, 1947.
(4) Buijs, F. W. and Ongering, F. E., *B.A.N.*, **10**, 347, 1948.
(5) Burns, K. and Meggers, W. F., *Pub. Allegheny Obs.*, **6**, 105, 1927.
(6) Cherrington, E., *Lick Obs. Bull.*, **17**, 161, 1935.

(7) Cittert, P. H. v., *Z. f. Phys.*, **65,** 547, 1930.
(8) Dufay, J. and Gauzit, J., *Ann. d'Ast.*, **3,** 13, 1940.
(9) Evershed, J., *M.N.*, **104,** 38, 1944.
(10) Fabry, C. and Buisson, H., *Ap. J.*, **28,** 169, 1908 ; **31,** 97, 1910.
(11a) Fabry, C. and Perot, A., *Ap. J.*, **15,** 73 and 261, 1902.
(11b) Fabry, C. and Perot, A., *C.R.*, **140,** 848, 1905.
(12) Geiger, F. E., *J.O.S.A.*, **39,** 249, 1949.
(13) Gehrke, E., *Interferenzen*, p. 39, 1906.
(14) Houtgast, J., *Variations in the Profiles of Strong Fraunhofer lines*, p. 20, 1942.
(15) Hulst, H. C. v. d., *Ann. d'Ast.*, **8,** 1, 1945.
(16) Kayser, H., *Ap. J.*, **19,** 157, 1904.
(17) Meissner, K. H., *J.O.S.A.*, **31,** 405, 1941 ; **32,** 185, 1942.
(18) Ornstein, L. S. and Minnaert, M., *Z. f. Phys.*, **43,** 404, 1927.
(19) Panofsky, H. A., *Ap. J.*, **97,** 180, 1943.
(20a) Redman, R. O., *M.N.*, **95,** 742, 1936.
(20b) Redman, R. O., *M.N.*, **98,** 311, 1938.
(21) Ritschl, R., *Z. f. Phys.*, **79,** 1, 1932.
(22) Shane, C. D., *Lick Obs. Bull.*, **16,** 76, 1932 ; **19,** 119, 1941.
(23) Thiessen, G., *Ann. d'Ast.*, **9,** 112, 1946.
(24) Tolansky, S., *High Resolution Spectroscopy*, p. 158, 1947.
(25) Williams, W. E., *Applications of Interferometry*, p. 99, 1928.
(26) Unsöld, A., *Physik d. Sternatmosphären*, p. 214, 1938.

THE DIFFERENTIAL CORRECTION OF ORBITS

J. G. Porter

(Received 1949 March 8)

Summary

This paper deals with the differential correction of the orbits of comets and minor planets in terms of certain elements and other constants. The formulae used are related to those of the Tietjen method, but are adapted for calculating machines. In the case of a comet which has been observed at a previous return, it is possible to link the two apparitions, thus obtaining a more reliable value of the correction to the mean motion. The resulting equations contain no more than three unknowns and afford a simple solution to the problem. An alternative to the usual least-squares solution is suggested.

There is an increasing need at the present time, with the rapid increase in the number of periodic comets which are discovered, for a method of improving orbits with a minimum of labour and by comparatively unskilled computers. The standard method is that of Schönfeld and is described in detail in Bauschinger's *Bahnbestimmung der Himmelskörper*. This method was intended for logarithmic working and, like many of the more modern methods which have been evolved, it entails the solution of normal equations with six unknowns. The labour involved in such a task is of doubtful value, for the essential requirement is a method of correcting an orbit so that a perturbation scheme may be started, capable of giving predictions of sufficient accuracy to facilitate detection of the body at subsequent returns. That the problem may be simplified, by a suitable choice of axes, was shown by Tietjen, and the method that follows is, in effect, an adaptation of Tietjen's method to calculating machines. The formulae that are given may be derived with much labour from those given by Bauschinger, but it has been thought better to derive the entire method *ab initio*, using direction cosines throughout, and thus avoiding the intricate system of spherical triangles as given by Bauschinger.

The equatorial constants.—If the heliocentric position of the comet (or planet) be referred to three axes, of which the first (P) is directed to the point of perihelion, the second (Q) to a point on the orbit where $v = +90°$ and the third (R) to the pole of the orbit, then the position of the comet is given by the coordinates $r\cos v$, $r\sin v$, 0. It is usual, however, to employ equatorial coordinates, which refer to three axes, X, Y, Z, of which the first is directed to the vernal equinox, the second to a point on the equator in R.A. 6 hours and the third to the north celestial pole. The coordinates of the comet in this equatorial system may be obtained by projection, the value of the X-coordinate being simply the sum of the projections of the original coordinates on the X-axis. Let P_x, P_y, P_z be the direction cosines of the point P with respect to the axes X, Y, Z, and let Q_x, Q_y, Q_z and

R_x, R_y, R_z similarly refer to the points Q and R respectively. Then the heliocentric equatorial coordinates of the comet are given by

$$\left.\begin{aligned} x &= r P_x \cos v + r Q_x \sin v \\ y &= r P_y \cos v + r Q_y \sin v \\ z &= r P_z \cos v + r Q_z \sin v \end{aligned}\right\} \quad (1)$$

If in these equations we make the substitutions

$$\left.\begin{aligned} r \cos v &= a(\cos E - e) \\ r \sin v &= a \cos \phi \sin E \end{aligned}\right\} \quad (2)$$

we derive the equations which are usually employed for the computation of an ephemeris:—

$$\left.\begin{aligned} x &= a P_x(\cos E - e) + b Q_x \sin E \\ y &= a P_y(\cos E - e) + b Q_y \sin E \\ z &= a P_z(\cos E - e) + b Q_z \sin E \end{aligned}\right\} \quad (3)$$

It will be seen that the R-coordinates do not appear in these equations, and for this reason they have been greatly neglected in cometary work. Their importance has been shown by a number of workers, particularly Smiley *, and it is the use of these R-coordinates which enables the present problem to be simplified. If the ordinary ecliptic elements of the comet are given, then the values of P and Q may be calculated on the machine in the normal manner, preferably by the simple device given by Merton †, and those for R follow at once from

$$\left.\begin{aligned} R_x &= \sin i \sin \Omega \\ R_y &= -\sin i \cos \Omega \cos \epsilon - \cos i \sin \epsilon \\ R_z &= -\sin i \cos \Omega \sin \epsilon + \cos i \cos \epsilon \end{aligned}\right\} \quad (4)$$

If, on the other hand, the equatorial constants are given (i. e. the values of P and Q) then the values of R are obtained from

$$\left.\begin{aligned} R_x &= P_y Q_z - P_z Q_y \\ R_y &= P_z Q_x - P_x Q_z \\ R_z &= P_x Q_y - P_y Q_x \end{aligned}\right\} \quad (5)$$

which are easily computed on a machine in cyclic order, with only three settings of the levers.

The differential corrections.—In the Schönfeld method, the six elements which are chosen to define the comet's orbit are the mean anomaly at epoch, M_0, the mean daily motion, which is here referred to as n, the angle of eccentricity ϕ and the three axes P, Q and R. Experience has shown the great convenience of this choice and, with the substitution of $e = \sin \phi$ instead of using the angle itself (which saves one further reference to the tables), the system is here used unchanged. The six differential corrections are thus dM_0, dn, $de(= \cos \phi \, d\phi)$, and the quantities dp, dq and ds, which are the respective *rotations* of the system about the three axes P, Q and R. Since we know the direction cosines of these three axes, it is at once clear that the differential corrections to the equatorial constants may be obtained by projection, and are given by

$$\left.\begin{aligned} dP_x &= Q_x ds - R_x dq & dQ_x &= R_x dp - P_x ds \\ dP_y &= Q_y ds - R_y dq & dQ_y &= R_y dp - P_y ds \\ dP_z &= Q_z ds - R_z dq & dQ_z &= R_z dp - P_z ds \end{aligned}\right\} \quad (6)$$

* C. H. Smiley, *A.J.*, **40**, No. 934, 1930.
† G. Merton, *M.N.*, **89**, 453, 1929.

These simple expressions eliminate the need for computing the corrections to the ecliptic elements ω, Ω and i, followed by an entire recomputation of the equatorial elements. These angles, in fact, as previous workers have remarked, are quite unnecessary, and the whole of the work can be carried out with the equatorial constants—a logical ideal, since we are using equatorial coordinates. The corrections to the values of R are given, if required, by

$$\left.\begin{aligned} dR_x &= P_x\,dq - Q_x\,dp \\ dR_y &= P_y\,dq - Q_y\,dp \\ dR_z &= P_z\,dq - Q_z\,dp \end{aligned}\right\} \tag{7}$$

and the results may be checked readily by the obvious fact that

$$\Sigma P\,dP = \Sigma Q\,dQ = \Sigma R\,dR = 0 \tag{8}$$

The equations of condition.—By differentiating (1) above, and using (6), we have:

$$\begin{aligned} dx = {} & r(Q_x\cos v - P_x\sin v)\,dv \\ & + r(Q_x\cos v - P_x\sin v)\,ds \\ & + (P_x\cos v + Q_x\sin v)\,dr \\ & + r(R_x\sin v)\,dp \\ & - r(R_x\cos v)\,dq \end{aligned} \tag{9}$$

with similar expressions for dy and dz.

Now an observation (α, δ) at date t may be represented by

$$\left.\begin{aligned} x + X &= \rho(\cos\delta\cos\alpha) \\ y + Y &= \rho(\cos\delta\sin\alpha) \\ z + Z &= \rho\sin\delta \end{aligned}\right\} \tag{10}$$

where ρ is the geocentric distance of the comet and X, Y, Z are the solar coordinates. Again, if M_0 is the mean anomaly at the osculation date t_0, we have:

$$\left.\begin{aligned} M &= M_0 + (t - t_0)n \\ M &= E - e\sin E \\ r &= a(1 - e\cos E) \\ n^2a^3 &= k \\ \tan\frac{v}{2} &= \left(\frac{1+e}{1-e}\right)^{\frac{1}{2}}\tan\frac{E}{2} \end{aligned}\right\} \tag{11}$$

From equations (10) and (11) we obtain, on differentiating, the following results:—

$$\left.\begin{aligned} \rho\cos\delta\,\Delta\alpha &= -\sin\alpha\,dx + \cos\alpha\,dy \\ \rho\,\Delta\delta &= -\sin\delta\cos\alpha\,dx - \sin\delta\sin\alpha\,dy + \cos\delta\,dz \\ dr &= \frac{r\,da}{a} + ae\sin E\,dE - a\cos E\,dE \\ dM_0 &= dM - (t - t_0)\,dn \\ dE &= \frac{a}{r}\,dM_0 + \frac{a}{r}(t - t_0)\,dn + \frac{a}{r}\sin E\,de \\ \frac{dv}{\sin v} &= \frac{dE}{\sin E} + \sec^2\phi\,de \\ da &= -\frac{2a}{3n}\,dn \end{aligned}\right\} \tag{12}$$

In this last equation, n is expressed in radians per day; when n is expressed in degrees, as usual, then

$$da = \frac{-38{\cdot}197\,a}{n}\,dn$$

Combining these equations with (9) gives the equations of condition. For simplicity, the following transformations are made:

$$\left.\begin{aligned} P_1 &= P_y\cos\alpha - P_x\sin\alpha \\ P_2 &= P_z\cos\delta - \sin\delta(P_y\sin\alpha + P_x\cos\alpha) \end{aligned}\right\} \qquad (13)$$

with similar expressions for Q and R.

Then if $K = \dfrac{38{\cdot}197}{n}$,

$$\left.\begin{aligned} G_1 &= \frac{a}{\rho}P_1 & F_1 &= G_1\cos v + G_2\sin v \\ G_2 &= \frac{a}{\rho}Q_1 & F_2 &= G_2\cos v - G_1\sin v \\ G_3 &= \frac{a}{\rho}P_2 & F_3 &= G_3\cos v + G_4\sin v \\ G_4 &= \frac{a}{\rho}Q_2 & F_4 &= G_4\cos v - G_3\sin v \end{aligned}\right\} \qquad (14)$$

we have the equations of condition in the form:

$$\begin{aligned} \cos\delta\,\Delta\alpha = {} & dM_0[F_2\sec\phi + G_2\tan\phi] \\ & + dn\left[(F_2\sec\phi + G_2\tan\phi)(t-t_0) - K\frac{r}{a}F_1\right] \\ & + de[F_2\sec\phi\sin E - G_1] \\ & + ds\left[\frac{r}{a}F_2\right] \\ & + dp\left[\frac{a}{\rho}R_1\cos\phi\sin E\right] \\ & - dq\left[\frac{a}{\rho}R_1(\cos E - e)\right] \end{aligned} \qquad (15)$$

$$\begin{aligned} \Delta\delta = {} & dM_0[F_4\sec\phi + G_4\tan\phi] \\ & + dn\left[(F_4\sec\phi + G_4\tan\phi)(t-t_0) - K\frac{r}{a}F_3\right] \\ & + de[F_4\sec\phi\sin E - G_3] \\ & + ds\left[\frac{r}{a}F_4\right] \\ & + dp\left[\frac{a}{\rho}R_2\cos\phi\sin E\right] \\ & - dq\left[\frac{a}{\rho}R_2(\cos E - e)\right] \end{aligned} \qquad (16)$$

These equations are identical with those of Schönfeld as given by Bauschinger, and may be used in this form for the solution of the problem. The Tietjen

method, however, offers many advantages and this system is derived by Bauschinger from a new set of spherical triangles. It is easy to see that all that is required is a single rotation of the Schönfeld system through an angle which Bauschinger refers to as Ψ.

In the present case, the terms in dp and dq are eliminated from one set of equations by multiplying (15) by R_2 and (16) by R_1 and subtracting; while a second set of equations is formed by multiplying (15) by R_1 and (16) by R_2 and adding. The subsequent simplification of the coefficients calls for a good deal of manipulation, but if we put

$$\left.\begin{aligned} \boldsymbol{P} &= P_x l + P_y m + P_z n \\ \boldsymbol{Q} &= Q_x l + Q_y m + Q_z n \\ \boldsymbol{R} &= R_x l + R_y m + R_z n \end{aligned}\right\} \tag{17}$$

where l, m, n are the direction cosines of the observation,

$$\left.\begin{aligned} G_c &= \frac{a}{\rho}\boldsymbol{P} & F_c &= G_s \sin v + G_c \cos v \\ G_s &= \frac{a}{\rho}\boldsymbol{Q} & F_s &= G_s \cos v - G_c \sin v \end{aligned}\right\} \tag{18}$$

then we note the following relations:

$$\left.\begin{aligned} R_1^2 + R_2^2 &= 1 - \boldsymbol{R}^2 = \boldsymbol{P}^2 + \boldsymbol{Q}^2 \\ R_2 G_2 - R_1 G_4 &= G_c & R_1 G_3 - R_2 G_1 &= G_s \\ R_2 F_2 - R_1 F_4 &= F_c & R_1 F_3 - R_2 F_1 &= F_s \\ R_1 G_1 + R_2 G_3 &= -G_c \boldsymbol{R} & R_1 G_2 + R_2 G_4 &= -G_s \boldsymbol{R} \end{aligned}\right\} \tag{19}$$

and thus obtain the equations of condition in the form:

$$\left.\begin{aligned} A &= B_1\, dM_0 + B_2\, dn + B_3\, de + B_4\, ds \\ D &= C_1\, dM_0 + C_2\, dn + C_3\, de + C_4\, ds + C_5\, dp + C_6\, dq \end{aligned}\right\} \tag{20}$$

in which

$$\left.\begin{aligned} A &= R_2 \cos\delta\, \Delta\alpha - R_1 \Delta\delta \\ D &= R_1 \cos\delta\, \Delta\alpha + R_2 \Delta\delta \end{aligned}\right\} \tag{21}$$

$$B_1 = F_c \sec\phi + G_c \tan\phi \qquad C_1 = -(F_s \sec\phi + G_s \tan\phi)\boldsymbol{R}$$

$$B_2 = B_1(t - t_0) + K\frac{r}{a}F_s \qquad C_2 = +C_1(t - t_0) + K\frac{r}{a}F_c\boldsymbol{R}$$

$$B_3 = F_c \sec\phi \sin E + G_s \qquad C_3 = -(F_s \sec\phi \sin E - G_c)\boldsymbol{R}$$

$$B_4 = F_c\frac{r}{a} \qquad C_4 = -F_s\frac{r}{a}\boldsymbol{R}$$

$$C_5 = +\frac{a}{\rho}\cos\phi \sin E(1 - \boldsymbol{R}^2)$$

$$C_6 = -\frac{a}{\rho}(\cos E - e)(1 - \boldsymbol{R}^2)$$

These equations are not the same as those of the Tietjen method, for they represent the Tietjen equations multiplied by the quantity which Bauschinger calls $\cos\chi$. It may be objected that the omission of this constant factor will have the result of reducing the weight of the observational equations, especially in those cases

where χ is a large angle. This may possibly occur when the comet passes close to the Earth and is seen in the direction of the pole of its orbit, but in such a case the evaluation of dp and dq (which depend on i and Ω) will necessarily be indeterminate, and the low weighting is justified.

In the case of a newly discovered comet, the method may be used exactly as given, and will be found very convenient for machine working. With such an orbit, or with one for which the perturbations from a previous apparition have not been worked with sufficient accuracy, it is advisable not only to obtain a provisional value of the correction dn (which is always the element which causes the most trouble), but also to express both the corrections to other elements and the observational errors in terms of dn, so that a possible range of solutions may be found, or a better solution obtained at a later date.*

If, however, the comet has been seen at a previous apparition, and perturbations have been computed for the ensuing revolution, then the two apparitions may be linked so as to give an improved value of dn. We may adapt Merton's suggestion† to these equations, thus simplifying the system still further.

Let M_{-1} be the mean anomaly at some previous epoch T (for example $M_{-1}=0$ at the previous perihelion passage), so that the mean anomaly at osculation t_0 is given by

$$M_0 = M_{-1} + n(t_0 - T) + (m)$$

where (m) represents the perturbation in mean anomaly. The value so obtained is in error by an amount dM_0 which we have to find, but the small errors in the orbit can scarcely affect (m). If we assume, then, that M_{-1} is correct at epoch T, we have the true state of affairs given by

$$M_0 + dM_0 = M_{-1} + (n + dn)(t_0 - T) + (m)$$

and therefore by subtraction

$$dM_0 = (t_0 - T)dn.$$

Substituting this value in equations (20), (21), we have the formulae in the following form:

$$A = B_2\,dn + B_3\,de + B_4\,ds$$

$$D = C_2\,dn + C_3\,de + C_4\,ds + C_5\,dp + C_6\,dq$$

in which B_2 is now

$$(F_c \sec\phi + G_c \tan\phi)(t - T) + K\frac{r}{a}F_s$$

with a similar expression for C_2. The first group of equations is thus reduced to three unknowns, so that a solution is possible from three observations only. It is advisable in practice to use a minimum of four observations as a check against undetected observational and computational errors.

Summary of method.—From the given orbit we require

M_0 at epoch t_0	$e = \sin\phi$
a	$\cos\phi$
n	$\sec\phi$
$K = \dfrac{38{\cdot}197}{n}$	$\tan\phi$

* See G. Merton, *M.N.*, **87**, 565, 1927, and *Memoirs R.A.S.*, **64**, 58, 1927.
† *Loc. cit.*

and the date of the previous perihelion passage T. The equatorial constants are computed if not already known:—

$$\begin{array}{lll} P_x & Q_x & R_x = P_y Q_z - P_z Q_y \\ P_y & Q_y & R_y = P_z Q_x - P_x Q_z \\ P_z & Q_z & R_z = P_x Q_y - P_y Q_x \end{array}$$

As a check on these values, we have $\Sigma PQ = \Sigma PR = \Sigma QR = 0$. Then for each date t, we compute:

$$\begin{array}{ll} l = \cos\delta\cos\alpha & \boldsymbol{P} = lP_x + mP_y + nP_z \\ m = \cos\delta\sin\alpha & \boldsymbol{Q} = lQ_x + mQ_y + nQ_z \\ n = \sin\delta & \boldsymbol{R} = lR_x + mR_y + nR_z \end{array}$$

$$R_1 = R_y\cos\alpha - R_x\sin\alpha$$

$$R_2 = R_z\cos\delta - \sin\delta(R_y\sin\alpha + R_x\cos\alpha)$$

As a check, $$\boldsymbol{P}^2 + \boldsymbol{Q}^2 = R_1^2 + R_2^2 = 1 - \boldsymbol{R}^2$$

The O–C residuals $\cos\delta\,\Delta\alpha$ and $\Delta\delta$ should be computed in units of the seventh place in circular measure. Thus if $\Delta\alpha^s$ is expressed in seconds of time, and $\Delta\delta''$ in seconds of arc, we have

$$\cos\delta\,\Delta\alpha = 727{\cdot}2\cos\delta\,\Delta\alpha^s$$

$$\Delta\delta = 48{\cdot}48\,\Delta\delta''$$

We also require from these same calculations the values of ρ, $\sin E$ and $\cos E$. From the latter are computed $r/a = 1 - e\cos E$ and also the values of $\sin v$ and $\cos v$. Then

$$\begin{array}{ll} G_c = \dfrac{a}{\rho}\boldsymbol{P} & F_c = G_s\sin v + G_c\cos v \\ G_s = \dfrac{a}{\rho}\boldsymbol{Q} & F_s = G_s\cos v - G_c\sin v \end{array}$$

$$A = R_2\cos\delta\,\Delta\alpha - R_1\,\Delta\delta$$

$$D = R_1\cos\delta\,\Delta\alpha + R_2\,\Delta\delta$$

$$B_2 = (F_c\sec\phi + G_c\tan\phi)(t-T) + K\frac{r}{a}F_s$$

$$B_3 = F_c\sec\phi\sin E + G_s$$

$$B_4 = F_c\frac{r}{a}$$

$$C_2 = -\boldsymbol{R}(F_s\sec\phi + G_s\tan\phi)(t-T) + K\frac{r}{a}F_c\boldsymbol{R}$$

$$C_3 = -\boldsymbol{R}(F_s\sec\phi\sin E - G_c)$$

$$C_4 = -\boldsymbol{R}\frac{r}{a}F_s$$

$$C_5 = +\frac{a}{\rho}\cos\phi\sin E(1-\boldsymbol{R}^2)$$

$$C_6 = -\frac{a}{\rho}(\cos E - e)(1-\boldsymbol{R}^2)$$

The equations for A are solved first by any suitable method:

$$A = B_2\,dn + B_3\,de + B_4\,ds$$

and the results are substituted in the equations for D:

$$D = C_2\,dn + C_3\,de + C_4\,ds + C_5\,dp + C_6\,dq$$

The resulting equations contain only two unknowns, dp and dq, and may again be solved by least squares, or any other suitable combination of the equations.

The values of dp, dq and ds are then used to correct the equatorial constants:

$$dP = Q\,ds - R\,dq \qquad \text{and} \qquad dQ = R\,dp - P\,ds$$

The correction de is applied directly to the value of e, while dn is converted to angle by

$$dn^\circ = 57{\cdot}2958\,dn$$

We then have $dM^\circ = (t_0 - T)dn^\circ$ as the correction to be applied to M_0, while the correction to a is given by

$$da = -K\,a\,dn$$

In the example which follows, this simple method is used, and a convenient method of setting out the work is illustrated.

Example: Comet Pons-Winnecke, 1945 a.

The four observations to be used were first corrected for parallax:

	1945	R.A. 1945·0 h	m	s	Dec. 1945·0 °	′	″	Obs.
May	17·13935	12	49	44·13	+42	07	26·2	U.S. Naval Obs.
June	5·20942	12	51	50 82	+32	51	47·6	Lowell
June	30·14104	13	22	09·87	+11	23	15·8	Yerkes
July	12·01742	13	47	07·91	− 2	33	22·8	Cordoba

The existing orbit, although unsatisfactory, had been used for a preliminary Encke scheme. Approximate perturbations were thus available and have been included as an illustration of the method, the computed position of the comet being obtained by adding the perturbations to the comet's heliocentric coordinates for the true time, together with the solar coordinates for the observed time.

	True time	Perturbations			O–C $\Delta\alpha^s$	$\Delta\delta''$
May	17·13569	−42	+ 60	−29	+2·62	+103·0
June	5·20619	−63	+113	−48	+1·16	+105·5
June	30·13829	−72	+216	−68	+0·29	− 6·2
July	12·01478	−65	+283	−71	+1·41	−161·4

Epoch (t_0) 1945 March 26·0 U.T.

M_0 342°·92967	n 0°·16007814
e 0·6546999	a 3·3592941
P_x −0·0843156	Q_x +0·9257287
P_y −0·9376126	Q_y +0·0515361
P_z −0·3373034	Q_z −0·3746606

The previous perihelion passage occurred on 1939 June 22·7 = T .

$$t_0 - T = 2103{\cdot}3 \text{ days}$$

The various functions of E and v which were obtained in computing the above positions were rounded off to five figures in the following table, and the whole of the rest of the work carried out with five-figure tables. In the first part of the table (to line 28) the decimal point has been omitted, since there is little likelihood of confusion.

a 3·359294	$\sin\phi$ 0·65470	$\sec\phi$ 1·32295
n 0·160078	$\cos\phi$ 0·75589	$\tan\phi$ 0·86613
K 238·616		

P	Q	R
−08432	+92572	+36867
−93761	+05154	−34384
−33730	−37466	+86363

	Date	May 17	June 5	June 30	July 12
1	$t-T$	2155·4	2174·5	2199·4	2211·3
2	$\sin\alpha$	−21531	−22430	−35088	−45061
3	$\cos\alpha$	−97655	−97452	−93642	−89272
4	$\sin\delta$	+67074	+54264	+19745	−04460
5	$\cos\delta$	+74170	+83997	+98031	+99900
6	R_1	+41516	+41777	+45134	+47308
7	$R_y\sin\alpha+R_x\cos\alpha$	−28599	−28215	−22458	−17418
8	R_2	+83238	+87853	+89097	+85500
9	$\cos\delta\,\Delta\alpha$	+1413	+709	+207	+1024
10	$\Delta\delta$	+4993	+5115	−301	−7825
11	A	−897	−1514	+320	+4577
12	D	+4743	+4790	−175	−6206
13	l	−72431	−81857	−91798	−89183
14	m	−15970	−18841	−34397	−45016
15	n	+67074	+54264	+19745	−04460
16	$\boldsymbol{P}$	−01543	+06264	+33331	+51232
17	$\boldsymbol{Q}$	−93004	−97078	−94150	−83208
18	$\boldsymbol{R}$	+36715	+23164	−04964	−21253
19	$1-\boldsymbol{R}^2$	86521	94634	99754	95483
20	$R_1^2+R_2^2$ Check	1	5	4	3
21	$\boldsymbol{P}^2+\boldsymbol{Q}^2$	1	4	2	3
22	$\sin E$	−40602	−27615	−08466	+01114
23	$\cos E$	+91387	+96111	+99641	+99994
24	$\cos\phi\sin E=r/a\,.\sin v$	−30690	−20874	−06399	+00842
25	$\cos E-e=r/a\,.\cos v$	+25917	+30641	+34171	+34524
26	$1-e\cos E=r/a$	40169	37076	34765	34534
27	$\sin v$	−76402	−56301	−18406	+02438
28	$\cos v$	+64520	+82644	+98291	+99971
29	ρ	0·63504	0·56057	0·47575	0·45688
30	a/ρ	5·2899	5·9926	7·0610	7·3527
31	G_c	−0·0816	+0·3754	+2·3535	+3·7669
32	G_s	−4·9198	−5·8175	−6·6480	−6·1180
33	F_c	+3·7062	+3·5856	+3·5369	+3·6167
34	F_s	−3·2366	−4·5965	−6·1012	−6·2081
35	$26\times33=B_4$	+1·4887	+1·3294	+1·2296	+1·2490
36	26×34	−1·3001	−1·7042	−2·1211	−2·1439

	Date		May 17	June 5	June 30	July 12
37	$\sec\phi\times 33$		+4·9031	+4·7436	+4·6791	+4·7847
38	$\sec\phi\times 34$		−4·2819	−6·0809	−8·0716	−8·2130
39	$37\sin E+32$	$=B_3$	−6·9106	−7·1274	−7·0441	−6·0647
40	$38\sin E-31$		+1·8201	+1·3038	−1·6702	−3·8584
41	$35K$		+355	+317	+293	+298
42	$36K$		−310	−407	−506	−512
43	$37+31\tan\phi$		+4·8324	+5·0687	+6·7175	+8·0473
44	$38+32\tan\phi$		−8·5431	−11·120	−13·830	−13·512
45	1×43		+10416	+11022	+14774	+17795
46	1×44		−18414	−24180	−30418	−29879
47	$45+42$	$=B_2$	+10106	+10615	+14268	+17283
48	$46-41$		−18769	−24497	−30711	−30177
49	$-\boldsymbol{R}\times 36$	$=C_4$	+0·47733	+0·39476	−0·10529	−0·45564
50	$-\boldsymbol{R}\times 40$	$=C_3$	−0·66825	−0·30201	−0·08291	−0·82003
51	$-\boldsymbol{R}\times 48$	$=C_2$	+6891·0	+5674·5	−1524·5	−6413·5
52	24×30		−1·6235	−1·2509	−0·4518	+0·06191
53	25×30		+1·3710	+1·8362	+2·4128	+2·5384
54	19×52	$=C_5$	−1·4047	−1·1838	−0·4507	+0·0591
55	-19×53	$=C_6$	−1·1862	−1·7377	−2·4068	−2·4237

The checks which are given by lines 19–21 ensure that the values of $\boldsymbol{P}$, $\boldsymbol{Q}$ and $\boldsymbol{R}$ have the correct magnitude, but they do not check the signs of these quantities. The following additional formulae will therefore be found useful in checking the signs and magnitude of the values of F and G and of some of the coefficients as well:—

$$\left.\begin{aligned} \frac{r}{a}(G_s F_c - G_c F_s) &= \frac{a}{\rho} C_5 \\ \frac{r}{a}(G_s F_s + G_c F_c) &= -\frac{a}{\rho} C_6 \\ B_3 C_4 - B_4 C_3 &= \boldsymbol{R}\frac{a}{\rho} C_6 \end{aligned}\right\} \qquad (22)$$

The equations may be solved by any suitable method, but it would hardly be justifiable to use a least-squares solution, since we have no right to assume a normal distribution of the residual errors. Any simple combination of the equations which will lead to the solution of simultaneous equations would answer the purpose, but unfortunately such methods may lead to undue weight being given to one equation. The following method has the advantage of offering simple checks, and has the effect of dividing the observations into two groups, in each of which the sum of the residuals is zero.

To solve the equations in A, put

$$x = 10000\ dn \qquad y = 10\ de \qquad z = ds \qquad \text{Unit} = 1000$$

Then

$$\left.\begin{aligned} +1{\cdot}0106x - 0{\cdot}69106y + 1{\cdot}4887z &= -0{\cdot}897 \\ +1{\cdot}0615 \ -0{\cdot}71274 \ +1{\cdot}3294 \ &= -1{\cdot}514 \\ +1{\cdot}4268 \ -0{\cdot}70441 \ +1{\cdot}2296 \ &= +0{\cdot}320 \\ +1{\cdot}7283 \ -0{\cdot}60647 \ +1{\cdot}2490 \ &= +4{\cdot}577 \end{aligned}\right\} \qquad (23)$$

Change the signs (if necessary) so as to make all the coefficients of x positive, and sum the equations:

$$+5{\cdot}2272x - 2{\cdot}7147y + 5{\cdot}2968z = +2{\cdot}486 \qquad (24)$$

This equation is now used to eliminate x from the original equations:

$$\left.\begin{aligned} -0{\cdot}16621y + 0{\cdot}4647z &= -1{\cdot}378 \\ -0{\cdot}16146 + 0{\cdot}2538 &= -2{\cdot}019 \\ +0{\cdot}03658 - 0{\cdot}2162 &= -0{\cdot}359 \\ +0{\cdot}29111 - 0{\cdot}5023 &= +3{\cdot}755 \end{aligned}\right\} \qquad (25)$$

These equations are readily checked, since the sum of each set of coefficients must be zero.

Change the signs as before and add:

$$+0{\cdot}65536y - 1{\cdot}4370z = +6{\cdot}793 \qquad (26)$$

Eliminate y from the previous equations:

$$\begin{aligned} +0{\cdot}1003z &= +0{\cdot}345 \\ -0{\cdot}1002 &= -0{\cdot}345 \\ -0{\cdot}1360 &= -0{\cdot}738 \\ +0{\cdot}1360 &= +0{\cdot}738 \end{aligned}$$

Check as before, change the signs and add, and solve for z. The values of x and y are then obtained from (24) and (26).

$$x = +6{\cdot}433 \quad y = +20{\cdot}42 \quad z = +4{\cdot}584$$

These values are then substituted in the D equations, giving four equations with two unknowns. These are treated in the same way, and changing back to the original units, we have:

$dn = +0{\cdot}6433$	$dP_x = +4501$	$dQ_x = +\ 722$
$de = +2042$	$dP_y = -\ \ 4$	$dQ_y = +3985$
$ds = +4584$	$dP_z = -1115$	$dQ_z = +2333$
$dp = +\ 911$		
$dq = -\ 698$		

These corrections lead to the figures for the improved orbit:—

Epoch 1945 March 26·0 U.T. $M_0 = 342{\cdot}93742$

$e = 0{\cdot}6549041$ $n = 0{\cdot}16008183$

$a = 3{\cdot}3592425$

P	Q
$-0{\cdot}0838655$	$+0{\cdot}9258009$
$-0{\cdot}9376130$	$+0{\cdot}0519346$
$-0{\cdot}3374149$	$-0{\cdot}3744273$

$$x = -0{\cdot}2817246\,(\cos E - e) + 2{\cdot}3502566 \sin E$$

$$y = -3{\cdot}1496694 \qquad +0{\cdot}1318422$$

$$z = -1{\cdot}1334585 \qquad -0{\cdot}9505286$$

The O–C residuals may be computed from the observational equations, but this is, as a rule, an unnecessary labour. For the sake of comparison, the actual figures so obtained are here compared with those derived from the positions computed from the orbit above.

	O–C from equations		O–C from orbit	
	″	″	″	″
May 17	−2·8	−0·1	−2·6	−0·2
June 5	+0·5	−4·6	+0·6	−4·7
June 30	−0·4	+4·5	−0·1	+4·4
July 12	+1·5	−2·3	+1·6	−2·6

The development of this method has resulted in a number of fruitful discussions with Dr G. Merton, whose helpful interest is gratefully acknowledged.

Gillingham, Kent :
1949 *March* 6.

A MODIFICATION OF THE PERTURBATIONS-OF-ELEMENTS METHOD

G. Merton

(Communicated by the Director of the University Observatory, Oxford)

(Received 1949 May 10)

Summary

The division of the orbit of a comet or minor planet, into an integral number of parts, permits the construction of special tables which facilitate the calculation of the special perturbations, by the planets, in terms of the variations of the usual ecliptic elements. Such tables have been published, but the approximate methods usually employed with them are not, it is argued, accurate enough to be generally suitable for the predictions of the returns of periodic comets. A rigorous method, treating the time element as perturbed and the mean anomaly as the independent variable, is here derived, very simply, for use with these tables or with the new ones proposed. And the integration of the perturbations of the mean anomaly, involving a double integration, is replaced by a single integration of the perturbed time interval.

Introduction.—The classical method of computing special perturbations of the orbit of a comet (or planet), in terms of the variations of the usual ecliptic elements, is elegant and rigorous, but the computation is rendered relatively cumbersome by the need at each step to solve Kepler's equation for some odd value of the mean anomaly, and to obtain a considerable number of other quantities which are functions of the true anomaly and the eccentricity. It has however been found that in some cases the work can be lightened if the orbit is divided into an integral number of parts corresponding to equal intervals of mean anomaly, or of eccentric anomaly. A division of the orbit in this way enables the quantities referred to, v the true anomaly, r/a the radius vector in units of the semi-major axis, and most of the coefficients in the equations for the variations of the elements, to be tabulated in advance for the steps of the chosen interval of the independent variable (M or E), so that they may be used for more than one revolution (or more than one comet).

Theodore R. von Oppolzer (**12**) first devised such a method, making the division in equal intervals of 20° of eccentric anomaly, to obtain approximate values for the perturbations of the periodic comet Pons-Winnecke between 1819 and 1869; and he used one set of tabulated quantities to cover all nine revolutions. The writer (**9a**) used the same method in the investigation of the orbit of the periodic comet Grigg-Skjellerup. As a result of this experience he concluded that generally a mean anomaly division of the orbit would be preferable, and pointed out that this would enable special tables to be constructed for general use, since many of the quantities required are functions of the true anomaly and eccentricity only. A. C. D. Crommelin (**4**) subsequently published such tables, covering a range of values of eccentricity (0·37 to 0·84) sufficient for nearly all periodic comets.* The method given for the use of these tables, however, remained an approximate one, since it assumed, in each case, that one set of elements could

* These tables are now out of print.

be used over a long interval to represent the actual circumstances in the perturbed orbit.

The purpose of the present paper is: (*a*) to show why the approximate method, when it is employed for prediction purposes for comets, is not, in general, accurate enough, and (*b*) by a very simple modification, to derive a "rigorous" form of the mean anomaly method which will enable existing tables, or the new ones proposed, to be used for work of the highest accuracy over any period which has to be covered. The word "rigorous" is used in this paper in the sense that any desired order of accuracy can be attained in the calculations.

Failure of the approximate method in predictions.—When Crommelin's tables were published, the method was frequently used, to take account of the perturbations of Jupiter and Saturn, in calculating the predictions for the returns of periodic comets. The results have sometimes been far from satisfactory, and although faulty technique has accounted for some failures, it has become clear that the method, as it has been used, has not been exact enough, especially when the perturbations have been heavy. One needs an accuracy that will not only provide for the recovery of a comet at its next return but will give a reliable basis for future predictions, taking account too of the possibility that the comet may be unfavourably placed for observation at the next return or two.

The main difficulty lies in the value of the mean motion, since errors here quickly accumulate in the mean anomaly and thus alter the predicted perihelion date. It must be emphasized that the mean motion cannot be determined accurately from one apparition, nor corrected at the next without taking both of them into account as well as the intervening perturbations. If then the calculated perturbations are in error, the resultant value of the mean motion will be inaccurate and misleading, and could even lead to the subsequent loss of the comet. Unfortunately too, a fairly successful prediction is not a complete guarantee of the accuracy of the value of the mean motion.

If the accuracy of the original elements is to be maintained within the required limits the working elements must always be kept near their true values. The approximate method, in using one set of elements which are really only appropriate at the start, to cover a whole revolution (usually), allows the assumed path to deviate increasingly from the true and, unless the planetary attractions remain small, errors will grow and accumulate. It has happened that the original accuracy of the elements, especially that of the mean motion, has been so far destroyed that the elements became useless. And even if the assumed elements are "rectified" at intervals, it does not always meet the case, since the elements so used are not in fact the average elements over the interval in which they are employed.

Derivation of the modified method.—The weaknesses of the approximate method may be overcome, without losing the advantage of having special tables, by modifying the formulae and procedure to make them rigorous. To achieve this, the standard equations must be altered to make *time* one of the *perturbed* elements, and the mean anomaly rigorously the independent variable—it is not so in Crommelin's method.

The conventional method for computing the perturbed orbits of planets and comets, in terms of the variations of their elements, using time as the independent variable, has been fully set out in the standard works by Julius Bauschinger (**3a**) and others (**1**), and has been used extensively by computers of orbits for over

half a century. The method is rigorous and the results can be made correct to any order of accuracy by employing time intervals of integration sufficiently small, and sufficient figures in the calculation.

To arrange the formulae, for use with the mean anomaly as the independent variable, is found to require only simple changes; substantially it amounts to multiplying the differential equations for the variations of the elements by dt/dM and to integrating with respect to M instead of to t. Starting from the fundamental equation for the mean anomaly

$$M = M_{00} + n(t - t_0), \tag{1}$$

we obtain by a full differentiation with respect to M

$$1 = \frac{dM_{00}}{dM} + (t - t_0)\frac{dn}{dM} + n\frac{dt}{dM}.$$

Now put

$$\frac{dM_0}{dM} = \frac{dM_{00}}{dM} + (t - t_0)\frac{dn}{dM}, \tag{2}$$

where dM_0 has the same meaning as in the original method (**3b**). Then

$$\frac{dt}{dM} = \frac{1}{n}\left(1 - \frac{dM_0}{dM}\right) \tag{3}$$

and from this by integration

$$t = t_0 + \int_{M_{00}}^{M} \frac{dt}{dM} \cdot dM. \tag{4}$$

Thus instead of the mean anomaly we shall use time as the perturbed element, and consequently the time intervals between the steps in the integration will not be exactly equal. This integral (4) then gives the date t appropriate to the mean anomaly argument at any step in the integration table, so that the planetary coordinates may be obtained at that step. It will be noticed that the double integral of the variation of the mean motion, in the classical method, is thus replaced by the single integral of the variation of the time element.

In the standard formulae given by Bauschinger and others, the variations of the elements are expressed, as has been said, in terms of time as the independent variable ($w \cdot di/dt$, $w \cdot d\Omega/dt$, etc.); and the expressions for the forces S, T and W are given, for each planet, by

$$\left.\begin{aligned} \boldsymbol{S}_1 &= (k''wm_1)\sqrt{p}\left(\xi_1 K_1 - \frac{r}{\rho_1^3}\right), \\ \boldsymbol{T}_1 &= (k''wm_1)\sqrt{p}\eta_1 K_1, \\ \boldsymbol{W}_1 &= (k''wm_1)\sqrt{p}\zeta_1 K_1, \end{aligned}\right\} \tag{5}$$

where

$$K_1 = \frac{1}{\rho_1^3} - \frac{1}{r_1^3},$$

and ξ_1, η_1, ζ_1, are the coordinates of the perturbing planet relative to the moving axes of the comet, ξ from the Sun along the comet's radius vector, η at right angles and forward in the orbit, ζ at right angles and towards the pole of the orbit; and the interval w is in days, m is the mass of the perturbing planet (m_1 for Jupiter), $p = a\cos^2\phi$, and the Gaussian constant of gravitation k'' gives the perturbations in seconds of arc.

These equations are now to be multiplied by dt/dM, and the integration interval w units of time changed to units of mean anomaly. As dt/dM will be a common

factor, it is most conveniently included in the expressions for the forces S, T and W. To simplify the computation, and the tabulation of certain quantities to which we shall refer later, we put

$$\left.\begin{aligned} S_1 &= \boldsymbol{S}_1 \sec\phi \frac{dt}{dM}, \\ T_1 &= \boldsymbol{T}_1 \sec\phi \frac{dt}{dM}, \\ W_1 &= \boldsymbol{W}_1 \sec\phi \frac{dt}{dM}, \end{aligned}\right\} \tag{6}$$

and subsequently will multiply by $\cos\phi$ all the coefficients in the usual expressions for the variations of the elements. It is also convenient to alter the units so as to express the perturbations in units of the fourth decimal of a degree (0″·36), as this facilitates the integrations and the extraction of the osculating elements from them, as will be shown later. Thus we arrive at the expressions we need:

$$\left.\begin{aligned} S_1 &= (10^4 k^\circ m_1)\sqrt{a}\,.\,w \frac{dt}{dM}\left(\xi_1 K_1 - \frac{r}{\rho_1^3}\right), \\ T_1 &= (10^4 k^\circ m_1)\sqrt{a}\,.\,w \frac{dt}{dM}\eta_1 K_1, \\ W_1 &= (10^4 k^\circ m_1)\sqrt{a}\,.\,w \frac{dt}{dM}\zeta_1 K_1, \end{aligned}\right\} \tag{7}$$

with similar expressions for each of the other perturbing planets.

It will be seen that in evaluating these we require equation (3) for dt/dM; and in this equation we will now include the interval of integration w, thus

$$w\frac{dt}{dM} = \frac{1}{n}\left(w - 10^{-4} w \frac{dM_0}{dM}\right), \tag{8}$$

where n and w are in degrees and the result is in days. But (8) assumes a knowledge of the value of $w\,.\,dM_0/dM$ before it has in fact been calculated. In practice, however, this is usually a very small quantity at the start of an integration and can then, with sufficient accuracy, be taken as zero. We start therefore with $w\,.\,dt/dM = w/n$. If it should happen that $w\,.\,dM_0/dM$ when calculated is found to be appreciable, then a further approximation may have to be made to include it and to revise the evaluation of (7), but this should cause no difficulty as its value is not required to full accuracy for this purpose. At other stages of the work the value of $w\,.\,dt/dM$ itself can be extrapolated accurately enough for (7), at each step, from the preceding values in the integration table.

Summary of formulae.—For the convenience of computers the remaining equations, relative to this modification of the classical method, will not be given separately but will be included in a complete summary of the working formulae. The arrangement is that which has been found convenient for computation either with a machine or with logarithms (assuming the use of addition and subtraction logarithms).

The start is made with the osculating elements given, calculating say three steps, and commencing the integration tables in the usual way. Then, as the initial osculating value of the mean anomaly will usually not correspond to an exact argument (or mid-point) in the integration, some adjustment of the first summation columns may have to be made so as to represent the osculating

elements exactly at their epoch. After that, new elements i, Ω, ω, ϕ, n, and the date t, and the quantity $w.dt/dM$, are obtained at the commencement of each step, by extrapolation from the integration tables, with sufficient accuracy for the computation of that step.

Unless v and r/a can be obtained from special tables, they will be computed as follows:

$$\left.\begin{aligned} a &= \left(\frac{k^\circ}{n}\right)^{\frac{2}{3}}, \qquad e^\circ = 57{\cdot}29578 \sin\phi, \\ E - e^\circ \sin E &= M \quad \text{(Kepler's equation)}, \\ \frac{r}{a}\sin v &= \cos\phi \sin E, \\ \frac{r}{a}\cos v &= \cos E - e, \\ u &= v + \omega, \end{aligned}\right\} \tag{9}$$

where M is the tabular argument of the integration table at the step to be computed.

The coordinates for Jupiter for the date t, namely l_1, b_1, r_1, and the quantity $1/r_1^3$, are obtained by interpolation from the appropriate volume of Planetary Coordinates (*Pub. N.A. Office*, e. g. **10**); and similarly those for Saturn (l_2, b_2, etc.) and for any other planets it may be desired to include. Then in each case the coordinates of the planet relative to the plane of the comet's orbit are given by

$$\left.\begin{aligned} X_1 &= r_1 \cos b_1 \cos(l_1 - \Omega), \\ Y_1 &= r_1 \cos b_1 \sin(l_1 - \Omega)\cos i + r_1 \sin b_1 \sin i, \\ Z_1 &= -r_1 \cos b_1 \sin(l_1 - \Omega)\sin i + r_1 \sin b_1 \cos i, \end{aligned}\right\} \tag{10}$$

for which the computation of Y_1 and Z_1 may be conveniently arranged in the form

$$\left.\begin{aligned} (Y_1) &= r_1 \cos b_1 \sin(l_1 - \Omega), \\ (Z_1) &= r_1 \sin b_1, \end{aligned}\right\} \tag{10a}$$

and

$$\left.\begin{aligned} Y_1 &= (Y_1)\cos i + (Z_1)\sin i, \\ Z_1 &= -(Y_1)\sin i + (Z_1)\cos i. \end{aligned}\right\} \tag{10b}$$

Next, the coordinates relative to the moving heliocentric axes of the comet are

$$\left.\begin{aligned} \xi_1 &= X_1 \cos u + Y_1 \sin u, \\ \eta_1 &= -X_1 \sin u + Y_1 \cos u, \\ \zeta_1 &= Z_1. \end{aligned}\right\} \tag{11}$$

Then

$$\rho_1^2 = (\xi_1 - r)^2 + \eta_1^2 + \zeta_1^2, \tag{12}$$

and, as a check which should always be computed,

$$\rho_1^2 = r^2 + r_1^2 - 2r\zeta_1. \tag{13}$$

This check may not be perfect, when the distance ρ_1 is small, since, under such conditions, (13) gives ρ_1^2 as the difference of large nearly equal quantities. If any computational error seems indicated, there are as additional checks

$$r_1^2 = X_1^2 + Y_1^2 + Z_1^2, \tag{14}$$

$$r_1^2 = \xi_1^2 + \eta_1^2 + \zeta_1^2, \tag{15}$$

to compare with r_1^2 obtained from the tabular value of r_1.
Then

$$K_1 = \frac{1}{\rho_1^3} - \frac{1}{r_1^3}, \tag{16}$$

and

$$A_1 = (10^4 k^\circ m_1)\sqrt{a} \,.\, w \frac{dt}{dM}, \tag{17}$$

where, for Jupiter, $m_1 = 1/1047{\cdot}35$, $10^4 k^\circ m_1 = 9{\cdot}4105$.

At the start of the work, where we put $w \,.\, dt/dM = wn$, equation (17) reduces to $A_1 = 9{\cdot}548\, wa^2$.

For other planets we multiply A_1 (Jupiter) by the ratio of the masses, namely

$$A_2 = A_1 \frac{m_2}{m_1}, \tag{18}$$

where, for Saturn, $m_2 = 1/3500$ and $m_2/m_1 = 0{\cdot}29924$.

The quantities representing the perturbing forces are then

$$\left.\begin{aligned} S_1 &= A_1 K_1 \xi_1 - A_1 \frac{r}{\rho_1^3}, \\ T_1 &= A_1 K_1 \eta_1, \\ W_1 &= A_1 K_1 \zeta_1, \end{aligned}\right\} \tag{19}$$

for Jupiter, and similarly S_2, T_2, W_2 for Saturn, and so on; the sums being denoted by S, T, W. The accuracy of these quantities should be to one decimal place, if integrations are to be in units of $0^\circ{\cdot}0001$ in the angular elements.

Finally the variations of the elements (in units of the fourth decimal of a degree, except for n and t) are

$$\left.\begin{aligned} w\frac{di}{dM} &= W(\mathrm{i})\cos u, \\ w\frac{d\Omega}{dM} &= W(\mathrm{i})\sin u \operatorname{cosec} i, \\ w\frac{d\omega}{dM} &= S(\mathrm{ii}) + T(\mathrm{iii}) - \cos i \,.\, w\frac{d\Omega}{dM}, \text{ or} \\ w\frac{d\varpi}{dM} &= S(\mathrm{ii}) + T(\mathrm{iii}) + 2\sin^2\frac{i}{2} \,.\, w\frac{d\Omega}{dM}, \\ w\frac{d\phi}{dM} &= S(\mathrm{iv}) + T(\mathrm{v}), \\ w\frac{dM_0}{dM} &= S(\mathrm{vi}) + T(\mathrm{vii}), \\ w\frac{dn}{dM} &= 3\times 10^3 n_c\,(S(\mathrm{viii}) + T(\mathrm{ix})) \text{ in units of 7th decimal,} \\ &\quad \text{where } n_c \text{ is in circular measure, and } 3\times 10^3 n_c = 52{\cdot}3599n, \\ w\frac{dt}{dM} &= \frac{1}{n}\left(w - 10^{-4} w\frac{dM_0}{dM}\right) \text{ days,} \\ &\quad \text{where } w \text{ is the integration interval in degrees of mean anomaly;} \end{aligned}\right\} \tag{20}$$

and where the coefficients are

$$\left.\begin{aligned}
&(\mathrm{i}) = \frac{r}{a}\sec\phi, \\
&(\mathrm{ii}) = -\cot\phi\cos v, && \text{Tab.} \\
&(\mathrm{iii}) = \cot\phi\sin v(1+(\mathrm{i})\sec\phi), && \text{Tab.} \\
&(\mathrm{iv}) = \sin v, && \text{Tab.} \\
&(\mathrm{v}) = \cos v + \cos E && \text{Tab.} \\
&\quad = \cos v\left(1+\frac{r}{a}\right)+\sin\phi, \\
&(\mathrm{vi}) = -(\mathrm{ii})\cos\phi - 2\frac{r}{a}, && \text{Tab.} \\
&(\mathrm{vii}) = -(\mathrm{iii})\cos\phi, \\
&(\mathrm{viii}) = -(\mathrm{iv})\tan\phi, \\
&(\mathrm{ix}) = -\frac{1}{(\mathrm{i})}.
\end{aligned}\right\} \qquad (21)$$

The integrations of the variations in (20) are performed in the usual way, and the single integral for any element (x) at any step M_s is obtained by

$$\int_{M_{00}}^{M_s} w\frac{dx}{dM}.dM = f'(x)_{s-\frac{1}{2}} + \tfrac{1}{2}f(x)_s - \tfrac{1}{12}f'(x)_s + \ldots, \qquad (22)$$

where $f'(x)_s$ is the mean of the adjacent first differences, $f'(x)_{s-\frac{1}{2}}$ and $f'(x)_{s+\frac{1}{2}}$. The variation $w.dM_0/dM$ is not integrated; it is only used in evaluating the $w.dt/dM$ equation at each step.

It will be found convenient to include the values of the elements themselves (in degrees and decimals) in the first-summation columns of the integration tables, and the Julian dates in the case of $'f(t)$. This enables the changes in the elements to be watched easily so that new osculating values of the elements may be taken out and introduced into computations whenever the changes are sufficient to necessitate it. The Julian date t is of course required at each step but frequently may be extrapolated with sufficient accuracy to enable several steps to be computed simultaneously.

The coefficients in the forms given in (21) are easily derived from the standard ones after multiplying by $\cos\phi$, which is made necessary by equation (6). The five coefficients marked "Tab." are those it is suggested might be tabulated, together with v and r/a, in special tables. The remainder are so easily calculated that their tabulation would offer no saving of time and might, moreover, lead to some loss of accuracy where interpolation is not linear.

Difficulties arise when either the inclination or the eccentricity of the orbit is small. In the former case the ascending node is poorly determined, and hence also the argument of perihelion ω; in fact when $i=0$ there is no node relative to the ecliptic. Nevertheless the longitude ϖ of the perihelion point will not be badly determined unless also the eccentricity is small. When therefore i is small, and the factor cosec i in the equation for $w.d\Omega/dM$ is consequently large, it will probably be best to integrate $w.d\varpi/dM$ instead of $w.d\omega/dM$, and to obtain ω

from $\varpi - \Omega$. In this way any small errors in Ω resulting from the cosec i multiplication will be compensated in ω, and the accuracy of the longitude of perihelion will be maintained.

When the eccentricity is small the perihelion point in the orbit is poorly determined and changes rapidly, even when the perturbations are altering the shape of the orbit only slightly. This affects ω, ϖ and M. It makes itself felt through the factor $\cot\phi$ in the coefficients (ii), (iii) and (vii) in (20). This factor will be large when the eccentricity is small.

If either the inclination or the eccentricity is so small that the normal method is impracticable, recourse may be had to the special formulae by Tietjen and Neugebauer, which employ four substitute elements (**3c**). These however complicate the computation, especially in the case of the small eccentricity, and although the integration in terms of the mean anomaly might still be possible, the computer would almost certainly be wise to use another method. The Cowell method (**2**) of integrating the actual perturbed rectangular coordinates suggests itself, but consideration might now also be given to the new method of the variations of special constants (closely related to the usual P_x, Q_x, etc. constants in ephemeris work) recently proposed by Samuel Herrick (**6**).*

When, in the general case, the highest accuracy is not required, it will be possible to work with fewer figures, using the same elements for a number of steps and carrying out the computations for them simultaneously; and it may be feasible too to increase the integration interval in some parts of the orbit from, say, $7\frac{1}{2}°$ to 15°. When a comet is distant from both Jupiter and Saturn it will be safe to compute half a dozen or more steps simultaneously, much of the work being done to three-figure accuracy; and even a slide-rule calculation may suffice in the latter stages of each step, that is after the distance ρ has been found. It is in fact on account of the smaller number of figures employed in the calculations, and the longer integration intervals possible, that this method (well suited for logarithmic calculation) will be found in general to be quicker than the Cowell method, which requires seven or eight decimal places to be retained in the integrations of the coordinates, and the integration intervals to be much shorter, and hence the steps at least twice as numerous. When perturbations are very heavy, however, and very short intervals have to be used even in the elements method, the Cowell method appears to be unsurpassed if a calculating machine is available.

Modifications for the use of Crommelin's and Stracke's Tables.—Before coming to the description of the special tables which it is suggested should be constructed for the new method, mention must be made of the two existing sets of tables which can be adapted for the purpose: those by Crommelin, already referred to, and those by Stracke for approximate minor planet work. The modifications necessary for the use of these tables will now be given.

One point must be emphasized. As the computation of the perturbations can now be made rigorously, these tables can be used for the most exact investigations of orbits, so far as the integration intervals and the number of significant

* It appears that Herrick's method too could be arranged for integration with the mean anomaly as independent variable, enabling tables to be made for a number of the quantities required. In this the integration of his $[\dot{T}]$ would be replaced by that of the perturbed time element, that is of $dt/dM = (1 - [\dot{M}])/n$. If however time is retained as independent variable, it is suggested that the numerical integration of M directly from $\dot{M} = n + [\dot{M}]$ might prove more convenient than using the perturbation $[\dot{T}]$.

figures in the tables permit. When a stage is reached at which the accuracy is inadequate, or the tabular intervals are too long, steps at shorter intervals can be fully computed to all the accuracy required without any break in the sequence of the computation, or in the integrations, until such time as the tables are once again adequate. This should afford a considerable saving in the total computing time expended in such cases.

Crommelin's Tables.

Instead of the original equations for $\boldsymbol{S}$, $\boldsymbol{T}$, $\boldsymbol{W}$ in (5), namely

$$\boldsymbol{S}_1 = (k''wm_1)\sqrt{p}\left(\xi_1 K_1 - \frac{r}{\rho_1^3}\right), \text{ etc.}$$

Crommelin (**4a**) put

$$S_1 = \frac{\boldsymbol{S}_1}{F}, \text{ etc.}, \qquad \text{where} \qquad F = \frac{wk''m_1\sqrt{p}}{a^2}, \tag{23}$$

and included the quantity F in the values of his tabulated coefficients I to X. Remembering that w in (5) and (23) is in units of time (days) and noting that

$$\frac{wk''}{3600\,a^{\frac{3}{2}}} = \frac{wn}{3600} = w^\circ \text{ (degrees of mean anomaly)}, \tag{24}$$

we have, more simply than Crommelin gave it,

$$F = 3600w^\circ m_1 \cos\phi. \tag{25}$$

With his tabular interval $w^\circ = 7\frac{1}{2}^\circ$, and Jupiter's mass 1/1047·35, this yields his value of the constant, $\log F\sec\phi = 1{\cdot}41127$. Since (6) has already removed $\cos\phi$ from (5), the first modification necessary to use his tables will be to divide A_1 in (17) by this constant $F\sec\phi = 25{\cdot}779$. Instead of (17), therefore, we use

$$A_1 = 0{\cdot}36504\sqrt{a}\,.\,w\frac{dt}{dM} \tag{26}$$

to obtain the results in units of the fourth decimal of a degree, instead of the seconds of arc he employed. At the start of the work where we put $w\,.\,dt/dM = w/n$, this reduces to $A_1 = 2{\cdot}778a^2$, for $w = 7\frac{1}{2}^\circ$.

The formulae for A_2 and S_1, T_1, W_1 remain as in (18) and (19), but for the accuracy here suggested it will now be necessary to retain three decimal places in S, T and W (with a tolerance of about $\pm 0{\cdot}004$). Crommelin's coefficients I and II are not usable and must be replaced by

$$\left.\begin{aligned} \text{I}' &= (F\sec\phi)\frac{r}{a}\sec\phi \\ &= 25{\cdot}779\,\frac{r}{a}\sec\phi. \end{aligned}\right\} \tag{27}$$

And since his tabulated dn/dt coefficients contain the factor w^2 for a double integration, instead of w for the single integration required here, they must be multiplied by $1000n/7\frac{1}{2}$ to rectify this and to give the results for this element in

units of the seventh decimal place of a degree instead of the fourth. Thus instead of (20) we compute

$$\left.\begin{aligned}
w\frac{di}{dM} &= WI'\cos u,\\
w\frac{d\Omega}{dM} &= WI'\sin u\,\mathrm{cosec}\,i,\\
w\frac{d\phi}{dM} &= S\,\mathrm{III}+T\,\mathrm{IV},\\
w\frac{d\omega}{dM} &= -S\,\mathrm{V}+T\,\mathrm{VI}-\cos i\,.\,w\frac{d\Omega}{dM},\ \text{or}\\
w\frac{d\varpi}{dM} &= -S\,\mathrm{V}+T\,\mathrm{VI}+2\sin^2\frac{i}{2}\,.\,w\frac{d\Omega}{dM},\\
w\frac{dM_0}{dM} &= S\,\mathrm{VII}+T\,\mathrm{VIII},\\
w\frac{dn}{dM} &= 133{\cdot}33n\,(S\,\mathrm{IX}+T\,\mathrm{X})\ \text{units of 7th place},\\
w\frac{dt}{dM} &= \frac{1}{n}\left(7{\cdot}5-10^{-4}w\frac{dM_0}{dM}\right)\ \text{days},
\end{aligned}\right\}\qquad(28)$$

where the coefficients III to IX, except VIII, are taken from Crommelin's tables. The values of VIII and X may conveniently be obtained directly, thus saving the interpolations, from

$$\left.\begin{aligned}
\mathrm{VIII} &= -\mathrm{VI}\cos\phi,\\
\mathrm{X} &= -3Fw\frac{2\pi}{360}\frac{a}{r}\\
&= -\frac{260{\cdot}97}{\mathrm{I}'}\,.
\end{aligned}\right\}\qquad(29)$$

Stracke's Tables.

G. Stracke (**16**) published tables similar to Crommelin's, but for the range of eccentricities required for minor planet work, namely for ϕ between 0° and 35° ($e=0$ to 0·57) at 1° intervals and an integration interval of 12° of mean anomaly. These tables were however designed for approximate work and are only to three-figure accuracy.

The modifications required in using these with the present method are similar to those for Crommelin's tables. The tabulated values of the coefficients contain the mass of Jupiter and the integration interval 12°, and give the results in units of the third decimal of a degree (fourth decimal for n). Stracke put

$$F=12{,}000m_1=11{\cdot}457,\qquad(30)$$

corresponding to Crommelin's constant $F\sec\phi$. The value of A_1 in (17) must therefore be divided by this factor, and in place of it we must use

$$A_1=0{\cdot}82142\sqrt{a}\,.\,w\frac{dt}{dM}\qquad(31)$$

to obtain results in units of the fourth decimal. At the start of the work, where we put $w\,.\,dt/dM=w/n$, this reduces to $A=10a^2$, for $w=12°$.

The formulae for A_2 and S_1, T_1, W_1 remain as in (18) and (19), and one decimal place should be retained in the latter quantities. Stracke's coefficients I and II are not usable and must be replaced by

$$\left.\begin{aligned} \mathrm{I}' &= F\frac{r}{a}\sec\phi \\ &= 11{\cdot}457\,\frac{r}{a}\sec\phi. \end{aligned}\right\} \tag{32}$$

And, as before, since the tabulated dn/dt coefficients contain the factor w^2 instead of w, they require multiplication, in this case by $100n/12$, to rectify this and to give the results for this element in units of the seventh decimal place of a degree. Instead of (20) then, we compute

$$\left.\begin{aligned} w\frac{di}{dM} &= W\mathrm{I}'\cos u, \\ w\frac{d\Omega}{dM} &= W\mathrm{I}'\sin u\,\mathrm{cosec}\,i, \\ w\frac{dn}{dM} &= 8{\cdot}33n(S\,\mathrm{III}+T\,\mathrm{IV}),\ \text{units of 7th place}, \\ w\frac{d\varpi}{dM} &= (S\,\mathrm{V}+T\,\mathrm{VI})\,\mathrm{cosec}\,\phi+2\sin^2\frac{i}{2}.w\frac{d\Omega}{dM}, \\ w\frac{dM_0}{dM} &= S(\mathrm{VII}-\mathrm{V}\cot\phi)-T\,\mathrm{VI}\cot\phi, \\ w\frac{d\phi}{dM} &= S\,\mathrm{VIII}+T\,\mathrm{IX}, \\ w\frac{dt}{dM} &= \frac{1}{n}\left(12-10^{-4}w\frac{dM_0}{dM}\right)\ \text{days}, \end{aligned}\right\} \tag{33}$$

where the coefficients III to IX are taken from Stracke's tables.

If greater accuracy is required than can be obtained with these tables, and the eccentricity is below the limit of Crommelin's tables, the full computation of equations (9) to (22) will be necessary. It may however to some extent be facilitated by obtaining v and r/a from existing tables : to four-figure accuracy by Peters and Stracke (**13**), or to five-figure accuracy from Innes's (**7**) tables of elliptical coordinates.

Special tables for the method.—Experience with Crommelin's tables has shown that a new arrangement is desirable for a number of reasons; for example: smaller intervals are needed around perihelion, the number of tabulated quantities could be reduced with advantage, and the values should be given in natural numbers (with printed differences) instead of logarithms, so as to reduce errors in interpolation.

The tables it is proposed should be constructed would give v and r/a, and the coefficients (ii) to (vi) in (21), for every 3° of mean anomaly near perihelion, say from 0° to 24° (and 336° to 360°), and 6° for the rest of the revolution. The values between 180° and 360° are the same as between 0° and 180° (i. e. as $360° - M$) except for some changes of sign. The 3° interval around perihelion (equivalent to about 20 days for an average periodic comet), it is expected, would be small enough to give reasonably smooth differences, and to permit perturbations by the

Earth and Venus to be taken into account in most cases. An interval of 6° at aphelion, on the other hand, would enable approaches to Jupiter to within about 1½ A.U. to be handled with sufficient accuracy with the tables, in the case of an average periodic comet ($P=7$ years). For closer approaches the interval of integration would have to be reduced and some steps fully calculated. Where high accuracy is demanded it would be necessary to reduce the integration intervals at an earlier stage, to abandon the tables for a while, and to calculate the steps separately with more significant figures.

The table for each argument in M would occupy one page and would show the natural values of the coefficients tabulated against the vertical argument of the eccentricity e at intervals of 0·01, from say 0·30 to about 0·87 (according to the space available on the page).

It is intended that v and r/a should be given to five-figure accuracy (viz. 0°·001 and 0·00001); and the coefficients to four-figure. It is of no practical use to carry the accuracy of the latter beyond the four-figure order, as Crommelin did, for if the perturbations are large enough to require it, then v and r/a will be needed to greater accuracy than the five-figure given, because the distance ρ will be small and not accurately enough determined without it. Moreover the 6° integration interval will then anyhow be too great. Further, linear interpolation in the tables is insufficient in many places if more than four-figure values are used. For this same reason it would be advisable to print the natural four-figure values (and first differences) and not their logarithms.

If such tables were considered of use in future minor planet work, the range of those just proposed could be extended at the lower end to cover eccentricities from say 0·05 to 0·30, for intervals of M of 6° for the whole revolution. In that case the coefficients (ii), (iii) and (vi) had best be tabulated as $\tan\phi$ (ii), $\tan\phi$ (iii) and $\tan\phi$ (vi), to remove the $\cot\phi$ factor which would render easy interpolation impossible within the proposed tabular intervals of eccentricity.

Numerical example and discussion.—It was considered of interest to compute the perturbations for an object assumed to have an orbit with the period and eccentricity of an average short-period comet, namely $P=7$ years and $e=0{\cdot}6$, for a moderately close approach to Jupiter over a short interval. The data were adjusted to make the minimum distance two units exactly in the unperturbed orbit. To simplify the calculation the inclination to the ecliptic was assumed zero, and the closest approach arranged for a date when the latitude of Jupiter was zero. The perturbations of the inclination and node were then ignored, and those of ϖ (longitude of perihelion) computed instead of those of ω. The assumed elements, together with those obtained from the rigorous and approximate calculations nineteen steps (about 950 days) later, were as follows. The results by the rigorous method for 1950 February 6·650, when M was 330°, have been adjusted to compare directly with those from the approximate method for February 8·0.

	Assumed	Rigorous	Approx.	R–A
Epoch	1947 August 23·0	1950 February 8·0		
	°	°	°	°
M	195·0000	330·2038	330·2012	+0·0026
ϖ	90·9202	91·3328	91·3364	− ·0036
ϕ	36·8699	37·1650	37·1651	− ·0001
n	0·1500000	0·1512035	0·1512027	+ ·0000008

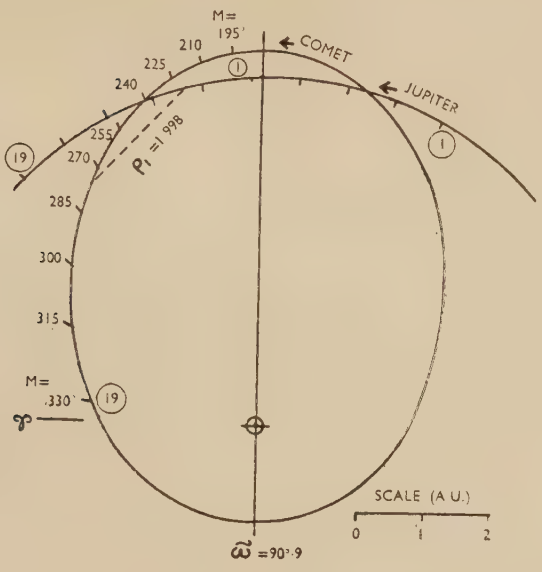

M	ρ_1	R–A	$w\frac{d\varpi}{dM}$	R–A	$w\frac{d\phi}{dM}$	R–A	$w\frac{dn}{dM}$	R–A	$'f(t)$	$w\frac{dt}{dM}$
°										
187½	3·4573	− 3	− 59	0	+102	−1	+185	0	243	49·864
195	3·3079	0	− 50	0	118	−1	201	0	2395·570	49·859
202½	3·1541	+ 5	− 36	0	136	−1	221	−1	2445·429	49·856
210	2·9974	7	− 18	0	157	0	249	−1	2449·285	49·855
217½	2·8402	12	+ 6	0	179	−1	285	−1	2545·140	49·857
225	2·6845	13	38	−1	204	−1	332	−2	2594·997	49·865
232½	2·5334	12	80	−1	230	−1	394	−2	2644·862	49·879
240	2·3907	12	134	−1	255	−1	474	−3	2694·741	49·901
247½	2·2609	+ 7	200	−2	278	−1	575	−3	2744·642	49·934
255	2·1494	0	277	−2	293	0	698	−3	2794·576	49·976
262½	2·0635	− 8	359	−2	294	0	837	−1	2844·552	50·025
270	2·0106	−16	433	−3	276	+1	975	0	2894·577	50·070
277½	1·9990	−25	483	−3	236	+1	1088	+3	2944·647	50·098
285	2·0363	−25	496	−3	180	0	1144	+4	2994·745	50·094
292½	2·1274	−25	466	−4	119	+1	1128	+4	3044·839	50·053
300	2·2756	−22	405	−4	64	+1	1044	+3	3094·892	49·982
307½	2·4832	−16	329	−4	+ 22	0	911	+1	3144·874	49·896
315	2·7518	−12	251	−4	− 4	+1	754	0	3194·770	49·809
322½	3·0847	−11	180	−3	− 17	+1	588	−1	3244·579	49·732
330	3·4877	−12	119	−3	− 20	+1	422	0	3294·311	49·670
337½	3·9685	−17	+ 69	−2	− 16	0	+254	−1	3343·981	49·624

The equations for the relative Jupiter coordinates simplified, in this case, to

$$\left.\begin{aligned}\xi_1 &= r_1 \cos(l_1 - L),\\ \eta_1 &= r_1 \sin(l_1 - L),\end{aligned}\right\} \qquad (34)$$

where $L = v + \varpi$; and $\zeta_1 = 0$.

The figure on page 433 represents the circumstances of the approach. The table gives the distance, and the variations of the elements in units of the fourth decimal of a degree for ϕ and ϖ, and of the seventh decimal for n. The differences (R–A), between the values obtained from the rigorous and approximate methods, are also tabulated. The last columns give the perturbed time interval and the first summation for obtaining the perturbed Julian date.

It will be noted that the values of the variations in the table only exceed three significant figures in one element, the mean motion, and then only for four steps. Differencing of the values, moreover, shows the higher differences to be of reasonable size. We conclude therefore that the $7\frac{1}{2}^\circ$ interval of Crommelin's tables is adequate for such a case as this. The run of the R–A errors moreover shows that several steps could safely be computed simultaneously, using one set of osculating elements, provided the osculating value also of $w.dt/dM$ were used in obtaining t and A_1. Not only are the R–A errors seen to be small but most of those occurring before the closest approach cancel out to a considerable extent afterwards. We note, in particular, that the final error in the mean motion is negligible.

It might be thought from this that the remarks made earlier in this paper (p. 422), about errors resulting from the use of the approximate method, were perhaps not justified. The example, however, was not well chosen to illustrate this; the circumstances were not exacting enough and the approach was of too short a duration. As the distance throughout was between two and three and a half units, the perturbations had to accumulate sufficiently to affect the three-figure accuracy of the elements before their neglect caused errors in the subsequent computed three-figure values of the variations of the elements.

Under other circumstances, especially during closer or longer approaches, one could not expect such compensations in the errors as occurred in this example, and the cumulative effects of errors would then rapidly make themselves felt once the three-figure accuracy of the starting elements was affected by them. The example does give indications of the beginning of this. The R–A errors in the S and T components of the perturbations of the mean motion were separated and found to total $+32$ and -36 respectively—small but appreciable. The R–A differences of the relative Jupiter coordinates, at first negligible, started to increase rapidly after the closest approach and amounted, at $M = 330^\circ$, to $+0{\cdot}0204$ astronomical units in $\xi_1 - r$ and $+0{\cdot}0113$ in η_1; that is, these errors were then affecting the accuracy of the computations in the third significant figure. A practical point of interest is that the comparatively large differences between the elements used, on account of the accumulating perturbations, only caused such relatively small errors.

Acknowledgments.—The author gratefully acknowledges the encouragement and help he has received, especially from Dr J. G. Porter who experimented with the modified method, assisted in designing the computational arrangements for it now in use in the Computing Section of the British Astronomical Association, and taught it to a number of computers. The author's thanks are also due to

Mr D. H. Sadler for valuable suggestions regarding the presentation of the method and the planning of new tables for it.

University Observatory,
Oxford :
1949 *May* 8.

References

(1) See (8), (11), (14), (15a) and (17) below.
(2) See (5), (9b), (10) and (15b) below.
(3) Julius Bauschinger, *Die Bahnbestimmung der Himmelskörper*, Leipzig, 1906 and 1928. (a) Chap. 30. (b) 1st edition, pp. 493, 495 ; 2nd edition, pp. 501, 503. (c) 1st edition, pp. 511–515 ; 2nd edition, pp. 519–523.
(4) A. C. D. Crommelin, " Tables for Facilitating the Computation of the Perturbations of Periodic Comets by the Planets ", *Mem. R.A.S.*, **64,** part 5, 1929. (a) p. 150.
(5) Paul Herget, *The Computation of Orbits*, published privately by the author, Cincinnati, 1948, pp. 98–105.
(6) Samuel Herrick, " A Modification of the ' Variation-of-Constants ' Method for Special Perturbations ", *Pub. A.S.P.*, **60,** No. 356, 321–323, 1948.
(7) R. T. A. Innes, " Tables of X and Y (Elliptic Rectangular Co-ordinates) ", *Union Observatory Circular*, No. 71, 1926.
(8) W. Klinkerfues and H. Buchholz, *Theoretische Astronomie*, Braunschweig, 1899 and 1912, Chap. 98.
(9) G. Merton, " The periodic Comet Grigg (1902 II)-Skjellerup (1922 I) ", *Mem. R.A.S.*, **64,** part 3, 1927. (a) See especially p. 100. (b) pp. 60–70.
(10) H.M. Nautical Almanac Office, *Planetary Co-ordinates for the Years* 1800–1940, H.M. Stationery Office, London, 1933, pp. ix–xviii.
(11) Th. R. von Oppolzer, *Lehrbuch zur Bahnbestimmung der Planeten und Kometen*, Leipzig, 1880, Vol. II, Chap. II C.
(12) Th. R. von Oppolzer, " Über der Winnecke'schen Komet ", *Sitzungsberichte der Wiener Akademie* (*Math. Classe*), **62,** 655, 1870.
(13) J. Peters and G. Stracke, " Tafeln zur Berechnung der Mittelpunktsgleichung und des Radiusvektors in elliptischen Bahnen (für Exzentrizitätswinkel von 0° bis 26°) ", *Veröffentlichungen des Astronomischen Rechen-Instituts*, No. 41 (2nd Ed.), Berlin, 1933.
(14) H. C. Plummer, *An Introductory Treatise on Dynamical Astronomy*, Cambridge, 1918, pp. 149–152, 227–228.
(15) G. Stracke, *Bahnbestimmung der Planeten und Kometen*, Berlin, 1929. (a) Chap. 20. (b) Chap. 18.
(16) G. Stracke, " Tafeln zur genäherten speziellen Störungsrechnung ", *Veröffentlichungen des Astronomischen Rechen-Instituts*, No. 48, Berlin, 1930.
(17) J. C. Watson, *Theoretical Astronomy*, Philadelphia, 1868, pp. 489–503, 516–523.

LINE-INTENSITIES IN STARS OF TYPE G5 TO K5

A. D. Thackeray

(Revised version received 1949 March 8*)

Summary

The paper presents results of measured intensities of certain lines, in the green-yellow region, of 78 stars of type G5 to K5. Homogeneity of the material has been ensured by using the same 2-prism spectrograph throughout at an unchanged setting. Quantitative mean variations with spectral type and absolute magnitude (based on Mt. Wilson and Victoria classifications) are derived. The deviations from these means are studied statistically and the observed dispersion is found in most cases to exceed slightly that attributable to observational errors ; in particular, the excess dispersions of $H\beta$ and *Mg* 5183 are more than twice their standard errors.

The numerous physical factors contributing to line-intensities are briefly discussed. But, provided the abundance of the relevant element makes no significant contribution to the atmospheric opacity nor to the classification of type and luminosity, such residual dispersions indicate upper limits to the dispersion in abundance for stars of the same type and luminosity. The upper limits so found amount to ± 18, ± 20 and ± 29 per cent for the abundance of *Na*, *Mg* and *H* respectively. The approximate nature of these results is stressed, especially for *H*.

Corrections to types and absolute magnitudes, as well as observed deviations in individual stars, are listed in Table IV. One outstanding case is ζ Aurigae whose visual spectrum at phase 0·69 is that of a normal giant ($M_v = +0{\cdot}5$). The existence of a number of sub-giants is confirmed.

The following results in connection with the variations with type and luminosity are noteworthy : (1) the strength of certain satellite lines of a low-level *Fe* multiplet in supergiants, (2) the strength of *Mg* 5183 in dwarfs, (3) the failure of subordinate lines of the neutral metals to show a maximum earlier than K5, (4) the strengthening of *Cr* lines from K0 to K5 compared with the relative insensitivity of *Ti* lines.

---

1. *Introduction.*—To a first approximation stellar spectra may be classified in a single sequence according to surface temperature. When finer details are examined, certain "sensitive" lines provide a second parameter by which giant and dwarf stars may be distinguished or arranged in a sequence of luminosity-classes. A few stars with lines due to certain elements unusually strong or with other peculiarities are distinguished by the letter "p", but in general two parameters of type and luminosity suffice for modern classifications, and this fact together with calculations based on ionization theory may be taken as indicating the roughly constant composition of stellar atmospheres.†

In 1938 a spectrophotometric programme of line-intensities in K-type stars was begun with the 25-inch Newall refractor of the Solar Physics Observatory, Cambridge. The programme was conceived with the following questions in mind:

(1) To what extent are line-intensities in stellar spectra determined by the two parameters, spectral type and absolute magnitude?

* Originally submitted 1948 November 8.

† C. H. Payne, *Stellar Atmospheres*, Cambridge, Mass., 1925.

(2) Can abnormal line-intensities be explained in terms of abnormal abundance and, if so, what is the dispersion in abundance of various elements in a sub-class of stars of the same type and luminosity?

(3) What relation, if any, exists between the phenomenon of abnormal line-intensities and large discrepancies between spectroscopic and trigonometric parallaxes (e.g. α Bootis)?

It is not practicable to choose a sufficiently large group of stars of identical spectral type and luminosity for accurate comparison of line-intensities. Instead, a certain range of spectral type was chosen and as many stars as possible in this range were observed without any restriction on the luminosities. Before question (1) could be answered therefore the subsidiary question, of great astrophysical interest in itself, of how lines vary from star to star with type and luminosity had to be tackled, and then the appropriate corrections for these two parameters could be applied.

The range of spectral types selected was G5 to K5 (Victoria classification) and the range of spectrum recorded in focus and of suitable density was from 4800 to 5900 A. This "visual" range is well suited to the Cambridge equipment, especially for K stars. With the OG plus correcting lens focused on the spectrograph slit at the flattest portion of the colour curve in the green (roughly coinciding with the minimum sensitivity of panchromatic emulsions) a remarkably long portion of the spectrum, for a refractor, is obtained simultaneously and of density suitable for photometry. The range includes several strong lines in G5 to K5 stars (especially *Hβ*, *Mg* 5183, D_1 and D_2 besides several *Fe* lines) and in general the problem of blending is not so severe as in the "photographic" region more usually studied. Finally, for the statistical problem in hand, namely the dispersion of line-intensities, it is a decided advantage to study lines which have played no part in the observational determination of type and luminosity, since, as has been mentioned above, the observations have to be corrected for these two parameters and reduced to some standard.

2. *Observational Material.*—The instrument used throughout was the 2-prism spectrograph, with 20-inch camera, attached to the Newall refractor, giving a dispersion of 51 A./mm. at *Mg* 5183. The lines selected for measurement, together with their corresponding ionization and excitation potentials, are listed in Table I. Equivalent widths of the lines *Hβ*, *Na* ($D_1 + D_2$) and *Mg* 5183 were measured, while for the other lines only the central intensities were recorded; these could then be transformed into equivalent widths by means of a calibrating curve, which in fact largely depended upon *Mg* 5183. The method of reduction was the same as that formerly used by the writer *, namely after drawing in the background of continuous spectrum, curves corresponding to 95, 90, 80, 70, etc. per cent of the background were drawn in on the tracings. The widths of the line contours were measured at these depths and the equivalent width derived by a simple summation which effectively treated each contour as the sum of a series of trapezia. The error involved in this approximation is no larger than the many others arising from various sources. The prime interest in our problem is *relative* not absolute line-intensities and for an accurate comparison from star to star the chief essential is homogeneity of material; the requisite homogeneity has been achieved by using the same spectrograph at identical setting throughout

* *M.N.*, **94**, 99, 1933. See also *M.N.*, **99**, 492, 1939; this latter paper, hereafter referred to as Paper I, describes preliminary results on variations with type and luminosity.

the programme. The photometric calibration with step-slit standardizer, development and emulsion type (for all but a few of the brighter stars Ilford Hypersensitive Panchromatic) were also kept uniform and, though calibration curves for three wave-lengths from $H\beta$ to D were always derived, it was found that there was remarkably little change from one plate to another or even at the various wave-lengths, so that usually a single average calibration curve sufficed for each plate.

TABLE I

Absorption Lines measured for Central Intensity and Equivalent Width

Wave-length	Chief Contributor	E.P. (volts)	I.P.	C.I.	E.W.
4861·3	$H\beta$	10·1	13·5	×	×
5890·0	*Na*	0·0	5·1	×	×
5895·9				×	
5183·6	*Mg*	2·7	7·6	×	×
5269·6				×	
5328·0	*Fe* (*a*)	0·9	7·8	×	
5371·5				×	
5247·1				×	
5250·2	*Fe* (*b*)	0·1	7·8	×	
5254·9				×	
4890·7, 4891·5				×	
4919·0, 4920·5	*Fe* (*c*)	2·8	7·8	×	
4957·3, 4957·6				×	
5206·0				×	
5208·4	*Cr*	0·9	6·7	×	
5298·3				×	
4934·1	Ba^+	0·0	5·2	×	
4856·0	*Ti*	2·2	6·8	×	
5036·5		1·4		×	

At one time it was hoped to include all stars brighter than apparent magnitude 4·6 and north of declination $-10°$ in the programme. (There are 103 stars in the Victoria classification satisfying the criteria.) At the outbreak of war in 1939 September, 80 such stars had been photographed, all but five of them at least twice. Reduction of the material proceeded and was completed during 1941. Final discussion of the results was held up in the hope of obtaining more material after the war. However, the programme was not in fact resumed, for a variety of reasons (the chief of which was that post-war material would not have been strictly homogeneous with pre-war). The number of stars obtained prior to 1939 September does seem to be adequate for a discussion of our main problem and it would probably require more than double the material in order to achieve a sensible gain in weight of the results.

Mean widths and central intensities as measured in 80 stars are given in Table V.

3. *Variations with Type and Luminosity.*—After measurement of the line-intensities on all plates in the series, and derivation of means for each star, the variation of each line (or group of lines) was studied in the manner described in Paper I, viz. by successive approximations, and the variation of line-intensity with spectral type and absolute magnitude was derived.

For spectral type the mean of Victoria (V), Mt. Wilson (W) and Harvard (H) classifications were used:

$$T = \frac{4V+3W+H}{8},$$

this system of weighting being suggested by an intercomparison of the three classifications.* For absolute magnitude the mean of the Mt. Wilson and Victoria values was used.

Figs. 1A and B show the mean curves which best describe the variation of the lines with type and luminosity. Two successive approximations were used as

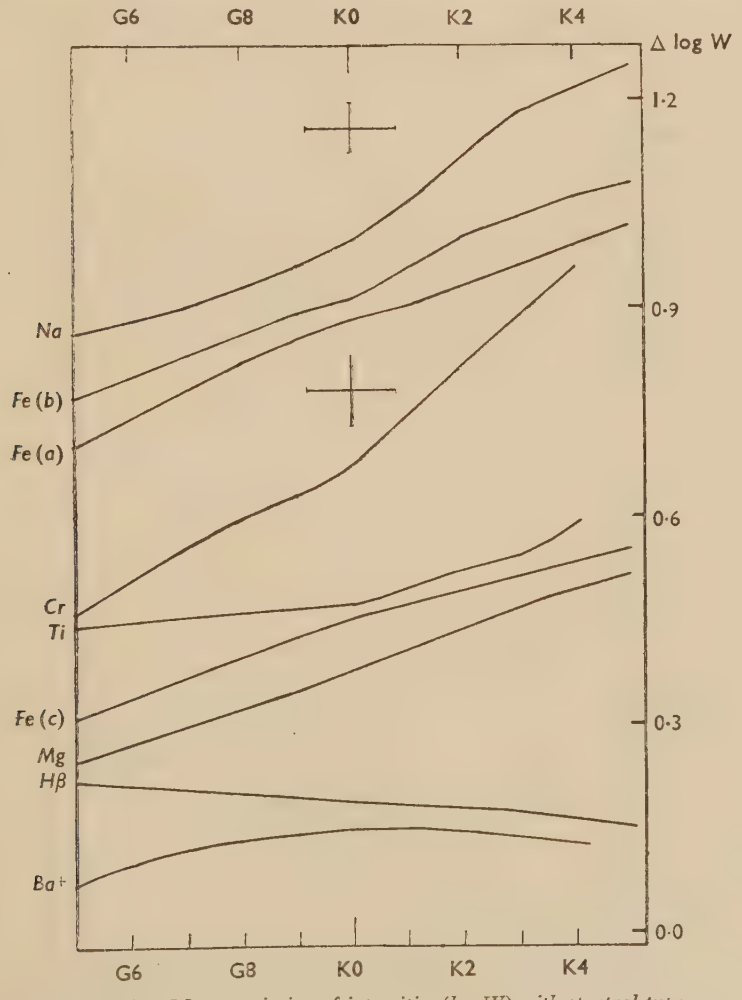

FIG. 1A.—f_1: *Mean variation of intensities (log W) with spectral type. Zeros are arbitrary for each intensity curve but each interval corresponds to a twofold increase in equivalent width. The size of observational errors is indicated.*

* H. E. Butler and A. D. Thackeray, *M.N.*, **100**, 450, 1940.

in Paper I in deriving these curves which have been drawn free-hand through points representing means at successive magnitudes or tenths of a spectral type. The size of the observational errors for an individual star is indicated on the figures; about eight stars form the mean for each tenth-type. Figs. 1C and D show the individual plots of central intensity ($\Delta \log I$) against type for the *Cr* group of lines, and against M for the *Fe* (*b*) group. Other examples of such figures (based on about half the present material and with a poorer sample of supergiants and dwarfs) appear in Paper I.

It should be mentioned that for those lines whose central intensities only were measured, the transformation central intensity to equivalent width by means of the calibrating curve was only made after the mean curves connecting central intensity and spectral type or M (such as Figs. 1C and D) had been drawn out.

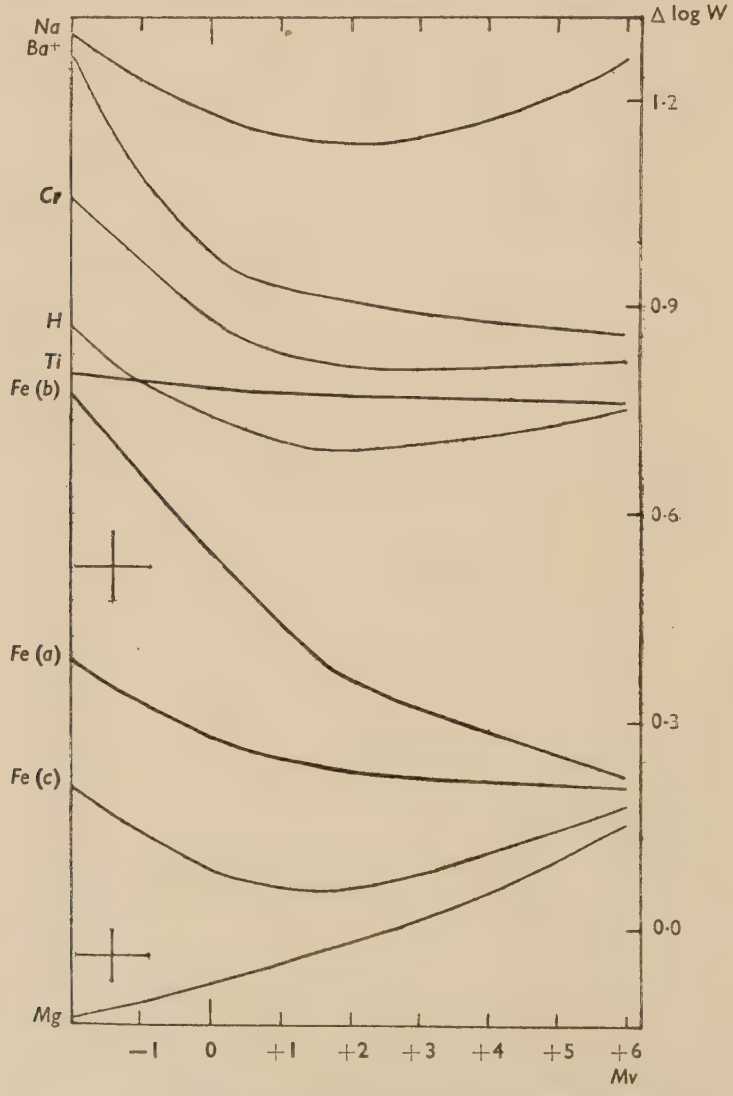

FIG. 1B.—ϕ_M: *Mean variation of intensities with absolute magnitude. Zeros are arbitrary for each intensity curve. Each interval corresponds to a twofold increase in equivalent width. The size of observational errors is indicated.*

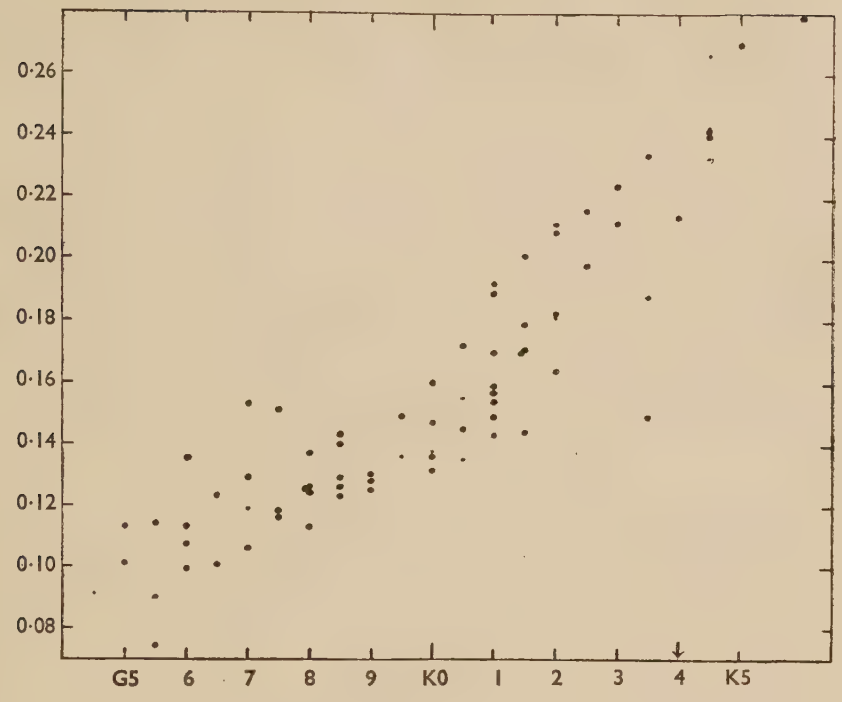

FIG. 1C.—*Variation of Cr* (λλ 5206, 5208, 5298) *with spectral type.*
Abscissae: *Spectral type.*
Ordinates: *Central intensities* $\Delta \log I$ *(reduced to* $M_v = 0$*).*
Note: *ζ Aurigae (with* $M_v = -2{\cdot}5$*) lies off the figure in the direction of the arrow at K4.*

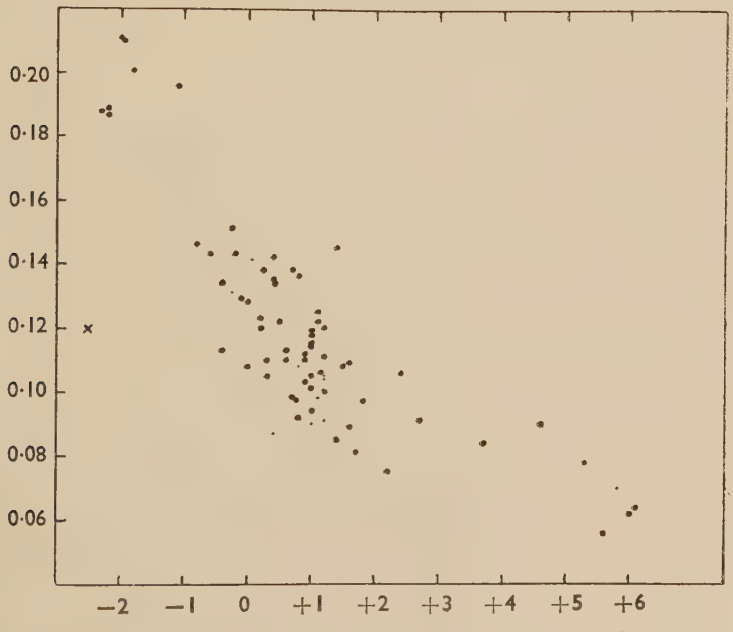

FIG. 1D.—*Luminosity variation of Fe* (*b*) (λλ 5247, 5250, 5254) *in K0 stars.*
Abscissae: M_v.
Ordinates: *Central intensities* $\Delta \log I$ *(reduced to K0).*
X: *denotes ζ Aurigae (with* $M_v = -2{\cdot}5$*).*

4. *Dispersion of the Intensities.*—Let us express the equivalent width of a line in a star of type t and absolute magnitude M as

$$\log W = f_t + \phi_M + \delta,$$

or when the central intensity only is measured,

$$\Delta \log I = f_t' + \phi_M' + \delta'.$$

Here f_t, ϕ_M represent the variations with type and luminosity respectively and may be read off from the curves of Fig. 1. δ represents the deviation of the log (width) in that star from the mean for its type and luminosity. (It will be noted that this procedure implicitly assumes that the variations f_t with temperature and ϕ_M with absolute magnitude are mutually independent. So long as the range in spectral type is not too large, there is no reason to believe that the luminosity effect varies appreciably and no such variation for the stars used in this programme has been detected when the material is divided into two groups earlier and later than Ko.)

Now our main objective is to study the true deviation from the mean, both for individual stars and statistically for the whole group. It is quite clear that for each individual star the derived δ will be composed, to a greater or less extent, of observational errors and only partly of a true deviation due to some physical cause. However, if we form the root mean square deviation

$$\bar{\delta} = \{(\Sigma\delta^2)/n\}^{\frac{1}{2}}$$

over all n stars studied, then

$$\bar{\delta}^2 = \sigma^2 + \tau^2,$$

where σ represents the observational error and τ represents the true dispersion due to physical causes. The observational error σ will be composed of various parts, viz.

(*a*) Observational error of the measurement of line-intensity, including all photometric errors of calibration, Eberhard effect, etc.

(*b*) Error of spectral type. This has been estimated * as $\pm 0{\cdot}85$ (in tenths of a spectral type) for K stars, using the same system of weighting as has been adopted here. The effect of this standard error on line-intensities is determined by applying the results from Fig. 1, giving the change of intensity with spectral type.

(*c*) Error of absolute magnitude. This has been calculated † for the Mt. Wilson spectroscopic values used here as $\pm 0{\cdot}80$ mag. For the mean of the independent determinations by Victoria and Mt. Wilson we divide this by $\sqrt{2}$, i.e. $\pm 0{\cdot}56$ mag. The effect of this error is similarly determined by applying the results of Fig. 1.

The influence of the criteria for type and luminosity on these derived errors is considered in a later section.

The only way to estimate σ_a, the observational error of measurement of line-intensity, is by comparing measures of duplicate plates of the same star.

The procedure adopted was as follows. Write $x_1 = \log W_1$, $x_2 = \log W_2$ for the log (equivalent widths) from duplicate plates of the same star. Calculate the function

$$\sigma_a = \left[\frac{1}{n}\Sigma\{\tfrac{1}{2}(x_1 - x_2)\}^2\right]^{\frac{1}{2}}$$

* H. E. Butler and A. D. Thackeray, *op. cit.*, p. 453, where $\sigma^2 = 0{\cdot}72$ for K stars.

† H. N. Russell and C. E. Moore, *Ap. J.*, **87**, 413, 1938.

for the n stars for which duplicate measures are available. This quantity represents the standard error (s.e.) of $\frac{1}{2}(x_1 - x_2)$ which is $1/\sqrt{2}$ (the s.e. of a single measure of x); but this is also the s.e. of the mean of two measures $\frac{1}{2}(x_1 + x_2)$ and this latter is the quantity required.

It will be noticed that this procedure implicitly assumes that the error follows a Gaussian distribution when expressed in log W rather than in W, in other words, that the s.e. of an observed width is directly proportional to that width rather than that they are independent. In fact the truth lies somewhere between these two alternatives, as can be seen from Table II, where the calculation of σ_a for *Na* and *Mg* is given subdivided into groups of stars having different average line-intensities. The data are rather scanty for a conclusive distinction.

TABLE II

Frequency Distribution of $\frac{1}{2}(x_1 - x_2)$, grouped by types, and Calculation of σ_a

$\frac{1}{2}(x_1-x_2)$ $(=y)$	*Na*(D$_1$+D$_2$) G4/6	G6·5/K1	K1·5/K5	All	*Mg* 5183 G4/6	G6·5/K1	K1·5/K5	All
0·00	3·5	10·5	8	22	16·5	6	6	28·5
0·01	11·5	1·5	6·5	19·5	12·5	14	16·5	27
0·02	6·5	9	9	24·5	8·5	14	9·5	32
0·03	8·5	3·5	10	22	6	6	7	19
0·04	3·5	8·5	4	16	6·5	2·5	3·5	12·5
0·05	4	7·5	5	16·5	0	3	1·5	4·5
0·06	4·5	3	1	8·5	1	1	0·5	2·5
0·07	2·5	1	0·5	4		1		1
0·08	2	1·5		3·5				0
0·09				0				0
0·10	2			2				0
0·11		0·5		0·5				0
0·12							0·5	0·5
$\sigma_a=(\Sigma y^2/n)^{\frac{1}{2}}$	0·0427	0·0390	0·0298	0·0377	0·0217	0·0261	0·0227	0·0236
log $\overline{W}$	0·15	0·28	0·39	0·28	0·16	0·25	0·35	0·25
log $\bar{\epsilon}$	$\bar{1}$·16	$\bar{1}$·25	$\bar{1}$·24	$\bar{1}$·24	$\bar{2}$·87	$\bar{1}$·04	$\bar{1}$·08	$\bar{1}$·00

Consider the last three lines of this table. The first gives the standard error σ_a as defined, in log W, for the group of stars concerned; this being the average, $\frac{1}{2}\log(W_1/W_2)$ may be written approximately as $\log(1+\bar{\epsilon}/\overline{W})$, where $\bar{\epsilon}$ is the mean linear error in angstroms and $\overline{W}$ the average width of the sample. log $\overline{W}$ is given in the second line, and derived from the two preceding lines by the approximate relation, log $\bar{\epsilon}$ is given in the last line.

For both *Na* and *Mg*, the linear error $\bar{\epsilon}$ increases as we measure stronger lines; with *Mg* the increase is roughly proportional to $\overline{W}$, while with *Na* the proportional error is rather smaller for strong lines, but the change is not sufficient to outweigh the increase in $\overline{W}$. Thus, so far as the evidence goes, it appears that our assumption that the error of the observed width is proportional to that width is better than that the two quantities are independent.

The difference between the size of the standard errors found in Table II for *Na* and *Mg* emphasizes the need to calculate this quantity for each line (or group

of lines), and this has been done; the relatively greater error for *Na* probably arises from the fact that the doublet is not fully resolved.

We are now in a position to summarize the results on the dispersion among the observed intensities and the extent to which the observed dispersion may be attributed to the various sources of observational error. Table III (*a*) gives the results for *Na*, *Mg* and *Hβ* for which equivalent widths were measured, while Table III (*b*) gives similar results from the central intensities measured in the lines *Fe* (*a*), (*b*), (*c*), *Cr* and *Ba*$^+$. Results for the two *Ti* lines are too scanty for such an analysis.

TABLE III

Standard Dispersion of Line-intensities

(*a*) Equivalent Widths. (Unit=0·01 in log *W*)

	Na	*Mg*	*H*
δ^2	39·4±7·6	27·6±5·4	48·0±8·9
σ_a^2	14·2±2·3	6·0±1·5	12·3±2·5
σ_b^2	14·4±2·3	6·5±1·1	0·2±0
σ_c^2	5·1±0·7	2·9±0·5	5·1±0·7
σ^2	33·7±3·3	15·4±1·9	17·6±2·6
$\delta^2-\sigma^2$	+5·7±8·3	+12·2±5·7	+30·4±9·3

(*b*) Central Intensities. (Unit=0·001 in Δ log *I*)

	Fe (*a*)	*Fe* (*b*)	*Fe* (*c*)	*Cr*	*Ba*$^+$
δ^2	403±70	216±36	660±118	249±44	456±82
σ_a^2	175±30	108±19	471± 96	131±23	251±53
σ_b^2	86±15	50± 9	53± 10	176±31	1
σ_c^2	92±16	164±27	55± 10	92±16	83±15
σ^2	353±37	322±34	559± 97	399±42	335±55
$\delta^2-\sigma^2$	+50±79	−106±49	+101±153	−150±61	+121±98

In these two tables, first appears δ^2, the observed dispersion as described above with its s.e. calculated from the formula* $\delta^2\sqrt{2/(n-1)}$, next come the three contributions to the dispersion, (*a*) calculated as in Table II, (*b*) the dispersion due to a s.e. of ±0·85 tenths of a spectral type, (*c*) the dispersion due to a s.e. of ±0·56 in absolute magnitude. The rate of change of intensity with spectral type is in all cases fairly uniform, but the change with *M* varies rapidly among supergiants (see Fig. 1); consequently the allowance for errors in *M* would be improved by a further breakdown into luminosity groups, but the quantity of material did not warrant it. In the next row appears σ^2 the sum of the three preceding entries, i. e. the square of the total calculated dispersion due to the various observational errors. Finally appears the difference $\delta^2-\sigma^2$, that is the amount by which the square of the observed dispersion exceeds that of the observational error. Standard errors of all these quantities, calculated in the usual manner, are tabulated.

5. *Discussion of the observed residual dispersions in line-intensities.*—It will be seen that in all three cases of Table III (*a*), $\delta^2-\sigma^2$ is positive and in the case of

* When the error curve has appreciable kurtosis this quantity should be multiplied by the factor $(1+(\beta-3)/n)^{\frac{1}{2}}$ (Yule and Kendall, *Introduction to Theory of Statistics*, p. 400). This has in fact been done for Table III (*a*) for the s.e. of δ^2 and σ_a^2. But the correction was always small and the refinement was not carried out for Table III (*b*).

Mg and *Hβ* considerably exceeds its s.e. Further, in Table III(*b*), $\delta^2 - \sigma^2$ is positive in three out of five cases. These results suggest that in a group of K stars of identical spectral type (*Sp*) and absolute magnitude *M* there is a real dispersion in intensities of certain lines, especially *Hβ* and *Mg* 5183, due to physical factors.

Before we can consider the reality of these residual dispersions as established we must examine further the meaning of the terms *Sp* and *M* and their computed errors. Spectral type and spectroscopic absolute magnitude are both defined as corresponding to the weighted mean of certain criteria—i. e. line-intensities or ratios of line-pairs used by various observatories.*

The error of *Sp* or *M* is composed of two parts, (1) a purely observational error which tends to be eliminated by repeating observations or by multiplying the criteria, (2) an error inherent in the criterion itself whereby certain stars of identical *Sp* or *M*, as determined by criterion *A*, will differ when criterion *B* or *C* is used.

Our determination of σ_b^2 by a straight intercomparison of different classifications would be composed entirely of observational errors (1) if identical criteria were used. As it is, there is a slight amount of overlap of the criteria; e. g. *Ca* 4227 is used by all three observatories while *H*/*Fe* is used by Mt. Wilson and Harvard. σ_b^2 is thus composed of both (1) and (2).

Now it might be objected that in view of the partial correlation of *Sp* due to overlapping criteria σ_b^2 has been underestimated and that if proper allowance were made the residual dispersions of Table III would disappear completely. This begs the question of intensity-dispersion in a group of stars of the same *Sp* and *M*. If, as seems highly probable, the use of different criteria leads to varying estimates of *Sp* and *M* owing to imperfections of the criteria, this is only another way of saying that there *are* differences in intensity for a given *Sp* and *M*. It is not so much begging the question as the answer, in that the critic assumes the truth of the proposition which he is endeavouring to disprove. It might further be objected that σ_c^2 has been underestimated owing to the use of the same calibration data (trigonometrical parallaxes, double stars, etc.) in the determination of *M*: but these will involve systematic errors in *M* which do not concern us after reduction to standard *Sp* and *M*, although they may of course affect the shape of the curves of Fig. 1B.

What does emerge from this discussion is that if we observe a dispersion in intensity for a given line *A* in a group of stars of the same *Sp* and *M* as determined by criteria *B* and *C*, then the dispersion may be attributable to variations in the lines *A*, *B* or *C*. In practice "*B*" and "*C*" correspond to a number of lines due to different elements as observed at different observatories; *A* corresponds to one line or to closely related lines (usually in the same multiplet) of one element. It is therefore more reasonable to suppose that the residual dispersions of Table III, when significant, are due chiefly to variations in the observed line, and not to the imperfections of criteria *B* or *C*.

In the writer's opinion there are more insidious dangers of having underestimated σ_a^2 from comparing but two (or sometimes three) measures of the same

* For the various criteria of spectral type see H. E. Butler and A. D. Thackeray, *M.N.*, **100**, 455, 1940, Table II, and of absolute magnitude see W. S. Adams, A. H. Joy, M. L. Humason and A. M. Brayton, *Ap. J.*, **81**, 188, 1935, and R. K. Young and W. E. Harper, *Publ. D.A.O.*, Victoria, III, 7, 23, 1924.

star than of having underestimated σ_b^2 or σ_c^2. However, inspection of Table III (*a*) shows that in order to explain away the residual dispersions of *Mg* and $H\beta$ in this way, it would be necessary to increase σ_a^2 threefold and this may be regarded as excessive. We are thus led to the conclusion that there probably is a small dispersion in line-intensities in stars of type G5 to K5 (particularly for *Mg* and $H\beta$) over and above what may be attributed to differences in type and luminosity.

6. *Interpretation of the residual dispersions.*—Accepting the reality of some of the observed residual dispersions of Table III, it is of some interest to enquire into the various physical factors which may contribute to them. It is well known that the equivalent width of a line depends primarily on the ratio of line to continuous absorption in the atmosphere, and hence upon a great many physical factors. Thus, the line-coefficient, dependent on the number of atoms in the appropriate energy level, is a function of temperature and pressure at standard optical depth, the excitation and ionization potentials and the abundance of the element: the continuous absorption, still imperfectly understood, depends on the concentration of electrons provided by all elements, of negative ions and probably also of molecules in K-type stars. The line-absorption may also be affected by such factors as Doppler motions (thermal, turbulent or rotational), re-emission within the line, collision effects upon the damping constant, Stark effect and (as recently discovered by H. W. Babcock) by Zeeman effect due to general or localized fields. Oscillator strengths are of course eliminated in our comparison of the same line in different stars.

In recent years the standardized procedure of building up a "curve of growth" (*W*, *Nf*) has provided a powerful method of allocating physical variables to individual stellar atmospheres. Stellar spectrographs of high dispersion, knowledge of laboratory *f*-values and work on the theory of formation of absorption lines have united to favour this procedure. In the present work a different approach is used. Instead of concentrating on one star (observationally more convenient when using high dispersion) and comparing lines formed in one atmosphere with the same lines produced in a controlled and highly simplified laboratory tube, we compare the same line (or group of closely related lines) produced in a number of different atmospheres which superficially resemble each other rather closely. In doing so we build up two other curves of growth (*W*, *Sp*) and (*W*, *M*) which have hardly been studied at all spectrophotometrically. Yet, if more theoretical work were done in relating spectral type and absolute magnitude to the physical variables in a normal stellar atmosphere, such curves might well yield valuable new information.

The procedure described in Section 4 above effectively reduces line-intensities in some 80 stars to a standard *Sp* and *M* and yields individual deviations δ from the normal intensity in those standard conditions. If one could demonstrate that many lines due to the same element in one star showed individual deviations of similar sign and magnitude, we might be justified in inferring that the deviations were due to abnormal values of the abundance of the relevant element. Unfortunately the only suitable case for such an intercomparison is provided by the *Fe* groups (*a*), (*b*), (*c*) and little weight can be placed on group (*c*) as each line consists of an unresolved pair. The correlation coefficients for δ among these groups are +0·47 for (*a*) and (*b*), +0·36 for (*a*) and (*c*). These values are similar to others calculated for other pairs of lines due to different elements. This result throws doubt on the interpretation of the residual dispersions mainly in terms of abundance.

Even though the results on individual stars may be inadequate to provide positive information about differences in abundance, the residual dispersions of Table III may give some indication of a probable *upper limit* to the statistical dispersions in abundance. Suppose we have a group of stars of identical *Sp* and *M*. The width W of a given line is to be expressed as a function $f(x_1, x_2 \ldots x_r)$ of physical variables x_r of which the abundance ϵ of the relevant element is one. If we observe a dispersion $\tau^2(=\delta^2-\sigma^2)$ in the widths among the stars, then theoretically we may express it in the form *

$$\tau^2 = \Sigma\left(\frac{\partial f}{\partial x_r}\right)^2 \sigma^2(x_r),$$

provided the variables are independent, where $\sigma(x_r)$ is the dispersion of x_r in the group. In practice many of the variables are mutually dependent, but at the moment we are interested only in those which are dependent on the abundance ϵ, and of these the most important is clearly the atmospheric opacity. If ϵ makes no significant contribution to the opacity then

$$(\partial f/\partial\epsilon)^2\sigma^2(\epsilon) \leqslant \tau^2,$$

in other words the observed dispersion sets an upper limit to the dispersion of ϵ in the group of stars. Moreover we can express the upper limit numerically if we know $\partial f/\partial\epsilon$. The lines considered here are all strong enough to lie on the square-root portion of the curve of growth † for which $\partial \log W/\partial \log \epsilon = \frac{1}{2}$.

Let us now take some numerical examples from Table III to consider such upper limits. For *Mg* 5183 we find $\tau^2 = +12{\cdot}2 \pm 5{\cdot}7$. We can therefore say that τ^2 is unlikely to exceed 17·9, i. e. τ is unlikely to exceed 0·0423 in log W and, provided *Mg* makes no appreciable contribution to the opacity, an upper limit to its dispersion in log N is 0·0846. This corresponds to an upper limit of ± 20 per cent in abundance of *Mg*. Values of ± 18 and ± 29 per cent are similarly found for *Na* and *H* respectively. (With a Gaussian distribution this means that there is a chance of 0·32 *at most* of finding a star outside these limits; probably the chance is less.)

It is clear that the condition that the abundance be independent of the variables, and especially of the opacity, is a restrictive one which is hardly likely to be realized in the case of hydrogen. The relatively large residual dispersion found for *H* may well be due to other factors than abundance or, if it *is* due to variations in abundance, the upper limit of ± 29 per cent will have to be increased by some factor which makes proper allowance for the dependence of opacity on hydrogen abundance.

Let us consider now the qualitative effect of variations in atmospheric opacity which are *not* due to the element in question. Consider a "normal" star A of standard *Sp* and *M* (say K0, $M=0$) and another star B with higher atmospheric opacity but identical in other respects to A and particularly in the relative abundance of an element X. The increased opacity will tend to weaken all lines, and those formed at lowest levels most. Since the dominant lines in K types are all strengthening towards later types, the effect will be to a first approximation that the star with higher opacity will be classified earlier (say G8); there may be a

* David Brunt, *Combination of Observations* (1917 Edn.), p. 48, Cambridge.

† In justification of this we refer to the curve of growth derived by Miss S. E. A. van Dijke (*Ap. J.*, **104**, 36, 1946) for α Bootis. Collisional effects which may distort the upper portion of the curve of growth are likely to be negligible in the giants to which the present data nearly all refer (A. Unsöld, *Sternatmosphären*, Table 65, p. 343).

relative strengthening of "enhanced" lines, characteristic of the solar chromosphere, which would mean that the star would be classified brighter than $M=0$ (say $M=-1$). The important question is whether a (K0, $M=0$) star classified as (G8, $M=-1$) due to a high value of k, will differ from a normal (G8, $M=-1$) star, which we may denote C, in the intensity of any selected line due to the element X. To a first approximation we may expect that if the abundance of the element X is the same in all three stars A, B, C, they will show the same deviation δ in our analysis *despite the difference in opacity of B*. It will be noticed that this argument once again assumes the opacity to be independent of the abundance of X.

The remarks of Section 5 relating to criteria of classification also have some bearing on the question of upper limits to the abundance-dispersion. If the relevant element X is used as a criterion for *Sp* and *M*, then changes in the abundance of X will produce, in part, errors of classification, similar to those due to opacity in the hypothetical case above. This complication does not arise for *Na* or *Mg*, but *H* is used as a criterion, as are lines due to *Fe* and *Cr*, and it is of interest to note that the latter two elements provide the only two negative cases of τ^2 in Table III. Possibly some improved method could be devised for estimating σ_b^2 and σ_c^2, when the element concerned is used as a criterion for *Sp* and *M*, but none has occurred to the writer.

The reader will appreciate that in view of the numerous complications the upper limits set to abundance-dispersions by the results of Table III can only be taken as indicating orders of magnitude. It is true that the method of comparing a few lines in a large number of similar stars does not enable one to explain individual deviations in terms of any one of the physical factors. But the position is not dissimilar to that of building star-models on the three parameters T_e, L and chemical composition, combined with a theoretical opacity law for the interior, and this latter procedure forms one of the corner-stones of modern ideas about hydrogen abundance. Our group of stars reduced to standard *Sp* and *M*, corresponding to one point in the Russell-Hertzsprung diagram, must have nearly constant surface temperature and gravity; there may be a small dispersion * even so in T and P_e, but this does not affect the argument presented above with regard to upper limits to the abundance-dispersion.

One final remark must be made about this question of abundance. If there are progressive changes in abundance with type and luminosity these will be reflected in the curves of Fig. 1 and will have been eliminated in our method of analysis. The results refer to the standard *Sp* and *M*, and most of the stars considered are *giants* of type G5 to K5.

7. *Intensity-deviations in individual stars.*—In Table IV the results for individual stars are summarized. The first column gives the number of the star in Schlesinger's 1930 Bright Star Catalogue, the second the name of the star. The third column gives the mean type (weighted mean of *W*, *V* and *H*) followed by corrections (in units of a twentieth of a spectral type) derived from the data as described below. In the fourth appears the absolute visual magnitude (mean of Mt. Wilson and Victoria) followed by a correction, also derived from this material, in units of $\frac{1}{2}$ mag. Then follows under each element the tabular quantity δ/σ, i. e. the observed deviation from the mean for the given star's type and magnitude, *in units of the total observational error for that line*, found as in Table II. The column headed *Fe* refers to the mean of the three groups of *Fe* lines (*a*), (*b*) and (*c*) weighted in the ratio 3, 2, 1 (see Table I).

* Pointed out by a referee.

TABLE IV

Summary of Individual Deviations

(Unit=standard error for each line)

1930 BSC	Star	Type		M_v		$H\beta$	*Na*	*Mg*	*Fe*	*Cr*	Ba^+	*Ti*
165	δ Andr	K3	+2	0·8	+1	+2	+1	+3:	+2:	+1	0	0
168	α Cass	G75	+1	0·0	0	0	+1	+1	0	0	0	0
402	θ Ceti	K0	−1	1·8	−1	+2:	−2	0	−1	−1	+1	0
464	51 Andr	K2	+3	0·8	+1	+2:	+1	+2	+3	+1	−1	0
509	τ Ceti	G6	−1	5·8	0	0:	−2	+1	0:	0	0:	+2
603	γ^1 Andr	K1	+3	−0·6	−1	+2:	+1	+2	+1	+2	0	+1
617	α Arie	K15	−1	0·8	+2	+2:	−1	+2	−1	−2	0	−1
834	η Pers	K35	+1	−2·2	+1	−1	−2:	0	−1	−2	0	0
941	κ Pers	G85	+2	1·2	+1	+1:	+1	+1	0	+1	−1:	0
1030	ο Taur	G7	−5	0·4	0	0:	0	−3	−3	−2	−1:	−1:
1084	ε Erid	K15	0	6·1	−1	0	−1	−1	+2	0	+1:	−1
1136	δ Erid	G95	+3	4·6	−1	−1:	+2	+1	+1	0	0:	0
1256	37 Taur	K0	0	1·1	+1	0:	+1:	−1:	0:	0:	0:	−1:
1325	o^2 Erid A	K0	0	6·0	+2	0	0	+2	−1	0	−1	−1
1346	γ Taur	G8	+2	1·0	−1	+4:	+1	0	0	+1	+1	0:
1373	δ Taur	G85	−1	1·2	−3:	+2:	+1	−2	0	0	+2:	+2:
1409	ε Taur	G8	+3	1·4	+1	+2:	+1	+1:	+1:	0:	0:	+1:
1457	α Taur	K75		0·2		+2:	...	...	...	...	+1:	...
1577	ι Auri	K35	−1	−0·5	0	+1	0	+1	+1	0	0	+1
1612	ζ Auri	K4		−2·5		...	−4	+1	−8	−8	−3	−5
2012	ν Auri	K05	−2	1·0	−2	+0:	−0:	−4:	−1:	−1:	+2:	0:
2473	ε Gemi	G8	+2	−2·0	0	−1	+1	+1	+2	0	0	0:
2973	σ Gemi	K05	+1	1·2	+2	+1:	+1:	0:	0:	0:	−2:	+1:
2985	κ Gemi	G7	+1	0·9	0	+1	+1	0	0	+1	0	0
2990	β Gemi	G9	+1	1·6	+1	+2	+1	0	0	0	+1	0
4057	γ^1 Leon	G85	−1	0·5	+1	−1	−1	+1	−1	0	0	−1
4058	γ^2 Leon	G5	0	1·0	0	−3:	0	−1	...	...	0:	−1:
4069	μ U Maj	K45		0·3		−1	...	...	...	...	−1:	−2
4301	α U Maj	G6	+4	0·7	−1	−1	+1	+1	+2	+2	0	0
4335	ψ U Maj	K05	0	1·0	−2	0	−1	0	+1	+1	+1	−1
4377	ν U Maj	K2	0	−0·1	−2	−2:	−1	+1	−1	+1	+1	0:
4518	χ U Maj	K05	−4	0·3	+1	−1	−3	0	−2	0	−2	−1
4608	ο Virg	G55	−3	0·3	+1	−2:	−0	−2	−2	−1	...	...
4932	ε Virg	G65	−1	0·9	0	+2:	0	0	0	0	−1	+2
5340	α Boot	K0	0	0·2	+2	+1	−2	+4	−2	0	−1	0
5429	ρ Boot	K25	0	0·4	+1	−2	−3	+2	+1	+1	−1	0:
5502	ο Boot	G7	−2	0·6	+1	−1	−1	0	0	−1	+1	−2
5506	ϵ^1 Boot	G75	+3	0·4	0	+3:	−1	+1	+1	+2	0	+2
5544	ξ^1 Boot	G6	−1	5·3	−1	0	−1	0	0	0	+2:	0:
5563	β U Min	K45		−0·4		−2:	..	..	..	..	0	..
5602	β Boot	G45		0·5	−1	0	...	...	...	...	+1:	...
5681	δ Boot	G5	+4	1·0	−1	−1:	+2	0	+1:	+2	+1	+2:
5744	ι Drac	K15	+1	0·9	+2	−2	0	+1	0	0:	−1	0
5854	α Serp	K2	+1	1·2	−1	−2	+1	0	+1	0:	+1	+2
5901	κ Cor B	K1	0	2·3	+2	0:	0	0	0	−1	0:	...

TABLE IV.—*Continued*

1930 BSC	Star	Type		M_v		$H\beta$	*Na*	*Mg*	*Fe*	*Cr*	Ba^+	*Ti*
5947	ϵ Cor B	K1	−1	0·6	+1	−2:	−1	−1	−1	0	−2:	−2:
6075	ϵ Ophi	G8	−4	0·7	0	0	−1	−2	−3	−2	−1	...
6132	η Drac	G55	+2	1·2	−1	+1	+1	−1	+1	+1	0	0
6220	η Herc	G6	−1	1·0	+1	−1	0	0	−1	0	−2	−1
6299	κ Ophi	K2	−1	1·4	+2	−2	0	0	−1	−1	0	0
6418	π Herc	K4	0	0·0	0	0	−1	−1	0	0	0	...
6603	β Ophi	K15	+3	1·1	0	−2:	+2	+2	+3	+1	+1	+1
6623	μ Herc	G45		3·9		+1:	...	...	...	...	+1	...
6688	ξ Drac	K25	+1	1·2	+2	−4:	0	+1	+1	0	0	0:
6695	θ Herc	K1	0	−1·1	0	−0	−1	+1	+2	0	−1	0
6698	ν Ophi	G9	+1	0·5	−1	+2:	+2	0	0	0	0:	−1:
6703	ξ Herc	G75	−1	1·0	0	+2	0	−1	−1	0	0	0
6705	γ Drac	K45		0·1		−1	...	...	...	...	...	0
6752	70 Ophi A	K1	−1	5·6	−1	−2	+1	−3	−1	0	0	−1
6869	η Serp	G9	−2	1·7	−1	−2:	0	0	−2	0	+2:	−1:
6872	κ Lyra	K15	0	1·6	−3	−2	0	−2	+1	0	+1	0
6895	109 Herc	K2	0	1·1	0	−2:	0:	−1:	...	0	*	−1:
7310	δ Drac	G85	−2	0·7	+1	+2	−2	−1	−1	+1	−1	−1
7314	θ Lyra	K1	−1	−0·8	0	+1:	0	−1	−1	−1	+1	0
7525	γ Aql	K3	0	−0·6	−1	0:	0	−2	+1	0	+1	0
7602	β Aql	G8	0	3·7	−1	+2	0	0	0	0	+1:	0:
7615	η Cygn	G95	0	1·5	0	0	+1	0	0	0	0	+1
7949	ϵ Cygn	G85	−1	1·0	+1	+2:	0	−1	0	0	−2:	+1
7957	η Ceph	G7	+1	3·3	0	+1	−1	0	+2	0	+1	0
8079	ξ Cygn	K45		−1·8	+1	−4:	...	+2:	...	...	+1:	+2:
8115	ζ Cygn	G55	−2	−0·4	+2	−4	0	+1	−1	−2	0	−2:
8308	ϵ Pegs	K1	+3:	−2·0	+2	−1:	−1	+4	+1	+2	0	+1
8465	ζ Ceph	K35	−1	−2·2	+1	+1	−3	−1	−2	−4	−1	0
8572	5 Lacr	K45		−2·3	0	+1:	−3:	...	...	...	0:	0:
8667	λ Pegs	G65	+1	0·4	−1	0	0	0	+1	+1	0:	+1
8694	ι Ceph	K0	+1	1·1	−2	+3	0	−1	+1	+1	+2	0
8961	λ Andr	G7	+5	2·4	−1	−4:	+1	+2	0	+2	...	−2
8974	γ Ceph	K1	0	2·7	0	0:	0	0	+1	0	0	0

* Very weak.

8. *Corrections to Type and Absolute Magnitude.*—In certain cases lines appear systematically strong or weak for the corresponding spectral type. Thus an attempt at improvement of spectral type on the basis of these quite independent measures may be justified. (It must be remembered that the classifications are based on an entirely different set of lines in the photographic region.)

The deviation from the normal for *Sp* and *M* could be transformed into a correction for *Sp* by means of Fig. 1A. Such corrections were calculated for the measured lines of *Na*, *Mg*, *Fe* and *Cr*. All three groups of *Fe* lines were lumped together as one unit, being weighted $(a):(b):(c)::3:2:1$. For stars earlier than K0 the four sets of lines were given equal weight; for stars of type K0 and later *Na* and *Cr* were given double weight owing to their greater sensitivity to

type. The correction thus derived appears in the third column of Table IV in units of 0·05 spectral type.

A similar correction to absolute magnitude was calculated on the basis of Fig. 1B. Lines due to *Mg*, *Fe* (*b*), Ba^+ and *Cr* were used. Since the standard error of such corrections must be of the order of 0·5 mag. they have been rounded off and appear in the fourth column of Table IV in units of 0·5 mag.

9. *Discrepancies between spectroscopic and trigonometric parallaxes.*—Attempts to correlate such discrepancies with the intensity deviations of Table IV proved disappointing. (Both quantities must of course include a large proportion of observational error.) There is a weak correlation with *Mg* deviations in the sense that when $\pi_t - \pi_s > 0$ *Mg* 5183 tends to be strong; this is probably due to π_s being underestimated—as a consequence of its luminosity effect, *Mg* 5183 will then appear strong for its class. The corrections to luminosity listed in Table IV will in fact go some way towards explaining significant discrepancies between π_t and π_s; see for example, κ Lyra, κ Ophi, ζ Cygn, κ Cor B, δ Taur, ξ Drac, ι Drac and o Boot; on the other hand, for the well-known case of α Boot and for ι Ceph the discrepancy is increased.

The most interesting case is that of ζ Aurigae. In the analysis the Mt. Wilson value of M_v ($-2{\cdot}5$) for this star was used alone. Nearly all the lines appeared too weak and it was at first thought that this was due to the presence of the B-type spectrum, although this should affect the visual spectrum far less than the photographic. However, *Mg* 5183 appears slightly *too strong* for type K4 and $M_v = -2{\cdot}5$. As this is the only line in Fig. 1B which increases from supergiants to normal giants, the measures are entirely accordant with a large luminosity correction. The best determination that can be made from these data, using all the lines, is $M_v = +0{\cdot}5$. In other words, the visual spectrum of ζ Aurigae on our plates is that of a *normal giant*, not a supergiant *; the two plates used were both taken on 1939 March 10, phase 0·69. I am indebted to Dr A. Beer for calculating that on this date 55 per cent of the K disk visible at the Earth was exposed to radiation from the B star.

The intensity deviations found for ζ Aurigae were regarded as special cases and were not indicated in the foregoing statistical discussion.

10. *Subgiants.*—The interesting group of subgiants lying between the normal giants and the dwarfs calls for special comment. The lines *Mg* 5183 and *Fe*(*b*) provide rather sensitive criteria for these stars. All five stars whose absolute magnitudes (mean of Mt. Wilson and Victoria) are greater than $+2{\cdot}0$, and yet are not dwarfs, are confirmed by our measures as subgiants: the stars are κ Cor B, γ Ceph, λ Andr, β Aqil and η Ceph. Further, luminosity corrections bring the following stars into this category (Victoria values of M_v are given in brackets): σ Gemi (2·0), α Arie (1·2), ξ Drac (1·8) and κ Ophi (2·2).

11. *Discussion of Variations of Intensity with Type and Luminosity.*—The material of Fig. 1 provides useful data for comparison with the predictions of ionization theory. It is true that the smallness of the spectroscopic dispersion involves incalculable risks in the measures due to blends with faint lines; these risks are almost certainly greater in considering the curves of Fig. 1 as reflecting real variations of one line than in considering the quantities in Table IV as reflecting

* W. E. Harper, in *D.A.O.*, III, 156, 1927, revised the earlier Victoria determination of M_v from $+0{\cdot}6$ to $-0{\cdot}5$.

TABLE V

Mean Widths and Central Intensities

BSC	Star	Type	M_v	Equivalent Widths (Unit=0·1 A.)			Measured Central Intensities, $100A \log_{10} I$									Number of plate
				$H\beta$	5183 *Mg*	D_2+D_1	$H\beta$	*Mg*	D_2	D_1	*Fe* (*a*)	*Fe* (*b*)	*Fe* (*c*)	*Cr*	*Ba*+	*Ti*	
165	δ Andr	K3	0·8	15	27:	50	22	44:	33	25	29:	14:	27:	22	14	15	3
168	α Cass	G75	0·0	14	14	28	28	30	17	14	19	11	19	13	14	14	2
402	θ Ceti	K0	1·8	14:	17	21	27	34	15	11	19	10	19	13	15	14	2
464	51 Andr	K2	0·8	14:	23	42	24:	44	30	21	30	16	23:	21	11:	13:	2
509	τ Ceti	G6	5·8	15:	22	20	32:	41	15	12	16	05:	19:	10	10:	14	2
603	γ^1 Andr	K1	−0·2	17:	20	41	29:	40	23	19	26	15	25	20	15	16	2
617	α Arie	K15	0·8	14	22	28:	27	38	16:	14:	21	11	21	14	13	12	2
834	η Pers	K35	−2·2	16	19	49	38	38	33	27	31	22	29	26	22	22	2
941	κ Pers	G85	1·2	14:	17	26	27	31	20	12	21	09:	20	14	09:	13	2
1030	ο Taur	G7	0·4	13:	11	23	24:	23	14	13	15	07:	15:	09	10:	12:	2
1084	ε Erid	K15	6·1	14	28	39	29	48	25	20	26	08	28	18	14:	11:	3
1136	δ Erid	G95	4·6	13:	23	36	23:	39:	27	21	22	09	22	14	13:	11:	2
1256	37 Taur	K0	1·1	12:	17:	29:	22:	32:	19:	16:	21:	11:	20:	13:	13:	12:	1
1325	o^2 Erid A	K0	6·0	14	31	33	23	48	21	15	19	06	21:	13	09	10	2
1346	γ Taur	G8	1·0	18:	15	26	40:	34	19	13	20	10	24	14	16	13:	2
1373	δ Taur	G85	1·2	14:	14	27	35:	28	16	13	18	10	21	12	17:	15:	2
1409	ε Taur	G8	1·4	14:	15:	25	28:	31:	17	15	21	13	20	12:	12:	13:	2
1457	α Taur	K65	0·2	14:	24*	45	26	32:	27	22	29	15	26	29	15	16	2
1577	ι Auri	K35	−0·5	14	21	48	36	42	31	25	28	18	29	26	16	20	2
1612	ζ Auri	K4+B	−2·5	(23:)	19	51	37	30	33	24	24	16	20	22	14	17:	2
2012	ν Auri	K05	1·0	12:	13:	30:	28:	28:	19:	16:	22:	09:	21:	13:	18:	12:	1
2473	ε Gemi	G8	−2·0	18	14	36	39	30	26	18	27	20	25	19	21	19	2
2973	σ Gemi	K05	1·2	13:	18:	35:	28:	29:	22:	19:	20:	10:	27:	15:	08:	14:	1
2985	κ Gemi	G7	0·9	14	15	23	30	31	15	11	19	09	17	13	11	11	2
2990	β Gemi	G9	1·6	15	17	26	29	32	17	13	20	08	24	12	14	13	3
3748	α Hyda	K45	−0·5	...	...	50:	...	...	29:	22:	32:	17:	...	27:	...	...	1
4057	γ^1 Leon	G85	0·5	12	17	22	23	30	15	11	18	13	18	13	12	11	3
4058	γ^2 Leon	G5	1·0	10:	12	20	25:	23	13	10	15	08	13:	10	11:	10:	3
4069	μ U Maj	K45	0·3	10	19*	41	25	26	26	20	28	16	24:	27	12:	13	2
4301	α U Maj	G6	0·7	12	14	23	24	28	14	11	20	11	16	14	13	11	2
4335	ψ U Maj	K05	1·0	12	17	25	23	33	18	12	23	12	21	17	15	12	2
4377	ν U Maj	K2	−0·1	10:	21	34	25:	35	21	17	24	15	21	22	17	15:	2
4518	χ U Maj	K05	0·3	11	17	27	26	30	13	09	20	11	18	15	10	11	2
4608	ο Virg	G55	0·3	10	11	22	35:	22	11	10	15	08	...	10	...	...	2
4932	ε Virg	G65	0·9	15:	14	21	35	26	13	10	16	09	...	10	11	14	2
5340	α Boot	K0	0·2	13	22	24	24	33	13	09	19	12	18	15	11	13	2
5429	ρ Boot	K25	0·4	10	22	27	26	40	17	14	26	16	25	22	12	15:	2
5502	ο Boot	G7	0·6	11	14	20	29	29	14	10	18	09	19	11	14	12	3
5506	ϵ^1 Boot	G75	0·4	17:	16	22:	30	32	16:	10:	21	13	20:	16	13	16	2
5544	ξ^1 Boot	G6	5·3	16	18	23	35	35	15	11	15	05	24:	11	16:	19:	2

5681	δ Boot	G5	1·0	12	13	27	27	29	16	12	17	09	18	09:	13:	13	2
5744	ι Drac	K15	0·9	10	21	33	19	37	20	17	24	12	21	17	12	13	2
5854	α Serp	K2	1·2	10	20	40	23	37	25	19	25:	13	24	18:	15	15	2
5901	κ Cor B	K1	2·3	12:	20	30	22:	37	20	18	22	09	25:	14	11:	08:	2
5947	ϵ Cor B	K1	0·6	09:	18	29	24	35	19	13	22	12	16:	16	09:	10:	2
6075	ϵ Ophi	G8	0·7	13	13	21	27	27	13	10	15	08	17	11	11	10	3
6132	η Drac	G55	1·2	14	13	22	27	27	16	10	17	09	17	11	11	12	3
6220	η Herc	G6	1·0	12	13	21	24	24	15	10	15	08	14	10	08	10	2
6299	κ Ophi	K2	1·4	09	20	35	21	37	22	15	22	11	22	16	12	13	2
6418	π Herc	K4	0·0	12	20	44	26	38	29	22	28	16	28	22	13	18	3
6603	β Ophi	K15	1·1	10:	22	39	28:	44	30	21	27	14	27:	20	14	15	2
6623	μ Herc	G45	3·9	16:	17	21	24:	30	13	10	16	07	17	10	10:	09	2
6688	ξ Drac	K25	1·2	07:	23	38	20	43	25	16	25	12	21	19	12	13	2
6695	θ Herc	K1	−1·1	18	17	32	34	36	22	18	29	21	22	21	14	18	2
6698	ν Ophi	G9	0·5	15:	16	35	28:	33	22	15	28:	12	20	14	14:	11:	2
6703	ξ Herc	G75	1·0	14	14	22	29	27	14	13	17	08	17	12	12	11	2
6705	γ Drac	K45	0·1	10	23*	49	26	40	33	28	30	19	25	28	14	17	2
6752	70 Ophi A	K1	5·6	12	22	40	23	39	23	20	21	07	24	15	11	10	2
6869	η Serp	G9	1·7	10:	15	24	28:	31	15	13	17	07	21:	12	18:	10:	2
6872	κ Lyra	K15	1·6	09	16	30	26	36	20	14	25:	12	21	17	15	13	2
6895	109 Herc	K2	1·1	09:	19:	34:	19:	42:	19:	15:	18:	12:	21:	18:	vw	11:	1
7310	δ Drac	G85	0·7	16:	15	19	30:	29	11	09	19	09	19	14	11	11	2
7314	θ Lyra	K1	−0·8	20:	15	36	36	33	23	19	24	16	23	17	19	17	2
7417	β Cygn	K0	−0·5	...	...	35†	...	...	...	...	...	...	...	...	...	...	2
7525	γ Aqil	K3	−0·6	15:	22	47	34:	39	27	21	28	17	30	24	16	16	2
7602	β Aqil	G8	3·7	19	17	26	22	31	16	13	19	07	18	12	14:	12:	2
7615	η Cygn	G95	1·5	12	16	25	24	31	15	11	18:	10	18	13:	13	13	2
7949	ϵ Cygn	G85	1·0	17:	15	24	26	30	15	13	18	09	23:	12	09	14	2
7957	η Ceph	G7	3·3	15	18	19	28	34	14	11	21	07:	21	11:	13	11	2
8079	ξ Cygn	K45	−1·8	14:	23	54	42:	43	35	28	31	23	28	30	23:	27:	2
8115	ζ Cygn	G55	−0·4	11	13	23	28	28	16	13	17	09	16	09	13	11:	2
8308	ϵ Pegs	K1	−2·0	16:	22	46	49	41	30	22	30	22	29	26	21	22	2
8465	ζ Ceph	K35	−2·2	19	17	40	44	33	28	22	30	22	26	22	20	21	2
8572	5 Lacr	K45	−2·3	18:	14*	47	42:	35:	28	24	29	23	...	31:	22:	25:	2
8667	λ Pegs	G65	0·4	13	13	22	32	25	15	10	19	11	18	13	14	15	2
8694	ι Ceph	K0	1·1	15	16	27	32	35	17	12	22	12	24	16	17	14	2
8961	λ Andr	G7	2·4	10	19	24	20:	28	15	13	16	09	16	15	...	07	2
8974	γ Ceph	K1	2·7	12	21	30	20	40	21	15	23	10	23	15	13	11:	2

* Corrected for *TiO* band absorption

† From two plates at different setting of spectrograph ; not used in the analysis.

vw, very weak.

: Observation given half-weight.

Column 1.—Number of star in Schlesinger's 1930 Bright Star Catalogue.
,, 2.—Name of star.
,, 3.—Spectral type : weighted mean of Victoria (4), Mt. Wilson (3) and Harvard (1) classifications.
,, 4.—Absolute visual magnitude : straight mean of Victoria and Mt. Wilson determinations.
Columns 5, 6 and 7.—Measured equivalent widths of *Hβ*, *Mg* 5183, *Na* (D_1+D_2) in units of 0·1 A.
,, 8-17.—Measured central intensities $100A \log_{10} I$ for various lines or groups of lines of Table I of paper.
Column 18.—Number of plates.

true deviations from the average for each star's type and luminosity. Nevertheless certain trends which are well established will be discussed below.

Variation with spectral type (for giants with $M_v = 0$): (see Fig. 1A)

(*a*) Ba^+ 4934 shows a very flat maximum at type K0 to K1. This is of course in accord with the predictions of ionization theory for the resonance line of an ionized atom, and a maximum at such low temperature is to be expected for an atom with low I.P. (5·1) like *Ba*.

(*b*) None of the other lines measured, due to neutral metals, show a maximum, even though several have E.P. greater than 1·5 volts and might therefore be expected to do so at about K0. In particular *Mg* 5183, for which H. N. Russell * predicts a maximum at G9, increases in strength as far as the observations extend up to type K5; thereafter the effect of neighbouring *TiO* absorption becomes severe.

(*c*) The three groups of *Fe* lines with E.P. 0·1, 0·9 and 2·8 volts all increase at roughly the same rate; in the table below we compare the observed increase from type G6 to K4·5 with Russell's calculations for giants for *Fe* 4383 (E.P. 1·5) from $5040/T = 1{\cdot}1$ to 1·4 modified simply by the term $5040E/T$ for differences in excitation potential E.

Observed and predicted change of Fe lines from type G6 to K4·5

Line-group	E.P.	Observed $\Delta \log W$	Predicted $\frac{1}{2}\Delta \log N$
Fe (*b*)	0·1	+0·27	+0·23
Fe (*a*)	0·9	+0·26	+0·11
Fe (*c*)	2·8	+0·21	−0·17

The comparison of $\Delta \log W$ is to be made with $\frac{1}{2}\Delta \log N$ as all the lines are strong enough to lie on the square-root branch of the curve of growth. Since Russell's calculations, Wildt † has shown the importance of negative ions to the opacity of low-temperature atmospheres. This has the effect of diminishing the number of atoms N to about one-third but the weakening affects all the lines in the same proportion provided there is no important stratification causing lines of different E.P. to be formed at different depths. Making reasonable assumptions as to the values of P_e in the giant range from G6 to K4·5 we find that the increase in opacity due to negative ions is practically constant in this range. Hence the influence of negative ions cannot affect the conclusion to be drawn from the comparison with Russell that while the rate of change of the lines of lowest E.P. is of the correct order of magnitude, those of higher E.P. change too rapidly or even with the wrong sign. This result is only another example of the well-known Adams-Russell phenomenon in which lines of high E.P. appear too strong among giants of low temperature.

(*d*) The rapid increase of the *Na* resonance lines is not surprising (in fact it is not as rapid as theory predicts) but that of the subordinate lines of *Cr* is remarkable (see Fig. 1C). Both these sets of lines show a marked acceleration in rate of growth at type K0. The *Na* curve begins to flatten out at K3 but the observations do not extend to sufficiently late types to reveal the known falling-off in intensity in M giants.

* H. N. Russell, *Ap. J.*, **78**, 290, 1933.
† R. Wildt. *Ap. J.*, **89**, 295, 1939.

(*e*) In contrast with *Cr*, the two *Ti* lines (having much the same I.P. and E.P. as *Cr*) increase very slowly. Although the *Ti* lines are rather weak, this distinction from *Cr* cannot be attributed to a curve of growth effect, as both lines start from practically the same intensity at G5. It is believed that the slow increase of *Ti* lines may be associated with the commencement of molecular formation in K stars. The peculiarities of *Ti* lines in ρ Cassiopeiae at the stage when *TiO* bands were present has been noted elsewhere.

Variation with Absolute Magnitude

(*a*) The general rule, as is well known, is for most lines to appear very strong in supergiants; there is usually rapid increase from normal giants to supergiants and a much less pronounced difference between normal giants and dwarfs. The chief exception to this rule among the lines studied here is *Mg* 5183 whose peculiar strengthening from supergiants to dwarfs, in contradiction of theory, formed the subject of an earlier paper by the writer.*

(*b*) The most rapid increases among the supergiants are shown by Ba^{+} 4934 and *Fe* (*b*).

(*c*) The behaviour of *Fe* (*b*) with absolute magnitude is especially noteworthy in its continued decrease among the dwarfs (see Fig. 1B). The great strengthening in supergiants is another example of the strengthening of the weakest lines in multiplets in supergiants; these observations suggest that the phenomenon is associated more with supergiant characteristics than with M type, as was originally believed by the writer.† The three lines forming group *Fe* (*b*) are the satellite lines of multiplet No. 1 of *Fe* I in the "Revised Multiplet Table" and include λ 5250·2 which, as Evershed has remarked, is particularly sensitive to magnetic fields, having a Zeeman pattern with three times the normal separation.

(*d*) *Ti* is again exceptional in showing very little change throughout the whole range of absolute magnitude.

12. *Concluding Remarks.*—The foregoing paragraphs summarize a few points where theory seems to fail to account fully for the behaviour of the lines. The most notable instances are (*a*) the strengthening of weak lines in multiplets of supergiants, (*b*) the strength of *Mg* 5183 in dwarfs, (*c*) the failure of subordinate lines of the metals to show a maximum near type K0, (*d*) the relative insensitivity of *Ti* lines to type and absolute magnitude.

Little has been said in this paper of the problem of blends, but it is clear that, with moderate dispersion, all one observes is the cores of strong lines. Even on high dispersion the strong wings are found to be lost in the background of numerous lines in the spectra of these late type stars ‡; these wings must therefore form a quasi-continuum of absorption. In these circumstances it does not seem at all improbable that the whole normal basis for quantitative interpretation of line-strengths disappears. Processes which affect the line-core must dominate the apparent strength of a line. The effect of fluorescence or interlocking within multiplets has been mentioned on several occasions. Turbulence of course affects chiefly the line-cores but it is difficult to see how this could influence various lines so differently as we find here. Recently the effect of Zeeman patterns

* *M.N.*, **99**, 492, 1939. The writer regrets that in this paper he failed to notice that this behaviour of *Mg* 5183 in M dwarfs had previously been observed by Y. Öhman, "On the bands of Magnesium Hydride in Stellar Spectra", *Stockholm Obs. Ann.*, Bd. **12**, No. 8, p. 14.

† *M.N.*, **94**, 99, 1933.

‡ L. Spitzer, *Ap. J.*, **90**, 494, 1939.

due to stellar magnetic fields (localized or general) on the appearance of lines has been pointed out. If magnetic fields are responsible for the strength of the satellite lines (e.g. *Fe* (*b*) of this paper) in these late-type stars, then presumably the fields are localized in "star-spots" with different polarities, as Babcock* failed to find a general field in ϵ Pegs, one of the supergiants studied in this paper.

One conclusion is clear—the errors inherent in the measures are similar in size to those due to estimates of *Sp* and *M* (Table III). Thus the results on residual dispersions will not be appreciably improved by merely increasing the precision of the intensity-measures; improved types and magnitudes and, for such statistical discussions, the precisions of the various estimates must be known rather accurately. Extension of the material to include other lines would of course help to distinguish between explanations in terms of different physical factors. It would be of interest to follow up in this way those stars with the largest individual deviations in Table IV.

Acknowledgments.—The extensive observational material on which this paper is based could not have been obtained so rapidly without the welcome assistance of the following members of the staff of the Solar Physics Observatory and of visitors: T. G. Arthur, H. A. Brück, V. A. Goedicke, W. H. Manning, N. B. Slater, Professor F. J. M. Stratton and W. S. Tai.

The writer is also grateful to Professor R. O. Redman for a number of helpful criticisms.

Solar Physics Observatory,
Cambridge.
Radcliffe Observatory,
Pretoria:
1948 *October* 19.

* H. W. Babcock, *Ap. J.*, **105**, 105, 1947.

ON THE CONSTITUTION OF VENUS

K. E. Bullen

(Received 1949 May 13)

Summary

The constitution of Venus is discussed in the light of the density-pressure hypothesis stated by W. H. Ramsey. It is shown that on this theory, an increase in the precision of observations of the diameter of Venus may lead to a useful test on the question of the chemical homogeneity of the Earth's mantle. The bearing of the writer's compressibility-pressure hypothesis on the density distribution in Venus is discussed. Values of the density and pressure in Venus are also given on the older hypothesis that the Earth's mantle and core are composed of chemically distinct materials.

---

1. Kronig, de Boer and Korringa * have given calculations to show that at pressures which are of the order of those reached in the Earth's deep interior, substances in molecular states will be transformed into forms of higher density resembling metals. Ramsey † has followed the implications of the suggestion through to the question of the constitution of the terrestrial planets. At the time of receiving Ramsey's paper, the present writer had commenced a similar investigation. The results confirm the main calculations of Ramsey; the methods of computation differ, however, in a few small respects from those used by Ramsey, and bring into focus some additional points. In the present paper, the relation of the theory to various aspects of the constitution of Venus will be discussed in some detail.

2. The writer's earlier investigations ‡ of the density variation in the Earth are compatible with the view that between the crustal layers and the base of the mantle, the density ρ depends in the main on the pressure p alone rather than on change in chemical composition. The theory of the preceding paragraph leads to the hypothesis that, starting from just below the crustal layers, the subsequent density variation is in the main determined by pressure alone throughout the entire Earth. (This hypothesis ignores the possibility of chemical changes associated with the Earth's inner core; when more information is available, this possibility may have to be taken into account.)

If the pressure-density figures for the Earth are applied to the terrestrial planets, the suggestion then arises that the hypothesis may possibly lead to a reconciliation between observational astronomical data and the view that the terrestrial planets were all composed of the same original material. Actually, the carrying out of this investigation provides a test of the compatibility of four distinct pieces of evidence or theory:

(*a*) Observational data on the mass and mean diameter of the terrestrial planets.

* R. Kronig, J. de Boer and J. Korringa, *Physica*, **12**, 245, 1946.

† W. H. Ramsey, *M.N.*, **108**, 406, 1948.

‡ See Bullen, *An Introduction to the Theory of Seismology*, Cambridge University Press, 1947, p. 218; this book will be subsequently referred to as Reference I.

(*b*) The pressure-density figures for the Earth's interior.

(*c*) The above pressure-density hypothesis.

(*d*) The hypothesis that the terrestrial planets are of the same original composition.

It may be remarked that the pressure-density hypothesis (*c*) forms an interesting complement to the hypothesis:*

(*e*) That the incompressibility k depends only on p throughout all but the uppermost 1000 km. of the Earth.

(There is, however, a significant difference between (*c*) and (*e*) in that (*e*) in its simplest form assumes that k varies fairly smoothly throughout most of the Earth, while (*c*) involves a sharp discontinuity in ρ at the outer boundary of the central core.)

3. It should be pointed out that the hypothesis (*e*) has suggested certain amendments to (*b*). But as (*e*) has yet to be substantiated, it is proper method at this stage to use the pressure-density figures of Reference I. Ramsey has used the density figures in Reference I which correspond to an arbitrarily chosen density of 17·2 g./cm.^{3} at the Earth's centre (i. e. midway between the hypotheses (i) and (ii) of Reference I, p. 218), and these figures have also been used by the writer. Table I gives the figures (p in dynes/cm.^{2}, ρ in g./cm.^{2}) for the material below the Earth's crustal layers down to a pressure of $1{\cdot}37 \times 10^{12}$ dynes/cm.^{2} in useful tabular form, not given either in Ramsey's paper or in Reference I.

TABLE I

p	ρ	p	ρ	p	ρ
$0{\cdot}00 \times 10^{12}$	3·29	$0{\cdot}45 \times 10^{12}$	4·76	$0{\cdot}93 \times 10^{12}$	5·29
0·03	3·38	0·48	4·79	0·96	5·31
0·06	3·46	0·51	4·83	0·99	5·34
0·09	3·53	0·54	4·87	1·02	5·37
0·12	3·60	0·57	4·90	1·05	5·40
*0·14	3·64	0·60	4·94	1·08	5·43
0·15	3·72	0·63	4·98	1·11	5·46
0·18	3·94	0·66	5·01	1·14	5·49
0·21	4·11	0·69	5·04	1·17	5·51
0·24	4·26	0·72	5·07	1·20	5·54
0·27	4·38	0·75	5·10	1·23	5·57
0·30	4·49	0·78	5·13	1·26	5·59
0·33	4·57	0·81	5·17	1·29	5·61
0·36	4·63	0·84	5·20	1·32	5·63
0·39	4·58	0·87	5·23	1·35	5·66
0·42	4·72	0·90	5·26	†1·37	5·68

* Corresponds to the 20° discontinuity.

† Corresponds to the base of the Earth's mantle.

4. The procedure followed by the writer in the case of the planet Venus was to use the equations (also used by Ramsey, and with the same assumptions entailed, e. g. the assumption of hydrostatic conditions)

$$dp = -\gamma m\rho\, dr/r^2, \qquad (1)$$

$$dm = 4\pi r^2 \rho\, dr, \qquad (2)$$

* Bullen, *Nature*, **157**, 405, 1946; *M.N., Geophys. Suppl.*, **5**, 355, 1949. The latter of these references will be subsequently referred to as Reference II.

where γ is the constant of gravitation and m the mass within a sphere of radius r with centre at the centre of Venus; and to carry out a numerical integration starting from the external surface of Venus using astronomical data for the mass M and mean radius R and using the figures of Table I.

The crustal layers were taken to be equivalent to a single layer of thickness 30 km. and mean density 2·8 g./cm.^{3}. This differs very slightly from the procedure of Ramsey, but the difference is inconsequential.

In a first calculation made by the writer, the data for M and R were those used by Jeffreys * in an earlier paper, namely,

$$M = 4{\cdot}91 \times 10^{27}\,\text{g.}; \qquad R = 6150\,\text{km.}$$

On the hypotheses (*b*), (*c*) and (*d*), the radius and mass of the central core of Venus would then be given as 2667 km. and $0{\cdot}882 \times 10^{27}$ g. respectively. (The "20° discontinuity" in Venus would in this calculation occur at a depth of 470 km.) These results entail the value 11·10 g./cm.^{3} for the mean density of this central core.

It is evident that if the hypotheses (*c*) and (*d*) are compatible with each other, the mean density of the central core of Venus must be less than that of the Earth. The value of the latter mean density, corresponding to the figures in Table I, is 10·65 g./cm.^{3}, the corresponding core mass being $1{\cdot}87 \times 10^{27}$ g. The mean density of the core of Venus must therefore, further, be less than the mean density of the region E (Reference I, p. 209) of the Earth; the latter is found to be 10·3 g./cm.^{3}.

If then the hypotheses (*c*) and (*d*) are to work, the mean density ρ_0 of the Venus core must be reduced by more than 0·8 g./cm.^{3}. The main possible ways in which this might be brought about are:

(i) Amendment of the astronomical data (*a*).

(ii) Modification of the p-ρ figures on the lines suggested by the hypothesis (*e*) (Reference II).

(iii) Modification of the p-ρ figures in other ways.

The calculations leading to the data in Table I assume uniform chemical composition over the range in this table (except for the interval $0{\cdot}14 \leqslant p \times 10^{-12} \leqslant 0{\cdot}39$). Ramsey has estimated, under (iii), that the desired reduction in ρ_0 can in fact be brought about by assuming a moderately small deviation from chemical homogeneity, which he would attribute to gravitation of heavier elements towards the centre of the Earth, leading to increased density gradients. It may be remarked that in Ramsey's calculations the biggest of these increases in density gradient would take place in the Earth's inner core where, incidentally, a much increased density gradient is independently indicated by the hypothesis (*e*) (Reference II).

A major purpose of the present paper is to examine, in Sections 5, 6, respectively, the relation of (ii) and (i) to ρ_0.

5. The main effect of (*e*) in the Earth's mantle would be an appreciable raising of the level at which changes associated with the "20° discontinuity" set in and, at the same time, a slight lowering of the density in the Earth's mantle between depths of about 1000 km. and 2700 km. The essential effect is in the direction of increasing the proportion of the Earth's mantle through which the density variation is everywhere steady and slow.

An indication of the consequent effect in Venus may be estimated by taking the (artificial) extreme case in which the density, *a* say, of the Earth is taken

* Harold Jeffreys, *M.N., Geophys. Suppl.*, **4**, 62, 1937.

constant in the regions B, C, D between the crustal layers and the central core and equal to 4·55 g./cm.^{3}, the mean density of B-C-D on the figures of Table I. Let r_1 and r_2 be the internal and external radii of B-C-D, let m_1 and m_2 be the masses below the levels $r=r_1$ and $r=r_2$, and let p_1 and p_2 be the pressures at these levels. It is then easy to show that

$$m_1 = m_2 - 4\pi a(r_2^3 - r_1^3)/3, \tag{3}$$

$$p_1 = p_2 + \gamma a^2\{(r_1^{-1} - r_2^{-1})(m_2/a - 4\pi r_2^3/3) + 2\pi(r_2^2 - r_1^2)/3\}. \tag{4}$$

A calculation based on (4) gives $p_1 = 1{\cdot}248 \times 10^{12}$ dynes/cm.^{2}. When (3) and (4) are applied to the interior of Venus, it is found that a pressure of $1{\cdot}248 \times 10^{12}$ dynes/cm.^{2} is reached when r_1 (for Venus) is equal to 2585 km., the corresponding m_1 (i. e. the mass of the central core of Venus) being $0{\cdot}833 \times 10^{27}$ g. This would entail a mean density for the central core of Venus of 11·5 g./cm.^{3}.

It is to be expected that the influence of (*e*) would be in the direction of the case just considered, i. e. raising, not lowering, the previously indicated value of 11·1 g./cm.^{3} for ρ_0. Thus no help for Venus is derived from (*e*). It is desirable, however, that its influence should be thus examined, for it will be shown in a subsequent paper that the compressibility hypothesis (*e*) offers a way of fully removing the discrepancy in the case of Mars.

6. With a view to examining the influence of (i) of Section 4, the writer re-calculated the value of ρ_0, taking $R=6200$ km., and the same value of M as in Section 4; the latter value of R is the maximum value allowed in the range of uncertainty given in the paper of Jeffreys.* The result was $\rho_0 = 10{\cdot}74$ g./cm.^{3}, which reduces the discrepancy, but not sufficiently; the corresponding mass and radius of the central core of Venus are $0{\cdot}708 \times 10^{27}$ g. and 2505 km. respectively.

It is not possible to remove the discrepancy by changing the mass M by an allowable margin. Thus, for example, it is found that on the data

$$M = 4{\cdot}88 \times 10^{27}\text{ g.}, \qquad R = 6200\text{ km.},$$

ρ_0 is given as 10·71 g./cm.^{3}. (The depth of the "20° discontinuity" in Venus would be 480 km. on the figures of this and also the preceding paragraph.)

The above calculations are incidentally in agreement with the calculations of Ramsey, who finds that, taking the mass of Venus as $4{\cdot}88 \times 10^{27}$ g., the hypotheses (*b*), (*c*), (*d*) of Section 2 are compatible if $R=6285$ km. Extrapolating from our results, we find that when $R=6285$ km. and $M = 4{\cdot}88 \times 10^{27}$ g., ρ_0 is given as 10·1 g./cm.^{3} and the radius of the core as 2235 km.

The value $R=6285$ km., which reconciles (*b*), (*c*) and (*d*), is outside the stated range of uncertainty in the observational data available. The data quoted by Ramsey give $R = 6200 \pm 50$. But it may be remarked that half of this range lies beyond the estimated uncertainty in the figures used by Jeffreys in 1937, namely $R = 6150 \pm 50$. Therefore, it seems well within the bounds of possibility that the radius of Venus may be as much as 6285 km.

A special feature of the above results is that the value of ρ_0 is very sensitive to variations in R, rather than to allowable variations in M or the effect of the hypothesis (*e*). Hence this important conclusion emerges: assuming the hypotheses (*c*) and (*d*) to be correct, *a slightly increased precision in observations of the mean diameter of Venus would decide whether or not the density gradients previously assigned in the regions B, D, E of the Earth need to be increased.* This in effect would

* *Loc. cit.*

also test the validity of the assumption of chemical homogeneity in these regions, provided there are no complications connected with the Earth's inner core.

7. For general reference purposes, the distribution of pressure and density with depth d km. in the mantle of Venus is given in Table II, corresponding to the data $M = 4{\cdot}91 \times 10^{27}$ g. and $R = 6150$ km., calculated as described in Section 4.

TABLE II

d	r	p	ρ	m
30	6120	$0{\cdot}007 \times 10^{12}$	3·32	$4{\cdot}76 \times 10^{27}$
470	5680	0·14	3·64	4·20
800	5350	0·25	4·30	3·70
1200	4950	0·41	4·70	3·09
1600	4550	0·57	4·90	2·55
2000	4150	0·73	5·09	2·07
2400	3750	0·89	5·25	1·67
2800	3350	1·06	5·41	1·33
3200	2950	1·24	5·57	1·06
3483	2667	1·37	5·68	0·88

8. For further reference purposes, values of p, ρ and m in the core of Venus are given in Table III, as calculated on the older theory that the central cores of the Earth and Venus are quite distinct chemically from the mantle. In preparing Table III, it is assumed that the "20° discontinuity" is a pressure phenomenon, and no provision is made for the presence of an inner core inside Venus. On this older theory, the figures of Table II would apply down to a radius of 2944 km. which would be the radius of the central core of Venus. Table III extends the figures to the centre of Venus. The figures in Tables II and III may be compared with values found by Jeffreys * using earlier density data.

TABLE III

d	r	p	ρ	m
3206	2944	$1{\cdot}24 \times 10^{12}$	9·21	$1{\cdot}06 \times 10^{27}$
3483	2667	1·45	9·50	0·79
3600	2550	1·53	9·62	0·70
4000	2150	1·79	9·96	0·43
4400	1750	2·01	10·24	0·23
4800	1350	2·20	10·48	0·11
5200	950	2·34	10·65	0·04
5600	550	2·44	10·76	0·01
6000	150	2·48	10·80	0·00
6150	0	2·49	10·81	0·00

University of Sydney:
1949 *April* 27.

* *Loc. cit.*

ON THE SOLAR ELECTRIC FIELD ENGENDERED BY THE ROTATION OF THE SUN IN ITS MAGNETIC FIELD

V. C. A. Ferraro and H. W. Unthank

(Received 1949 July 5)

Summary

The rotation of the Sun in its magnetic field gives rise to an electrostatic field, the equipotential surfaces of which are the surfaces of revolution obtained by rotating the magnetic lines of force around the axis (**1, 2**). The same is true for any rotating star possessing a magnetic field. If the angular velocity of the star is not constant, then it seems likely to be uniform over these same equipotential surfaces. This law of isorotation must hold for the solar atmosphere and corona as well, and may extend to the surrounding interstellar space. Also the resulting surface and space charges and the magnetic field due to their motion around the axis are negligible, in apparent contradiction with certain conclusions of L. Davis.

---

1. *Introduction.*—In 1937 the problem of the rotation of the Sun in the presence of its magnetic field was discussed by one of us (**1**)* and it was shown that in a steady state the angular velocity of the Sun (ω), if not constant, must be uniform over the surfaces traced out by the revolution of a magnetic line of force about the magnetic axis, assumed to be coincident with the axis of rotation. This theorem was rediscovered independently by Alfvén in 1943, who called such surfaces "isorotational" and the theorem the "law of isorotation". It is a consequence of the condition that in the steady state the electric field, resulting from the radial polarization of the Sun by the deflecting force of the magnetic field on the rotating ionized gases, must be lamellar. The existence of this electric field, additional to the Pannekoek-Rosseland field, was first pointed out by Cowling.

It was also stated in a note at the end of Paper I that surface charges would be induced on the surface of the Sun and that these would tend to escape from the surface under their mutual repulsion largely along the magnetic lines of force. Similar conclusions have recently been obtained by Leverett Davis Jr. (**2**), who has considered the problem of the rotation of a star in its magnetic field; he states that "a positive space charge is built up on the equatorial plane while the star acquires a negative surface charge" (**2,** p. 633). But the Sun and stars are surrounded by an extensive ionized atmosphere and it seems unlikely that appreciable "surface" or "space" distributions can exist for any considerable period. Davis also points out that if there exist surface or space charges a positive ion will be accelerated towards the equatorial plane and a negative ion accelerated in the opposite direction until it strikes the star, but gives no details of the actual motions. It will be shown, however, that under the action of the electric field of these surface and space charges, such as might be expected to arise in any departure from a steady state, the speeds acquired would be far greater than those observed in the solar chromosphere and corona. In so far as order of magnitude is concerned, it will suffice to consider only the effect of possible surface charges.

* This paper will be referred to as Paper I.

2. *The electrostatic potential in a non-steady state.*—Suppose, as in Paper I, that (i) the law of isorotation holds good up to the photospheric layers but not beyond them, (ii) the magnetic field is derived from a function U analogous to Stokes' stream function and that $U \propto \sin^2\theta$, where θ is the colatitude of a point on the Sun's surface, (iii) outside the Sun the magnetic field is that of a dipole situated at the centre of the Sun in a direction opposite to that of the Sun's rotation, (iv) the angular velocity of the Sun is given by

$$\omega = \omega_0 + \omega_1 \cos^2\theta, \tag{1}$$

where ω_0 and ω_1 are functions of the radial distance r. At the surface the values of ω_0 and ω_1 derived from the motion of sunspots give

$$\omega_0 = 14{\cdot}54^\circ \text{ per day}, \qquad \omega_1 = -2{\cdot}81^\circ \text{ per day}. \tag{2}$$

The law of isorotation, which expressed formally is

$$\omega = f(U),$$

where f is an arbitrary function, requires, from (1), that (approximately) in this case

$$\omega = a + bU, \tag{3}$$

where a and b are constants. The electrostatic potential at points within the Sun, as was shown in Paper I (p. 465), is given by

$$V = \int^U f(x)\,dx + \text{constant}, \tag{4}$$

or using (3),

$$V = aU + \tfrac{1}{2}bU^2 + \text{constant}. \tag{5}$$

We recall that the equation $U = \text{constant}$ is the equation of a line of magnetic force, so that the equipotential surfaces of the electric field are the same as the isorotational surfaces.*

If we ignore the space charge outside the Sun formed by the escaping charges the potential outside the Sun can be found from potential theory. For the present purpose we may suppose that the magnetic field in the outer layers of the photosphere and beyond them is the same as that of a dipole field, so that

$$U = (A\sin^2\theta)/r, \tag{6}$$

where A is a constant.

Substituting (6) in (5) and expressing in terms of zonal harmonics, we find the potential outside the Sun to be given by

$$V = V_0 R/r - (V_2 R^3/r^3)P_2(\cos\theta) + (V_4 R^5/r^5)P_4(\cos\theta), \tag{7}$$

where R is the radius of the Sun and V_0, V_2, V_4 are constants. The values of V_2, V_4 are

$$V_2 = \frac{2}{3}\frac{aA}{R} + \frac{8}{21}\frac{bA^2}{R^2}, \qquad V_4 = \frac{4}{35}\frac{bA^2}{R^2}. \tag{7a}$$

V_0 is arbitrary and corresponds to a uniform distribution of surface charge which will not affect the field at internal points.

The existence of the general solar magnetic field has not yet been definitely established; the first observations of Hale and his collaborators gave the polar value of the magnetic field as of the order of 50 gauss. The corresponding value

* This is also stated (without proof) by Davis (**2**, p. 633).

of A in (6) is about $4{\cdot}2 \times 10^{33}$ e.m.u. Thiessen, on the other hand, has lately expressed the view that the Sun's general field may not exceed 10 gauss at the pole. We shall here suppose that $A = 4{\cdot}2 \times 10^{32}$ e.m.u. so as to underestimate the speed acquired by the charges. We must then have

$$a = 2{\cdot}37 \times 10^{-6} \text{ rad./sec.}, \qquad b = 0{\cdot}95 \times 10^{-28}. \tag{8}$$

From (7*a*) we then find (ignoring the smaller P_4 term)

$$V = V_0/r_1 - 3{\cdot}59 \times 10^5 \, P_2/r_1^3 \text{ e.s.u.}, \tag{9}$$

where $r_1 = r/R$ is the radial distance in terms of a solar radius as unit. At the Sun's surface, $r_1 = 1$, there is a difference of potential of the order of 10^9 volts between the pole and equator of the Sun, as was noted by Davis. The presence of space charge will affect the form, but not the order of magnitude, of the coefficients of P_2 and P_4 in (7).

3. *The surface charge in the non-steady state.*—The surface charge density, σ, is given by $[E_n]/4\pi$, where $[E_n]$ denotes the discontinuity in the normal component of the electric field. Assuming (6) and using (5) (ignoring the small P_4 term) we find the potential inside the Sun to be

$$V = \text{constant} + \frac{2}{3}\frac{aA}{r_1 R}(1 - P_2), \tag{10}$$

whence from (9) and (10) it follows that

$$\sigma = 1{\cdot}14 \times 10^{-12} V_0 - 4{\cdot}3 \times 10^{-7} - 7{\cdot}7 \times 10^{-7} P_2 \text{ e.s.u.} \tag{11}$$

Writing $V_2 = 3{\cdot}59 \times 10^5$, (9) may be written

$$V = V_2 \left[\frac{V_0}{V_2}\frac{1}{r_1} - \frac{P_2}{r_1^3} \right] \text{e.s.u.} \tag{12}$$

Thus σ is zero at the poles and positive elsewhere if $V_0/V_2 = 2{\cdot}93$. If $V_0/V_2 < 2{\cdot}93$, there will be a negative belt surrounding each pole.

4. *The motion of charged particles in the solar atmosphere.*—We next consider the motion of a charged particle in the combined electric and magnetic field of the Sun. Choose a system of cylindrical polar coordinates (ϖ, ϕ, z) with the origin at the centre of the Sun, Oz directed along the axis of rotation, and let e (e.s.u.) be the charge and m the mass of a charged particle moving in the combined fields; then the (non-relativistic) equations of motion of the charges are

$$m(\ddot{\varpi} - \varpi\dot{\phi}^2) = -e\partial V/\partial\varpi + (e/c)\dot{\phi}\,\partial U/\partial\varpi, \tag{13}$$

$$(m/\varpi)d/dt(\varpi^2\dot{\phi}) = -(e/\varpi c)(\dot{z}\partial U/\partial z + \dot{\varpi}\partial U/\partial\varpi), \tag{14}$$

$$m\ddot{z} = -e\partial V/\partial z + (e\dot{\phi}/c)\partial U/\partial z, \tag{15}$$

since U and V are independent of ϕ; (14) can be integrated at once to give

$$\varpi^2\dot{\phi} = -(e/mc)U + h, \tag{16}$$

where h is a constant.

We have further the equation of energy

$$\tfrac{1}{2}mv^2 + eV = E, \tag{17}$$

where E is the total energy and v the speed of the charge.

Inserting in (16) numerical values for the case of a particle of the mass of a calcium ion, we find that

$$\varpi^2\dot{\phi} = h - 1{\cdot}45 \times 10^{24}(\sin^2\theta)/r_1; \tag{18}$$

since the velocity of ions in the solar atmosphere at 6000 deg. K. is of the order of 10^5 cm./sec., it follows that at the instant when the particle leaves the solar surface the left-hand side of (18) is of the order of 10^{16}. Thus, except for very small values of $\sin^2\theta$ (near the poles), h must be of the order of 10^{25} and, so long as the speed of the particle does not approach the speed of light, we have approximately

$$h=(e/mc)U$$

or

$$r_1=k\sin^2\theta, \tag{19}$$

where $k=eA/mchR$. Thus, so long as the speed of the ions is less than the speed of light, the ion will move approximately along a magnetic line of force.

To obtain some indication of the order of magnitude of the speed involved, we assume that $V_0/V_2=2{\cdot}93$. The following table gives the variation of V (in e.s.u.) for $r=R$, $2R$, $3R$ and $\theta=0°$, $45°$, $90°$.

r \ θ	0°	45°	90°
R	$7{\cdot}0\times10^5$	$9{\cdot}6\times10^5$	$12{\cdot}3\times10^5$
$2R$	$4{\cdot}8\times10^5$	$5{\cdot}2\times10^5$	$5{\cdot}5\times10^5$
$3R$	$3{\cdot}4\times10^5$	$3{\cdot}5\times10^5$	$3{\cdot}6\times10^5$

Consider an ion leaving the Sun's surface in latitude 45° along the line of magnetic force for which $k=2$. It can be shown that it will have the potential gradient always in its favour and thus will cross the equatorial plane at a distance $r=2R$. From the table we see that the ion will lose potential energy of the order of $1{\cdot}2\times10^8$ electron volts. The ion will therefore acquire a speed of the order of 2×10^9 cm./sec.; the speed acquired by the electrons will be still greater, approaching the speed of light. For other values of the ratio V_0/V_2 (which is unlikely to be less than unity) speeds of the same order of magnitude are to be expected.

This then is the order of magnitude of the speeds acquired by the charges under the action of the electrostatic field of the supposed induced surface charges. Now the temperature of the corona, although as high as 10^5 deg. K., is low compared with the temperature which would correspond to ionic random velocities of the order of 2×10^9 cm./sec. We must therefore suppose that surface or space charge distributions are unlikely to exist in the solar atmosphere, except locally or for short periods, and that the law of isorotation must extend into the outer atmosphere of the Sun. This last fact is stated by Davis, but the resulting small space charge distribution is not determined by him. It is in fact not made clear that the space charges are indeed small and negligible (**3**).

5. *The law of isorotation.*—Certain slight modifications of the law of isorotation are necessary, however, since the mechanical equilibrium will be different from that of the solar interior. In addition, the flow of current will not be according to Ohm's Law, except along the magnetic lines of force (so that, for instance, equation (31) of Paper I no longer holds).

The equation of motion of an element of volume of charge ne (e.s.u.) and mass nm may be written

$$m\frac{\partial \boldsymbol{v}}{\partial t} - m\boldsymbol{v}\wedge \operatorname{curl}\boldsymbol{v} = -\operatorname{grad}\left(\int\frac{dp}{n} + \tfrac{1}{2}m\boldsymbol{v}^2 + m\phi + eV\right) + \frac{e}{c}\boldsymbol{v}\wedge\boldsymbol{H}, \tag{20}$$

where $\boldsymbol{v}$ is the velocity of the element, p the partial pressure of the gas of number density n, ϕ and V the gravitational and electric potential and $\boldsymbol{H}$ the magnetic field. Writing the vorticity

$$\boldsymbol{\zeta} = \tfrac{1}{2}\operatorname{curl}\boldsymbol{v}, \tag{21}$$

we have in the steady state

$$\operatorname{grad}\left(\int\frac{dp}{n} + \tfrac{1}{2}mv^2 + m\phi + eV\right) = \boldsymbol{v}\wedge\left(2m\boldsymbol{\zeta} + \frac{e}{c}\boldsymbol{H}\right) \equiv \boldsymbol{v}\wedge\boldsymbol{K}, \tag{22}$$

where $\boldsymbol{K} = 2m\boldsymbol{\zeta} + \dfrac{e}{c}\boldsymbol{H}$.

Since curl grad = 0, we have

$$\operatorname{curl}(\boldsymbol{v}\wedge\boldsymbol{K}) = 0. \tag{23}$$

As in Paper I, we suppose $\boldsymbol{H}$ to depend on z and ϖ only and to have axial symmetry, so that

$$H_\varpi = -\frac{1}{\varpi}\frac{\partial U}{\partial z}, \qquad H_\varphi = 0, \qquad H_z = \frac{1}{\varpi}\frac{\partial U}{\partial \varpi}. \tag{24}$$

We suppose further that $\boldsymbol{v} = \Omega\varpi\boldsymbol{e}$, where $\boldsymbol{e}$ is a unit vector in the direction of ϕ increasing. Then

$$\boldsymbol{\zeta} = \tfrac{1}{2}\operatorname{curl}\boldsymbol{v} = \tfrac{1}{2}\left(-\frac{\partial\Omega\varpi}{\partial z},\ 0,\ \frac{1}{\varpi}\frac{\partial\Omega\varpi^2}{\partial\varpi}\right). \tag{25}$$

Thus we have

$$K_\varpi = -\frac{1}{\varpi}\frac{\partial J}{\partial z}, \qquad K_\varphi = 0, \qquad K_z = \frac{1}{\varpi}\frac{\partial J}{\partial\varpi}, \tag{26}$$

where

$$J = \frac{e}{c}U + m\Omega\varpi^2. \tag{27}$$

Then the only non-vanishing resolute of (23) gives

$$\frac{\partial\Omega\varpi K_z}{dz} + \frac{\partial\Omega\varpi K_\varpi}{\partial\varpi} = 0,$$

or, by (26),

$$\frac{\partial}{\partial z}\left(\Omega\frac{\partial J}{\partial\varpi}\right) - \frac{\partial}{\partial\varpi}\left(\Omega\frac{\partial J}{\partial z}\right) = 0,$$

that is

$$\frac{\partial(\Omega, J)}{\partial(\varpi, z)} = 0,$$

which corresponds to equation (38) of Paper I. Thus the new isorotational law is

$$\Omega = F(J) = f\left(U + \frac{mc}{e}\Omega\varpi^2\right) \text{ say}, \tag{28}$$

where F and f are arbitrary functions.

Because of the slow angular speed of the Sun the modification is only slight. Thus, if Ω is constant, then by (28)

$$U+\frac{mc}{e}\Omega\varpi^2=\text{constant also,}$$

that is, by (6),

$$\left(\frac{A}{r}+\frac{mc}{e}\Omega r^2\right)\sin^2\theta=\text{constant.}$$

Since A is of the order 10^{32} e.m.u. and Ω of the order 10^{-6} rad./sec., the term A/r exceeds $\frac{mc}{e}\Omega r^2$ so long as $r<10^{13}$ cm. Thus in the solar atmosphere the correction needed is negligible.

The electrostatic potential, V, may now be deduced from (22). We first note that the gravitational energy $m\phi$, which is of order $m\times 10^{15}$ in the solar atmosphere, exceeds the kinetic energy of the particle which is of the order $4m\times 10^{10}$. Further, we may neglect the vorticity ζ compared with the magneto-gyrofrequency $e\boldsymbol{H}/mc$ in $\boldsymbol{K}$ and thus (22) becomes approximately

$$\text{grad}\,(\int dp/n+m\phi+eV)=(e/c)\boldsymbol{v}\wedge\boldsymbol{H}. \tag{29}$$

The resolutes of this equation are

$$\frac{\partial P}{\partial\varpi}=\frac{e}{c}\Omega\frac{\partial U}{\partial\varpi},\qquad \frac{\partial P}{\partial z}=\frac{e}{c}\Omega\frac{\partial U}{\partial z}, \tag{30}$$

where

$$P=\int dp/n+m\phi+eV; \tag{31}$$

and since $\Omega=f(U)$ very nearly, we have

$$P-(e/c)\int^U f(x)\,dx=\text{constant}$$

or

$$eV=(e/c)\int^U f(x)\,dx-m\phi-\int dp/n+\text{constant.}$$

This equation replaces (40) of Paper I. Moreover, in the outer chromosphere and corona the pressure is inadequate to support the material against gravity so that the pressure term may also be neglected. Thus we have finally

$$V=(1/c)\int^U f(x)\,dx-(m/e)\,\phi+\text{constant.} \tag{32}$$

6. *The space distribution in the steady state.*—The appearance of the term $(m/e)\phi$ in the equation (32) indicates a slight differential velocity between the ions and electrons. In fact the equations holding for each are respectively

$$V=(1/c)\int^U f_i(U)dU-m_i\phi/e+\text{constant}$$

and

$$V=(1/c)\int^U f_e(U)dU+m_e\phi/e+\text{constant,}$$

where $f_i(U)$ and $f_e(U)$ are the angular velocities of an ion and electron around the axis. Thus, in the absence of any toroidal component of the magnetic field, we have at any point

$$c\phi(m_i+m_e)e=\int^U\{f_i(x)-f_e(x)\}dx.$$

As a first approximation we take $f_i=\Omega_i=\text{constant}$, $f_e=\Omega_e=\text{constant}$, so that

$$\Omega_i-\Omega_e=c\phi(m_i+m_e)/eU.$$

The differential velocity of the particles is thus of the order of

$$c(m_i+m_e)\phi R/eU \text{ cm./sec.},$$

where R is the radius of the Sun; and inserting numerical values, taking m_i to be the mass of a calcium atom, this is of the order of 1 metre per second and small compared with the rotational velocity of the ions, viz. a few kilometres per second.

The space charge will therefore be of the same order of magnitude as was computed in Paper I. In fact, ignoring the effect of gravity, (32) gives for the electric potential in the atmosphere the expression

$$V=\text{constant}+\frac{2}{3}\frac{aA}{r}(1-P_2)+\frac{bA^2}{r^2}\left(\frac{4}{35}P_4-\frac{8}{21}P_2+\frac{4}{15}\right), \tag{33}$$

approximately; ignoring the last term we should have, apart from a constant,

$$V=(aA\sin^2\theta)/r,$$

which agrees with the expression given by Davis (**2** and **3**). Inserting numerical values we find from (33)

$$V=3{\cdot}16\times 10^5(1-P_2)/r_1.$$

The space charge density is of the order 10^{-16} e.s.u. or, say, 10^{-7} excess particles of one sign per c.c. Thus not only in the outer corona, where the particle density is of the order 10^5, but even in the surrounding interstellar space the excess charge could be amply supplied. The convection electric current density will thus be of the order $10^{-16}\times 100/c$ e.m.u. or $\frac{1}{3}\times 10^{-24}$ e.m.u. If this flowed through an annulus of radii R and $2R$, the total current would be $3\pi R^2\times\frac{1}{3}\times 10^{-24}$ e.m.u., or $1{\cdot}5\times 10^{-2}$ e.m.u., say. The resulting increase in the magnetic field across the annular radius would be of the order 10^{-3} gauss and this is negligible compared with solar magnetic fields.

7. *The approach of moving ionized gases in the solar atmosphere to the steady state.*—Consider next the motion of a charged particle in the solar atmosphere which violates the law of isorotation. The equation of motion is approximately

$$m\dot{\boldsymbol{v}}=e\left(\boldsymbol{E}+\frac{1}{c}\boldsymbol{v}\wedge\boldsymbol{H}\right),$$

where $\boldsymbol{E}$ is the electric field vector. We have here neglected gravity and we also neglect the effect of collisions for the present. Since, very nearly,

$$\boldsymbol{E}=-\frac{1}{c}\boldsymbol{v}_0\wedge\boldsymbol{H},$$

where $\boldsymbol{v}_0$ is the azimuthal velocity at the point considered, then

$$m\dot{\boldsymbol{v}}=\frac{e}{c}(\boldsymbol{v}-\boldsymbol{v}_0)\wedge\boldsymbol{H}.$$

Write

$$\boldsymbol{v}=\boldsymbol{v}_0+\boldsymbol{W},$$

then

$$m\dot{\boldsymbol{W}}=\frac{e}{c}\boldsymbol{W}\wedge\boldsymbol{H}-m\dot{\boldsymbol{v}}_0.$$

Now $\dot{\boldsymbol{v}}_0$ is the centripetal acceleration of the particle which is of the order of $m\Omega^2R$. The term on the right-hand side is of the order of $(e/c)WH$, where W is comparable with the speed of the particle. Thus the ratio of the centrifugal force to the magnetic deflecting force is $m\Omega^2Rc/eWH$. For a calcium atom

$mc/e = 4 \times 10^{-3}$; taking $W = 10^5$ cm./sec. (corresponding to the speed of thermal agitation at a temperature of 6000 deg. K.) and putting $R = 7 \times 10^{10}$ cm., $H = 10$ gauss, $\Omega = 2{\cdot}4 \times 10^{-6}$, this ratio is $1{\cdot}50 \times 10^{-9}$ and so the centrifugal term is negligible.

Hence, very nearly,

$$m\dot{\boldsymbol{W}} = e\boldsymbol{W} \wedge \boldsymbol{H}/c,$$

and the charge will thus spiral around a magnetic line of force with little change of speed, except when colliding with another particle.

It follows that any charged particle projected into the solar atmosphere will soon take up the general drift velocity cE/H and conform to the law of isorotation.

This will hold so long as the mean free path of the particle is large compared with the spiral radius. In an ionized atmosphere at 6000 deg. K. the spiral radii of a *Ca* and an *H* ion in a magnetic field of 10 gauss are 20 and $\frac{1}{2}$ cm. respectively. The mean free path of an ion in an ionized atmosphere at the same temperature is (**4**) $1{\cdot}2 \times 10^{11}/n$ cm., where n is the particle density. Thus the mean free path is greater than the spiral radius when n is less than 10^9 ions per c.c., i. e. in the higher chromosphere and corona. In these regions the particles will soon take up the general drift velocity.

When collisions are no longer negligible, much the same conclusions follow.* Consider an ionized electrically neutral cloud of particles projected into the atmosphere. The cloud will become polarized by the electric field of the Sun and the electric field set up by the polarization will tend to annul the electric field in the interior of the cloud. Space charges will be induced on the surface of the cloud by the polarization and these will tend to disperse mainly along the magnetic lines of force. Thus these surface charges must be constantly re-formed and an electric current will flow in the cloud in the direction of the electric field. The action of the solar magnetic field on this current will be to accelerate or retard the azimuthal motion of the cloud as a whole until its motion conforms to the law of isorotation. It is hoped to consider this question in greater detail in a later note.

8. *The increase of angular velocity with height in the solar atmosphere.*—The law of isorotation appears to hold good throughout the solar atmosphere and for the interstellar gases surrounding the Sun. Since the magnetic lines of force spread outwards from the Sun as from a magnetic dipole centred at the Sun's centre with its axis along the axis of rotation, it follows, from the observed variation of the surface angular velocity of the Sun, that the angular velocity of the atmosphere should decrease with height roughly in inverse ratio to the distance from the centre. The observations of Evershed (**5**) and St. John (**6**) show that, on the contrary, the angular velocity increases rather rapidly with height. It seems at first sight that other factors not taken into account must affect the motion of the charges. In deriving the law of isorotation, however, we assume that the atmosphere is devoid of any motion in meridian planes. If we suppose that the gases have a component of velocity in such planes, one way of accounting for this increase would be to suppose that the Sun possesses a small positive resultant charge; for the resulting increase of kinetic energy of a positive ion or electron would be accompanied by an increase of angular momentum. In fact, from (17) we have

$$\tfrac{1}{2}mv^2 = E - eV,$$

and to a first approximation, by (32),

$$V = \Omega U/c + \text{constant}.$$

* *Cf.* Davis (**2**) and (**3**).

Thus, very nearly,

$$\tfrac{1}{2}mv^2 = E - e\Omega U/c + \text{constant}. \tag{34}$$

Again, by (16),

$$\varpi^2\dot{\phi} = h - eU/mc, \tag{35}$$

so that eliminating U between (34) and (35) and remembering that E, h and Ω are constants we have

$$v^2 = \text{constant} + 2\varpi^2\Omega\dot{\phi}. \tag{36}$$

This equation shows that gain of kinetic energy is accompanied by gain of angular momentum about the Sun's axis in the same sense as the rotation. The observations of Evershed point to an increase in $\dot{\phi}$ of about 3×10^{-7} rad./sec. in a distance of about 1000 km. If (36) holds good and if we take $\Omega = 2 \times 10^{-6}$ rad./sec., $\varpi \doteq 7 \times 10^{10}$ cm., this implies that v^2 should increase by 6×10^9 in this distance. The corresponding increase in v, if this is 10^5 cm./sec. at the surface, is 3×10^4 cm./sec.

It does not seem improbable that such an increase in velocity may take place under the action of solar electric fields. An electric field of the same order as the Sun possesses in virtue of the positive charge acquired through the escape of electrons, with their thermal velocity of agitation at a temperature of 6000 deg. K., would suffice.* It suggests a possible way of accounting for the observed increase of angular velocity with height other than the suggestion put forward by Evershed in 1925.

University College of the South West,
Exeter:
1949 *June* 30.

References

(1) V. C. A. Ferraro, *M.N.*, **97**, 458, 1937.
(2) L. Davis, *Phys. Rev.*, **72**, 632, 1947.
(3) L. Davis, *Phys. Rev.*, **73**, 536, 1948.
(4) V. C. A. Ferraro, *M.N.*, **93**, 416, 1933.
(5) J. Evershed, *M.N.*, **85**, 607, 1925.
(6) C. E. St. John, *Mt. Wilson Contributions*, No. 278, 1924.

* For any other temperature T the positive charge on the Sun would be of the order of $3kTR/2e$, where k is Boltzmann's constant.

WAVE FUNCTIONS FOR *Fe* XIV

M. Tuberg Gold *

(Received 1949 March 30)

Summary

The results obtained by Hartree's self-consistent field method, without exchange, for the radial wave functions of *Fe* XIV, for both the ground configuration ($3s^2 3p$) and the lowest lying configuration ($3s3p^2$) combining with the ground configuration, are presented. The level separation in the ground configuration of *Fe* XIV and the probability of spontaneous transition between these two levels are computed from these wave functions. The spontaneous-transition probability and the *f*-value for the transition array $3s3p^2 \rightarrow 3s^2 3p$ are also given.

1. *Introduction.*—The emission lines in the spectrum of the solar corona have been identified by Edlén (**1**) as due to transitions from metastable levels in highly ionized atoms of iron, calcium and nickel. These metastable levels are believed to be excited by collisions between the coronal ions and free electrons, and de-excited by spontaneous transitions. Knowledge of the structure of these highly ionized atoms and of their collision cross-sections is a necessary preliminary to a physical theory of the solar corona.

The most intense of the coronal lines, $\lambda 5303$, is identified with the transition *Fe* XIV $(3s^2 3p)^2P_{\frac{3}{2}} - {}^2P_{\frac{1}{2}}$. This paper presents the results obtained by Hartree's (**2**) self-consistent field method, without exchange, for the wave functions of *Fe* XIV, for both the ground configuration ($3s^2 3p$) and the lowest lying configuration ($3s3p^2$) combining with the ground configuration. The values of the level separation in the ground configuration of *Fe* XIV and of the probability of spontaneous transition between these two levels are calculated from these wave functions. These wave functions are also used to determine the spontaneous-transition probability and the *f*-value for the transition array $3s3p^2 \rightarrow 3s^2 3p$. The lines in this transition array, though in the far ultra-violet and hence unobservable, are of interest in connection with observed ionization effects in the ionosphere.

In a later paper, the collision cross-section for the excitation of *Fe* XIV $(3s^2 3p)^2P_{\frac{1}{2}} - {}^2P_{\frac{3}{2}}$ by electron impact, computed from these wave functions, will be given.

2. *Calculation of the wave functions.* (a) *Method.*—Wave functions for *Fe* XIV were obtained by numerical integration of Hartree's non-exchange equation (in atomic units),

$$P''(nl;r) + \left[\frac{2Z_p(r)}{r} - \epsilon_{nl} - \frac{l(l+1)}{r^2}\right] P(nl;r) = 0, \qquad (1)$$

$P_N(nl;r)/r$ being the normalized radial wave function for a *nl* electron. The negative energy parameter, ϵ_{nl}, is determined in units of the ionization potential of hydrogen ($I_H = 13{\cdot}53$ e.V.). The field at a given radius, due to a *nl* group of

* This work was carried out during the tenure of a fellowship from the National Research Council, Washington, D.C.

electrons, containing $N(nl)$ electrons, and the corresponding nuclear charge, is equal to $Z(nl;r)/r^2$, where

$$Z(nl;r) = N(nl)\int_r^\infty P_N^2(nl;r)\,dr. \qquad (2)$$

The potential at a given radius, due to the same group of electrons and corresponding nuclear charge, is equal to $Z_p(nl;r)/r$, where $Z_p(nl;r)$ is found by solution of the differential equation

$$\frac{dZ_p(nl;r)}{dr} = -\frac{Z(nl;r) - Z_p(nl;r)}{r}, \qquad (3)$$

subject to the condition that $Z_p(nl;r) \to 0$ as $r \to \infty$. The total $Z_p(r)$ for the atomic field, acting on a nl electron at a given radius, is given by

$$Z_p(r) = C + 1 + \sum_{n'l'} Z_p(n'l';r) - \frac{1}{N(nl)} Z_p(nl;r), \qquad (4)$$

C being the net charge of the atom.

In starting self-consistent field calculations, it is necessary to make initial estimates of the values of Z for the separate groups of electrons. For the present calculations, values of Z, derived from appropriately scaled (**3**) Cu^+ wave functions (**4**), were used for the 1s, 2s and 2p electrons. The integrations for the wave functions were begun with values of P at small values of r, found by series expansion, and were performed outwards. Initial estimates for the parameters, ϵ, were made from the successive ionization potentials for iron, determined by Hartree (**5**). Different values of ϵ were tried until the desired function, approaching zero at large values of r, was obtained. A preliminary calculation of the wave function for the 3s electron in *Fe* XIV (3s) was done, and with the Z(3s) derived from it, the wave function for the 3p electron in *Fe* XIV ($3s^2 3p$) was computed. A self-consistent field solution was then carried out for the 3s electron in *Fe* XIV ($3s^2 3p$). The process of successive approximations converged rapidly and was continued until initial and final values of Z(3s) agreed to within 0·005. The wave function for the 3p electron in *Fe* XIV ($3s^2 3p$) was then redetermined with the final Z(3s) obtained. The wave function for the 3p electron in the $3s3p^2$ configuration of *Fe* XIV was also computed and found to differ slightly from the wave function for the 3p electron in the $3s^2 3p$ configuration. It was not thought necessary to do a further calculation of the wave function for the 3s electron in the $3s3p^2$ configuration. The initial estimates of Z for the 1s, 2s and 2p electrons were not improved, a small change in their values having a negligible effect on the wave functions computed for the 3s and 3p electrons. The wave functions for the 3s and 3p electrons in *Fe* XIV are of chief interest for astrophysical applications.

(b) *Results.*—The normalized wave functions, $P_N(nl;r)$, for the 3s and 3p electrons in *Fe* XIV, together with the values of the energy parameter, ϵ_{nl}, are listed in Table I. Table II gives the values of $Z(nl;r)$ for each nl group of electrons and the values of the total $2Z_p(r)$; the latter quantity is of use in further calculations of wave functions for lower stages of ionization of iron.

The only available energy value with which the energy parameter, $\epsilon = 27{\cdot}79$, for the 3p electron in the ground configuration of *Fe* XIV can be compared is that of the ionization potential for *Fe* XIV, $i = 29$, in units of I_H, determined by Hartree. The maximum possible error in this value for i is estimated to be less than 10 per cent.

TABLE I

Values of $P_N(nl\,;r)$ and ϵ_{nl}

	Fe XIV ($3s^2 3p$)		*Fe* XIV ($3s3p^2$)
r	(3s)	(3p)	(3p)
0·000	0·000	0·000	0·000
0·005	0·157	0·006	0·006
0·010	0·274	0·022	0·022
0·015	0·357	0·046	0·046
0·020	0·411	0·076	0·076½
0·025	0·440	0·112	0·112
0·030	0·448	0·151	0·151
0·035	0·439	0·193	0·193
0·040	0·416	0·236½	0·237
0·05	0·338	0·325	0·325
0·06	0·230	0·412	0·412
0·07	0·106	0·493	0·493
0·08	−0·024	0·565½	0·566
0·09	−0·154	0·628	0·628
0·10	−0·277	0·679½	0·680
0·12	−0·490	0·747½	0·748
0·14	−0·647	0·770	0·770
0·16	−0·744	0·751	0·751½
0·18	−0·784	0·696½	0·697
0·20	−0·772	0·613	0·613½
0·22	−0·718	0·507	0·507
0·24	−0·628	0·384	0·385
0·26	−0·512½	0·249	0·251
0·28	−0·377	0·108	0·110
0·30	−0·230	−0·035	−0·033
0·35	0·159	−0·385	−0·382
0·40	0·528	−0·695	−0·692
0·45	0·840	−0·946	−0·943
0·50	1·077½	−1·131	−1·128
0·55	1·240	−1·252	−1·250
0·60	1·332	−1·316	−1·314
0·7	1·350	−1·308	−1·308
0·8	1·225	−1·184	−1·185
0·9	1·033	−1·006	−1·007
1·0	0·828	−0·816	−0·818
1·1	0·638	−0·639	−0·641
1·2	0·477	−0·487	−0·488
1·3	0·348	−0·362½	−0·364
1·4	0·249	−0·265	−0·266
1·6	0·122	−0·135	−0·135
1·8	0·056½	−0·066	−0·066
2·0	0·025	−0·031	−0·031
2·2	0·011	−0·014	−0·014
2·4	0·004½	−0·006	−0·006
2·6	0·002	−0·003	−0·002½
2·8	0·000½	−0·001	−0·001
3·0	...	−0·001	−0·001
ϵ_{nl}	30·14	27·79	27·76

As the electrons in *Fe* XIV are so tightly bound, the effects of exchange terms on the wave functions are likely to be small, some indication of their magnitude being given by Hartree's calculations (**4, 6**) of the wave functions for Cu^+, with and without exchange. From the calculations of Williams (**7**) of the relativistic wave functions for Cu^+, it would appear that the relativistic corrections to the *Fe* XIV wave functions will also be small.

TABLE II

Values of $Z(nl\,;\,r)$ and Total $2Z_p(r)$

r	$(1s)^2$	$(2s)^2$	$(2p)^6$	$(3s)^2$	$(3p)$	Total $2Z_p$
0·000	2·00	2·00	6·00	2·00	1·00	52
0·005	2·00	2·00	5·99	2·00	1·00	51·08
0·010	1·97	2·00	5·99	2·00	1·00	50·18
0·015	1·92	1·99	5·99	2·00	1·00	49·30
0·020	1·84	1·99	5·99	2·00	1·00	48·46
0·025	1·73	1·98	5·99	1·99½	1·00	47·66½
0·030	1·61	1·97	5·99	1·99	1·00	46·92
0·035	1·48	1·96	5·98½	1·99	1·00	46·22
0·040	1·34	1·95	5·98	1·99	1·00	45·56
0·05	1·07	1·93	5·96	1·99	1·00	44·31
0·06	0·82	1·92	5·93	1·98½	1·00	43·20
0·07	0·61	1·92	5·88	1·98	0·99	42·18
0·08	0·44	1·91½	5·80	1·98	0·99	41·24
0·09	0·31	1·91½	5·69	1·98	0·99	40·36
0·10	0·22	1·91	5·56	1·98	0·98½	39·53½
0·12	0·11	1·88	5·23	1·98	0·97	37·98
0·14	0·05	1·82	4·82	1·96	0·96	36·59
0·16	0·03	1·72½	4·37	1·94½	0·95	35·35
0·18	0·01	1·60	3·89	1·92	0·94	34·26
0·20		1·44	3·41	1·90	0·93	33·33
0·22		1·28	2·95	1·87	0·93	32·52
0·24		1·11	2·51	1·86	0·92	31·83
0·26		0·95	2·11	1·84	0·92	31·26
0·28		0·80	1·76	1·83½	0·92	30·77
0·30		0·67	1·46	1·83	0·92	30·36
0·35		0·40	0·88½	1·83	0·92	29·46
0·40		0·23	0·51	1·82	0·90	28·80½
0·45		0·13	0·28½	1·77	0·87	28·30
0·50		0·07	0·16	1·67	0·81	27·88
0·55		0·03½	0·09	1·54	0·74	27·53
0·60		0·02	0·04½	1·37	0·66	27·23½
0·7		0·00½	0·01½	1·00	0·48	26·74½
0·8			0·01	0·67	0·33	26·42
0·9				0·41	0·20½	26·23
1·0				0·24	0·12	26·12
1·1				0·13	0·07	26·06
1·2				0·07	0·04	26·03
1·3				0·03	0·02	26·01
1·4				0·02	0·01	26·00½
1·6						26·00

3. *Spin-orbit interaction.*—In one-electron spectra, because of the spin-orbit interaction, a *nl* configuration splits into two levels, corresponding to $j=l+\frac{1}{2}$ and $j=l-\frac{1}{2}$. The displacement between these two levels is given (**8**) by

$$\Delta W_{nl}=R\alpha^2(l+\tfrac{1}{2})\int_0^\infty \frac{Z(r)}{r^3}\,P_N^2(nl;r)\,dr, \tag{5}$$

where R is the Rydberg constant, α is the fine structure constant and Z is the charge, which, when placed at the nucleus, gives the net attractive field on the *nl* electron at the radius r, the integral being expressed in atomic units. If the energy difference is measured in cm.$^{-1}$, $R\alpha^2$ has the value 5·841.

For the 3p electron in *Fe* XIV ($3s^23p$), the value calculated from equation (5) is $\Delta W=19{,}390$ cm.$^{-1}$. This value agrees well with the wave number of the coronal line, 18,852·5 cm.$^{-1}$, identified by Edlén as due to the transition $(3s^23p)\ {}^2P_{\frac{3}{2}}-{}^2P_{\frac{1}{2}}$ in *Fe* XIV. His identification is based on the wave-number coincidence between this line and the ground-term splitting for *Fe* XIV, found by extrapolation along the iso-electronic sequence of *Al* I, and is consistent with the identifications of the other coronal lines.

4. *Transition probabilities.* (a) *The transition Fe XIV* $(3s^23p)\ {}^2P_{\frac{3}{2}}-{}^2P_{\frac{1}{2}}$.—The transition *Fe* XIV $(3s^23p)\ {}^2P_{\frac{3}{2}}-{}^2P_{\frac{1}{2}}$ is associated with magnetic-dipole and electric-quadrupole radiation (**9**). For a magnetic-dipole line, the probability of spontaneous transition from the upper level γJ to the lower level $\gamma' J'$ has the value

$$A_m(\gamma J,\gamma' J')=\left(\frac{4\pi^2e^2h}{3m^2c^2}\right)\frac{\nu^3}{2J+1}\,S_m(\gamma J,\gamma' J'), \tag{6}$$

where $S_m(\gamma J,\gamma' J')$, the strength of the line, is defined by

$$S_m(\gamma J,\gamma' J')=\sum_{M,M'}|(\gamma JM|\vec{\mathrm{L}}+2\vec{\mathrm{S}}|\gamma' J'M')|^2. \tag{7}$$

The wave number ν is measured in cm.$^{-1}$ and $\vec{\mathrm{L}}$ and $\vec{\mathrm{S}}$ are measured in units of $\hbar$. The numerical factor is equal to $2{\cdot}698\times10^{-11}$. The evaluation of S_m does not involve the use of radial wave functions and for the line considered has the value $\frac{4}{3}$. The magnetic-dipole transition probability for the line, $\nu=18{,}852{\cdot}5$ cm.$^{-1}$, is then 60 sec.$^{-1}$.

The electric-quadrupole transition probability is given by

$$A_q(\gamma J,\gamma' J')=\frac{h^7}{40m^4e^6\pi^2}\,\frac{\nu^5}{2J+1}\,S_q(\gamma J,\gamma' J'), \tag{8}$$

where

$$S_q(\gamma J,\gamma' J')=\sum_{M,M'}|(\gamma JM|\eta'|\gamma' J'M')|^2. \tag{9}$$

Here, η' is the electric-quadrupole moment of the atom minus its spherically symmetrical component, measured in atomic units, ea_0^2. The wave number ν is measured in cm.$^{-1}$. The numerical factor is equal to $1{\cdot}680\times10^{-22}$. In one-electron spectra, the electric-quadrupole strengths can be expressed in terms of certain coefficients, which have been evaluated (**8**), multiplied by the squares of the radial integrals

$$\int_0^\infty r^2P_N(nl;r)P_N(n'l';r)\,dr. \tag{10}$$

This integral has the value 0·565 for the 3p electron in *Fe* XIV. The quadrupole strength of the line considered is equal to 0·17. The value of the quadrupole transition probability is then 0·017 sec.$^{-1}$. This line is almost entirely due to magnetic-dipole radiation, the quadrupole term in the transition probability giving only 0·03 per cent of the whole amount.

(b) *The transition array Fe XIV* $3s3p^2 \rightarrow 3s^2 3p$.—The transition array $3s3p^2 \rightarrow 3s^2 3p$ is associated with electric-dipole radiation. For an electric-dipole line, the probability of spontaneous transition (**8**) from the upper level γJ to the lower level $\gamma' J'$ is given by the expression

$$A_e(\gamma J, \gamma' J') = \left(\frac{4h^3}{3m^2e^2}\right) \frac{\nu^3}{2J+1} S_e(\gamma J, \gamma' J'), \tag{11}$$

where S_e, the strength of the line, has the value

$$S_e(\gamma J, \gamma' J') = \sum_{M, M'} |(\gamma J M | \vec{P} | \gamma' J' M')|^2. \tag{12}$$

The electric-dipole moment of the atom, $\vec{P}$, is measured in atomic units, ea_0. The wave number ν is measured in cm.$^{-1}$. The numerical factor is equal to $2{\cdot}026 \times 10^{-6}$. The f-value (**8**) associated with this line is given by

$$f(\gamma J, \gamma' J') = \left(\frac{1}{3R}\right) \frac{\nu}{2J'+1} S_e(\gamma J, \gamma' J'), \tag{13}$$

where R is the Rydberg constant. The value of the numerical factor is $3{\cdot}039 \times 10^{-6}$. For a complete transition array, A_e and f have the values:

$$A_e = 2{\cdot}026 \times 10^{-6} \frac{\Sigma \nu^3 S_e(\gamma J, \gamma' J')}{\Sigma 2J+1} \tag{14}$$

and

$$f = 3{\cdot}039 \times 10^{-6} \frac{\Sigma \nu S_e(\gamma J, \gamma' J')}{\Sigma 2J'+1}. \tag{15}$$

By extrapolation along the iso-electronic sequence of *Al* I, the lowest lying configuration combining with the ground configuration, $3s^2 3p$, in *Fe* XIV, is found to be $3s3p^2$. The mean wave number for the transitions between these two configurations is $\bar{\nu} = 300{,}000$ cm.$^{-1}$. By the sum rules (**10**), holding for any coupling, the total strength of the lines in the transition array $3s3p^2 \rightarrow 3s^2 3p$, is $30\sigma^2$. The quantity σ, in atomic units ea_0, is given by

$$\sigma = \frac{1}{\sqrt{4l^2-1}} \int_0^\infty r P_N(nl; r) P_N(n'l'; r)\, dr, \tag{16}$$

l being the greater of the two azimuthal quantum numbers involved in the transition. For the transition array considered, σ^2 has the value 0·164; the total strength of the lines in the array is, then, 4·92. The sum of the statistical weights of the levels in the terms (^{4}P, ^{2}D, ^{2}S, ^{2}P) of the higher configuration, $3s3p^2$, is 30; that of the levels in the ground term (^{2}P) is 6. The values of A_e and f for the complete transition array, found by introducing in equations (14) and (15) the mean wave number $\bar{\nu}$, are $A_e = 9{\cdot}0 \times 10^9$ sec.$^{-1}$ and $f = 0{\cdot}75$.

The writer is grateful to Professor D. R. Hartree and Mrs Bertha Jeffreys for their helpful advice during the course of this work.

Girton College,
Cambridge:
1949 *March* 28.

References

(1) Edlén, B., *Zs. f. Ap.*, **22,** 30, 1942.
(2) Hartree, D. R., *Proc. Camb. Phil. Soc.*, **24,** 89, 111, 1928.
(3) Manning, M. F. and Millman, J., *Phys. Rev.*, **49,** 848, 1936.
(4) Hartree, D. R. and W., *Proc. Roy. Soc.* A, **157,** 490, 1936.
(5) Hartree, D. R., *Proc. Camb. Phil. Soc.*, **22,** 464, 1924.
(6) Hartree, D. R., *Proc. Roy. Soc.* A, **141,** 282, 1933.
(7) Williams, A. O., *Phys. Rev.*, **58,** 723, 1940.
(8) Condon, E. U. and Shortley, G. H., *The Theory of Atomic Spectra*, Cambridge, 1935.
(9) Shortley, G. H., *Phys. Rev.*, **57,** 225, 1940.
(10) Menzel, D. H., *Ap. J.*, **105,** 126, 1947.

STELLAR PARALLAXES DETERMINED AT THE UNIVERSITY OF LONDON OBSERVATORY, MILL HILL

(Communicated by the Director)

(Received 1949 May 6)

The first plates for the determination of parallax with the Radcliffe 24-inch photographic refractor were taken in 1939 April. This work was interrupted from 1939 September 1 to 1946 April 3. Sixty-six stars were chosen for this first parallax programme, mostly on the advice of Sir Frank Dyson; the twenty stars which comprise the present list all had plates taken in 1939, thus providing a period of about nine years for the determination of proper motion in R.A. Nineteen of the stars were photographed for five epochs; No. 10 was photographed for an additional epoch because the 1939 epoch consisted of only three plates instead of the usual five. Two exposures were made on each plate, and these were measured in R.A. in the direct and reverse positions relative to rulings on reference plates. These plates were ruled at Greenwich through the kindness of the Astronomer Royal.

The average number of comparison stars was 5·2, having an average photographic magnitude of about 11·5 except where the parallax star was fainter than this magnitude. When brighter, the image of the parallax star was reduced to equality with an average $11^{m}\cdot5$ image by means of a rotating sector, there being one sector for each half magnitude. The average distance of the comparison stars and of the parallax star from the centre of mean position on the plate of the comparison stars was 15′·7 and 2′·4 respectively, and the average parallax factor was $0\cdot66 \pm 0\cdot04$. The plates used were Ilford Special Rapid (H and D 270), but in some cases, for the fainter stars, Ilford Iso-Zenith plates (H and D 700) were used. The normal time of exposure was $2\frac{1}{2}$ minutes for stars not fainter then 11·5 magnitude. For such exposures no guiding was required, as the errors of the polar axis were not allowed to exceed half a minute of arc in altitude or azimuth, and the hour angles were less than 10 minutes except in the case of a few stars near the zenith. Examination showed no positive correlation between the hour angle at observation and the residual. Most of the plates were measured by Mr R. W. Pring, and the remainder by Miss A. C. Robinson, Mr D. J. Gerhard and the Director. The plates were reduced following the method adopted by Schlesinger.

In the following list, the third column gives the approximate visual and photographic magnitudes. These are taken from various sources and should be looked upon as provisional only. Where the photographic magnitude is bracketed, its value is estimated from the plates. Two values of the annual proper motion in R.A. are given, the first being a catalogue value and absolute (as also are the proper motions in declination); the second value of the proper motion in R.A. is derived from the parallax plates and is relative; omitting stars Nos. 14 and 18, which are multiple systems, the average difference between this and the catalogue value is $\pm 0''\cdot016$.

Twelve stars have had previous determinations of parallax; in some cases these parallaxes are well determined and such stars were included as test objects.

Of the eight stars having no previous determinations, marked with an asterisk in the column headed Relative Parallax, it will be noted that the parallax is in each case positive, the largest being 0″·063. To obtain the absolute parallaxes of all the stars in the list, the value of the correction which must be *added* to the given relative parallax may be found from *Groningen Publication*, No. 29, p. 55, Table 26. The average value of this correction is 0″·002.

In the case of the double star No. 14, both components were measured independently using the same comparison stars and both sets of values are given. The parallaxes differ by 0″·065, which seems excessive.

It will be noticed that the probable errors for an *exposure* of unit weight are somewhat large, the average being ±0″·047 as compared with the value ±0″·026 given in the Greenwich parallax list for 1938 for a *plate* of unit weight. This is probably due in part to lack of experience in this type of plate measurement, and in part to a number of small changes of adjustment which were made from time to time in the relative position of the components of the 24-inch objective in order to remove a source of magnitude error. It was discovered that, when the two components of the object glass were "squared on" by the method of alignment of reflected images of small lights in the focal plane in the various lens surfaces, a small residual coma was present over the whole plate, and this was independent of small changes in focus. It was only detected by photographs taken with a Hartmann diaphragm, and it has now been removed. The effect of this error is to cause a scatter in the actual parallax measurements on account of the variation of the sizes and appearances of the images of the parallax and comparison stars when photographed on nights differing in atmospheric transparency. In order to obtain a higher degree of accuracy in the parallax determinations of the remainder of the stars in the first programme, and all those stars in a subsequent programme which is now in progress, an average of five plates per epoch are being taken at not less than seven epochs.

No.	Designation and B.D. No.	Mag. Vis. Phot.	Spec. Type	R.A. Dec. 1900·0	Proper Motion (Unit 0″·001) R.A.	Proper Motion (Unit 0″·001) Dec.	P.E. Unit Wt.	Relative Parallax	P.E.
				h m s					
1	McC. 6·7a	8·7	K0	0 33 30	− 225	− 59	32	+ 9*	±6
	30° 89	[9·5]		+30° 28′	− 251				±4
2	McC. 15·33	10·6	G5	1 4 18	+ 153	− 9	43	+ 17	8
	54° 234	[11·5]		+54° 45′	+ 163				5
3	Camb. IId, 29	8·7	G0	1 32 30	+ 142	− 68	42	+ 33*	9
	52° 393	9·3		+52° 44′	+ 156				6
4	Boss 3470	7·4	G0	13 18 39	− 128	+ 26	35	+ 31	9
	85° 222	7·5		+85° 17′	− 124				6
5	Radcl. 33·72	8·3	F6	13 50 6	− 151	+ 54	44	+ 13*	8
	45° 2137	9·8		+45° 13′	− 128				5
6	Green. 146	9·5		14 10 20	+ 184	− 549	46	+ 75	10
	81° 465	11·0		+81° 5′	+ 212				5

Unit 0″·001

No.	Designation and B.D. No.	Mag. Vis. Phot.	Spec. Type	R.A. Dec. 1900·0	Proper Motion R.A.	Proper Motion Dec.	P.E. Unit Wt.	Relative Parallax	P.E.
				h m s					
7	McC. 183·2	9·7	Ko	14 38 54	− 318	− 16	48	+ 49*	9
	27° 2411	[10·5]		+27° 11′	− 332				4
8	McC. 194·34	11·2	G5	15 24 30	+ 90	− 164	41	+ 8*	8
		[12·5]		+59° 28′	+ 36				4
9	Radcl. 60·77	...	G3	15 56 32	− 174	− 14	96	+ 30*	25
		12·6		+29° 49′	− 163				11
10	Lal. F. 2832	7·0	Go	16 37 45	+ 101	− 80	56	+ 21	11
	80° 519	7·3		+80° 0′	+ 127				8
11	Lal. 32047	6·3	Ko	17 25 19	− 539	+ 8	44	+ 63	9
	67° 1014	6·8		+67° 23′	− 516				4
12	McC. 222·27	9·1	Go	17 43 42	− 132	− 211	40	− 2	8
	27° 2891	[10·0]		+27° 51′	− 128				4
13	36 Dra	5·0	F2	18 13 9	+ 345	+ 29	40	+ 52	8
	64° 1252	5·5		+64° 22′	+ 354				4
14	Test 18·41	8·8	K5	18 41 42	−1490	+1770	48	+235	9
	Burn. 8798	[10·0]		+59° 29′	−1255				5
	59° 1915								
					[−1330]		63	+300	13
									7
15	Green. 457	...		19 1 8	+ 105	+ 508	49	+102	10
	A.C. 70° 8247	12·7		+70° 30′	+ 100				6
16	O.A. 21338	8·6	K2	20 51 18	0	− 770	47	+ 98	9
	61° 2068	[9·5]		+61° 48′	− 16				5
17	McC. 295·12	9·2	G5	21 12 48	+ 150	+ 258	42	+ 63*	8
	62° 1916	[10·0]		+62° 26′	+ 137				4
18	Camb. VIIb, 40	9·3	Mb	22 24 29	− 760	− 422	52	+238	11
	56° 2783	11·3		+57° 12′	− 892				5
19	McC. 321·18	10·9	K5	22 43 48	+ 177	+ 13	51	+ 21*	10
		[12·5]		+24° 12′	+ 176				6
20	Radcl. 19·142	10·2	A3	23 21 57	+ 470	+ 44	29	+ 23	6
	59° 2723	10·8		+60° 5′	+ 453				3

* No previous determination of parallax.

University of London Observatory,
Mill Hill Park:
1949 *May* 5.

MEAN AREAS AND HELIOGRAPHIC LATITUDES OF SUNSPOTS IN THE YEARS 1943 AND 1944

Royal Observatory, Greenwich

(Communicated by the Astronomer Royal)

(Received 1949 June 23)

The following results are in continuation of those given in *M.N.*, **108,** 505, 1948, and are derived from the measurement at Greenwich of photographs taken at the Royal Observatories of Greenwich and the Cape and at the Kodaikanal Observatory, India. Photographs for two days unrepresented in the series were kindly supplied by the Superintendent, U.S. Naval Observatory, Washington.

Table I gives the mean daily areas of umbrae, whole spots and faculae for each synodic rotation of the Sun included in the years 1943 and 1944; the means for each year as a whole are included in Table II, which summarizes the yearly values from 1933–44.

TABLE I

No. of Rotation	Rotation Commenced U.T.	Days Photographed	Mean Daily Areas: Projected* Umbrae	Projected* Whole Spots	Projected* Faculae	Corrected for Foreshortening† Umbrae	Corrected for Foreshortening† Whole Spots	Corrected for Foreshortening† Faculae
	1943							
1195	Jan. 9·63	27	17	81	309	11	57	383
1196	Feb. 5·97	27	161	1014	502	114	708	614
1197	Mar. 5·31	28	147	829	506	105	583	616
1198	Apr. 1·61	27	203	1155	662	138	798	776
1199	Apr. 28·88	27	69	356	830	57	288	1026
1200	May 26·10	27	16	67	693	11	46	849
1201	June 22·30	27	58	354	408	39	239	509
1202	July 19·50	28	33	182	401	28	152	490
1203	Aug. 15·72	27	50	236	447	38	181	562
1204	Sept. 11·97	27	81	413	278	39	308	358
1205	Oct. 9·25	28	32	161	252	26	137	300
1206	Nov. 5·55	27	32	165	364	22	116	444
1207	Dec. 2·86	27	74	453	339	51	311	430
1208	Dec. 30·18	28	3	19	222	4	20	261
	1944							
1209	Jan. 26·52	27	4	18	179	2	11	211
1210	Feb. 22·86	27	11	58	113	11	58	149
1211	Mar. 21·18	28	32	168	287	19	105	324
1212	Apr. 17·47	27	0	0	126	0	0	152
1213	May 14·70	27	5	24	98	6	34	125
1214	June 10·91	27	11	56	213	9	42	253
1215	July 8·11	27	5	18	263	5	22	311
1216	Aug. 4·32	28	30	131	523	20	87	621
1217	Aug. 31·56	27	63	317	299	48	247	383
1218	Sept. 27·83	27	51	265	448	41	223	545
1219	Oct. 25·12	27	24	127	370	21	109	443
1220	Nov. 21·42	28	115	667	294	82	488	351

* Expressed in millionths of the Sun's disk.

† Expressed in millionths of the Sun's hemisphere.

TABLE II

Year	No. of Days		Mean Daily Areas					
			Projected*			Corrected for Foreshortening†		
	Photographed	Without Spots	Umbrae	Whole Spots	Faculae	Umbrae	Whole Spots	Faculae
1933	365	234	24	120	225	18	88	267
1934	365	145	27	142	297	22	119	354
1935	365	21	152	810	910	117	624	1100
1936	366	0	288	1529	2106	217	1141	2545
1937	365	0	509	2795	2856	375	2074	3505
1938	365	0	501	2706	2578	371	2019	3205
1939	365	0	404	2163	1907	295	1579	2349
1940	366	0	279	1434	1224	200	1039	1522
1941	365	8	167	915	1041	120	658	1282
1942	365	16	112	591	666	79	423	809
1943	365	48	73	410	457	51	295	561
1944	366	157	30	160	281	23	126	338

* Expressed in millionths of the Sun's disk.
† Expressed in millionths of the Sun's hemisphere.

Table III gives for each rotation in the years 1943 and 1944 the mean daily area of the whole spots (corrected for foreshortening) and the mean heliographic latitude of the spotted areas for both northern and southern hemispheres.

The mean heliographic latitude of the entire spotted area and the mean distance from the equator of all spots are also tabulated. The mean values for the years 1943 and 1944 are included in Table IV.

Tables II and IV are in continuation of similar tables given in *Monthly Notices*: for the years 1874 to 1888—**49,** 381–382; 1889 to 1902—**63,** 465–466; 1901 to 1914—**76,** 402–403; 1913 to 1924—**85,** 1007–1008; 1923 to 1933—**94,** 870–871.

The rotations in Tables I and III are numbered in continuation of Carrington's series.

The two years (1943 and 1944) embracing a sunspot minimum may conveniently be reviewed together. The chief features of the record are as follows:—

(1) The continued decline in sunspot frequency and in the mean daily spotted area throughout 1943 to a minimum early in 1944, and the subsequent rise with a definite onset of the new cycle.

The smoother values given by the faculae (Table I) show these features even more clearly than the sunspots themselves. The mean daily area of 126 for whole spots in 1944 (Table II, column 8) may be compared with values of previous years of minimum, viz. 88 (1933): 55 (1923): 7 (1913): 29 (1901): 78 (1889) and 22 (1878).

(2) On 48 days in 1943 and 157 days in 1944, no sunspots were seen. Throughout one solar rotation (No. 1212) no sunspot was recorded.

(3) As in 1941 and 1942, the spotted area in 1943 predominated in the northern hemisphere, but the new cycle spots of 1944 favoured the southern.

(4) The number and distribution of spot groups (north and south of the equator) lasting for two days or more are shown below. Groups that were seen on one day only are tabulated separately: these were mostly very small.

	Duration			
	Two days or more		One day	
Year	1943	1944	1943	1944
North	41	22	13	4
South	26	40	10	16
Total	67	62	23	20

For short summaries of the more important spots of the period, see *Monthly Notices*, **104,** 108, 1944 and **105,** 135, 1945.

(5) The characteristic discontinuity in latitude between the old and new cycle spots in the years 1943 and 1944 is clearly seen from the weighted mean latitudes given in the last column of Table IV. The first spot of the new cycle came in Rotation 1199.

TABLE III

No. of Rotation	Rotation Commenced U.T.	Spots North of the Equator: Mean Daily Area	Spots North of the Equator: Mean Heliographic Latitude	Spots South of the Equator: Mean Daily Area	Spots South of the Equator: Mean Heliographic Latitude	Mean Latitude of Entire Spotted Area	Mean Distance from Equator of all Spots
	1943		°		°	°	°
1195	Jan. 9·63	24	7·65	33	6·20	− 0·28	6·80
1196	Feb. 5·97	703	7·83	6	3·19	+ 7·74	7·80
1197	Mar. 5·31	564	5·22	18	9·60	+ 4·75	5·36
1198	Apr. 1·61	641	7·37	157	11·82	+ 3·59	8·25
1199	Apr. 28·88	235	5·57	53	39·46	− 2·72	11·81
1200	May 26·10	45	7·95	1	3·60	+ 7·68	7·84
1201	June 22·30	232	13·96	7	1·53	+13·53	13·62
1202	July 19·50	101	12·04	51	3·36	+ 6·90	9·14
1203	Aug. 15·72	149	13·80	31	7·04	+10·18	12·63
1204	Sept. 11·97	285	15·32	23	6·70	+13·69	14·68
1205	Oct. 9·25	135	14·68	3	19·87	+13·98	14·78
1206	Nov. 5·55	109	13·11	7	8·74	+11·78	12·84
1207	Dec. 2·86	96	7·43	215	22·33	−13·14	17·73
1208	Dec. 30·18	19	9·50	1	23·80	+ 8·36	9·99
	1944						
1209	Jan. 26·52	11	9·10	0	...	+ 9·10	9·10
1210	Feb. 22·86	0	...	58	25·48	−25·48	25·48
1211	Mar. 21·18	2	5·50	103	24·30	−23·67	23·91
1212	Apr. 17·47	0	...	0	...	...	...
1213	May 14·70	28	0·50	5	24·35	− 3·34	4·19
1214	June 10·91	38	5·29	4	18·40	+ 3·23	6·43
1215	July 8·11	0·2	18·50	21	26·34	−25·88	26·26
1216	Aug. 4·32	7	13·62	80	14·72	−12·40	14·63
1217	Aug. 31·56	1	9·10	247	23·72	−23·60	23·67
1218	Sept. 27·83	63	21·49	161	24·60	−11·69	23·73
1219	Oct. 25·12	69	20·86	40	14·55	+ 7·76	18·53
1220	Nov. 21·42	182	20·77	306	21·87	− 5·96	21·46

As an appendix to Table I, the mean daily values are given of whole spots and of faculae (corrected for foreshortening and expressed in millionths of the Sun's hemisphere) for each calendar month, 1943–44. Monthly values, rather

than those based on the Sun's synodic rotation period, are sometimes more convenient for comparison with tabulated geophysical data, and they will continue to be given in these summaries.

Monthly Mean Daily Areas of Sunspots and Faculae

	1943		1944	
	Spots	Faculae	Spots	Faculae
Jan.	72	422	26	247
Feb.	552	536	2	183
Mar.	629	626	145	301
Apr.	753	781	1	209
May	249	989	9	52
June	37	678	52	234
July	242	522	25	309
Aug.	143	621	78	606
Sept.	242	443	250	410
Oct.	235	262	194	554
Nov.	127	387	178	357
Dec.	285	468	538	585

TABLE IV

Year	Days Photographed		Spots North of the Equator: Mean Daily Area	Spots North of the Equator: Mean Heliographic Latitude	Spots South of the Equator: Mean Daily Area	Spots South of the Equator: Mean Heliographic Latitude	Mean Latitude of Entire Spotted Area	Mean Distance from Equator of all Spots
				°		°	°	°
1933	365		86	10·60	2	8·35	+10·23	10·56
1934	365		44	16·45	74	28·09	−11·49	23·75
1934	365	Old Cycle	19	4·10	1	4·37	+ 3·79	4·11
		New Cycle	26	25·44	74	28·31	−14·46	27·57
1935	365		205	22·42	419	23·72	− 8·57	23·30
1936	366		463	19·36	678	21·02	− 4·63	20·35
1937	365		1317	17·63	757	15·96	+ 5·36	17·02
1938	365		899	15·55	1120	14·17	− 0·94	14·79
1939	365		649	14·64	931	12·57	− 1·39	13·42
1940	366		499	11·65	540	10·72	+ 0·03	11·17
1941	365		427	11·31	232	8·67	+ 4·28	10·38
1942	365		252	9·32	171	8·45	+ 2·14	8·99
1943	365		249	9·01	46	15·87	+ 5·11	10·09
1943	365	Old Cycle	249	9·01	27	8·33	+ 7·33	8·95
		New Cycle	0	...	20	26·13	−26·13	26·13
1944	366		42	19·00	83	22·81	− 8·70	21·53
1944	366	Old Cycle	7	4·17	6	7·61	− 1·14	5·72
		New Cycle	35	22·18	77	24·02	− 9·63	23·45

Royal Greenwich Observatory,
Herstmonceux Castle,
Sussex:
1949 *June* 20.